Atomic Layer Deposition of Noble Metal Oxide and Noble Metal Thin Films

Jani Hämäläinen

Laboratory of Inorganic Chemistry
Department of Chemistry
Faculty of Science
University of Helsinki
Finland

ACADEMIC DISSERTATION

To be presented, with the permission of the Faculty of Science of the University of Helsinki, for public criticism in Auditorium A110 of the Department of Chemistry, A. I. Virtasen Aukio 1, on May 17th, 2013, at 12 o'clock noon.

Helsinki 2013

Supervisors

Professor Mikko Ritala
Professor Markku Leskelä
Laboratory of Inorganic Chemistry
Department of Chemistry
University of Helsinki
Finland

Reviewers

Professor W.M.M. (Erwin) Kessels
Department of Applied Physics
Eindhoven University of Technology
Netherlands

Dr. Jeffrey W. Elam
Energy Systems Division
Argonne National Laboratory
USA

Opponent

Professor Mato Knez
Nanomaterials Group
CIC nanoGUNE Consolider
The Basque Country, Spain

© Jani Hämäläinen

ISBN 978-952-10-8794-3 (pbk.)
ISBN 978-952-10-8795-0 (PDF)
http://ethesis.helsinki.fi
Helsinki University Print
Helsinki 2013

Abstract

Atomic layer deposition (ALD) is a chemical gas phase deposition method to grow thin films which are highly uniform and conformal over large and complex substrate areas. Film growth in ALD is precise, remarkably repeatable, and combined with unparalleled control of the film thickness. These inherent properties make ALD an attractive method to deposit thin films for advanced technological applications such as microelectronics and nanotechnology. One material group in ALD which has matured in ten years and proven to be of wide technological importance is noble metals.

The purpose of this study was to investigate noble metal oxide film growth by ALD. The ALD of noble metal oxides has been very limited compared to the noble metal growth. Another aim was to examine noble metal film deposition at temperatures lower than required in the earlier ALD noble metal processes. In addition, the selection of noble metals that can be grown by ALD was expanded with osmium.

The results of the study showed that oxides of iridium, rhodium, platinum, and palladium can be deposited from the common noble metal precursors using ozone as the reactant at temperatures below 200 °C. The development of ozone-based ALD noble metal oxide processes led further on to the low temperature deposition of noble metals by adding a reductive molecular hydrogen step after every oxidative ozone step. The noble metal deposition via noble metal oxide growth was achieved at lower temperatures than required with the common oxygen-based ALD noble metal processes.

Film growth rates, resistivities, purities, and surface roughnesses resulting from the studied noble metal oxide and noble metal processes were reasonable. The processes showed some shortcomings but offer an alternative thermal ALD pathway to deposit noble metals and noble metal oxides compared to the oxygen-based ALD processes.

Keywords: atomic layer deposition, ALD, noble metal oxide, noble metal, thin film, ozone

Contents

Abstract 3

Contents 4

List of publications 6

Related publications by the same author 8

Other publications by the same author 9

List of abbreviations and acronyms 10

1 Introduction 12

2 Background 14

2.1 Noble metals 14

2.2 Noble metal oxides 15

2.3 Atomic layer deposition (ALD) 16

2.3.1 Thermal and plasma enhanced ALD 18

3 ALD of noble metals and their oxides 20

3.1 Reaction mechanisms in ALD processes of noble metals and their oxides 22

3.1.1 Oxygen-based processes 22

3.1.2 Ozone-based processes 25

3.1.3 Reductant-based processes 26

3.1.4 Plasma-based processes 28

3.2 Nucleation in ALD of noble metals and their oxides 29

3.3 Ruthenium 33

3.3.1 Metallocene precursors 38

3.3.2 β-Diketonate precursors 43

3.3.3 Other precursors 44

3.4 Ruthenium oxide 47

3.5 Osmium 52
3.6 Rhodium and rhodium oxide 52
3.7 Iridium 54
3.8 Iridium oxide 60
3.9 Palladium and palladium oxide 62
3.10 Platinum and platinum oxide 67
3.11 Silver 73
3.12 Gold, rhenium and their oxides 76
4 Experimental 77
4.1 Film deposition 77
4.2 Film characterization 78
5 Results and discussion 80
5.1 Iridium oxide and metal 80
5.1.1 Film growth with $Ir(acac)_3$ 80
5.1.2 Film growth with (MeCp)Ir(CHD) 82
5.1.3 Surface roughnesses 85
5.1.4 Resistivities 87
5.1.5 Impurity contents 89
5.2 Rhodium oxide and metal 91
5.3 Palladium oxide and metal 95
5.4 Platinum oxide and metal 100
5.5 General aspects of the low-temperature ozone-based ALD processes 107
5.6 Osmium 109
6 Conclusions 111
Acknowledgements 114
References 116

List of publications

Thesis is based on the following publications:

I J. Hämäläinen, M. Kemell, F. Munnik, U. Kreissig, M. Ritala and M. Leskelä
Atomic Layer Deposition of Iridium Oxide Thin Films from $Ir(acac)_3$ and Ozone
Chemistry of Materials **20** (2008) 2903–2907.

II J. Hämäläinen, F. Munnik, M. Ritala and M. Leskelä
Atomic Layer Deposition of Platinum Oxide and Metallic Platinum Thin Films from $Pt(acac)_2$ and Ozone
Chemistry of Materials **20** (2008) 6840–6846.

III J. Hämäläinen, F. Munnik, M. Ritala and M. Leskelä
Study on Atomic Layer Deposition of Amorphous Rhodium Oxide Thin Films
Journal of the Electrochemical Society **156** (2009) D418–D423.

IV J. Hämäläinen, E. Puukilainen, M. Kemell, L. Costelle, M. Ritala and M. Leskelä
Atomic Layer Deposition of Iridium Thin Films by Consecutive Oxidation and Reduction Steps
Chemistry of Materials **21** (2009) 4868–4872.

V J. Hämäläinen, T. Hatanpää, E. Puukilainen, L. Costelle, T. Pilvi, M. Ritala and M. Leskelä
(MeCp)Ir(CHD) and Molecular Oxygen as Precursors in Atomic Layer Deposition of Iridium
Journal of Materials Chemistry **20** (2010) 7669–7675.

VI J. Hämäläinen, T. Hatanpää, E. Puukilainen, T. Sajavaara, M. Ritala and M. Leskelä
Iridium Metal and Iridium Oxide Thin Films Grown by Atomic Layer Deposition at Low Temperatures
Journal of Materials Chemistry **21** (2011) 16488–16493.

VII J. Hämäläinen, E. Puukilainen, T. Sajavaara, M. Ritala and M. Leskelä
Low Temperature Atomic Layer Deposition of Noble Metals Using Ozone and Molecular Hydrogen as Reactants
Thin Solid Films **531** (2013) 243–250.

VIII J. Hämäläinen, T. Sajavaara, E. Puukilainen, M. Ritala and M. Leskelä
Atomic Layer Deposition of Osmium
Chemistry of Materials **24** (2012) 55–60.

The publications are referred to in the text by their roman numerals.

Related publications by the same author

1. E. Santala, J. Hämäläinen, J. Lu, M. Leskelä and M. Ritala
Metallic Ir, IrO_2 and Pt Nanotubes and Fibers by Electrospinning and Atomic Layer Deposition
Nanosci. Nanotechnol. Lett. **1** (2009) 218.

2. T. Ryynänen, K. Nurminen, J. Hämäläinen, M. Leskelä and J. Lekkala
pH Electrode Based on ALD Deposited Iridium Oxide
Proc. Eng. **5** (2010) 548.

3. T. Ryynänen, L. Ylä-Outinen, S. Narkilahti, J. M. A. Tanskanen, J. Hyttinen, J. Hämäläinen, M. Leskelä and J. Lekkala
Atomic Layer Deposited Iridium Oxide Thin Film as Microelectrode Coating in Stem Cell Applications
J. Vac. Sci. Technol. A **30** (2012) 041501.

4. M. J. Heikkilä, J. Hämäläinen, M. Ritala and M. Leskelä
HTXRD Study of Atomic Layer Deposited Noble Metal Thin Films Heat Treated in Oxygen
Z. Kristallogr. Proc. **1** (2011) 209.

5. M. Leskelä, T. Aaltonen, J. Hämäläinen, A. Niskanen and M. Ritala
Atomic Layer Deposition of Metal Thin Films
Proc. Electrochem. Soc. **2005-09** (2005) 545.

6. J. Hämäläinen, M. Ritala and M. Leskelä
Low Temperature ALD of Noble Metals
U.S. Pat. Appl. Publ. (2011), US 20110020546 A1.

7. J. Hämäläinen, M. Ritala and M. Leskelä
Atomic Layer Deposition of Noble Metal Oxides
U.S. Pat. Appl. Publ. (2007), US 20070014919 A1.

Other publications by the same author

1 J. Hämäläinen, J. Ihanus, T. Sajavaara, M. Ritala and M. Leskelä
Atomic Layer Deposition and Characterization of Aluminum Silicate Thin Films for Optical Applications
J. Electrochem. Soc. **158** (2011) P15.

2 J. Hämäläinen, J. Holopainen, F. Munnik, M. Heikkilä, M. Ritala and M. Leskelä
Atomic Layer Deposition of Aluminum and Titanium Phosphates
J. Phys. Chem. C. **116** (2012) 5920.

3 J. Hämäläinen, J. Holopainen, F. Munnik, T. Hatanpää, M. Heikkilä, M. Ritala and M. Leskelä
Lithium Phosphate Thin Films Grown by Atomic Layer Deposition
J. Electrochem. Soc. **159** (2012) A259.

4 J. Hämäläinen, F. Munnik, T. Hatanpää, J. Holopainen, M. Ritala and M. Leskelä
Study of Amorphous Lithium Silicate Thin Films Grown by Atomic Layer Deposition
J. Vac. Sci. Technol. A **30** (2012) 01A106.

5 M. Mäntymäki, J. Hämäläinen, E. Puukilainen, F. Munnik, M. Ritala and M. Leskelä
Atomic Layer Deposition of LiF Thin Films from Lithd and TiF_4 Precursors
Chem. Vap. Deposition, accepted.

6 M. Mäntymäki, J. Hämäläinen, E. Puukilainen, T. Sajavaara, M. Ritala and M. Leskelä
Atomic Layer Deposition of LiF Thin Films from Lithd, $Mg(thd)_2$ and TiF_4 Precursors
Chem. Mater., accepted.

7 J. Hämäläinen, J. Holopainen, T. Hatanpää, M. Ritala and M. Leskelä
Atomic Layer Deposition of Metal Phosphates and Lithium Silicates
U.S. Pat. Appl. Publ. (2012), US 20120276305 A1.

List of abbreviations and acronyms

acac	acetylacetonato, 2,4-pentanedionato
AES	Auger electron spectroscopy
ALD	atomic layer deposition
AFM	atomic force microscopy
APM	atomic probe microscopy
Be	benzene
CHD	cyclohexadiene
COD	cyclo-octadiene
Cp	cyclopentadienyl
CVD	chemical vapor deposition
DMPD	dimethylpentadienyl
EBID	electron beam induced deposition
ECH	ethylcyclohexane
EDX	energy dispersive x-ray spectroscopy
ERDA	elastic recoil detection analysis
Et	ethyl
FESEM	field emission scanning electron microscopy
GIXRD	grazing incidence x-ray diffraction
hfac	1,1,1,5,5,5-hexafluoroacetylacetonato
LIALD	liquid injection ALD
Me	methyl
od	2,4-octanedionato
ODS	octadecyltrimethoxysilane
OTS	octadecyltrichlorosilane
PEALD	plasma enhanced atomic layer deposition
PMMA	poly(methyl methacrylate)
PVP	poly(vinyl pyrrolidone)
Py	pyrrolyl
QCM	quartz crystal microbalance
QMS	quadrupole mass spectrometer
RBS	Rutherford backscattering spectrometry

RT	room temperature
sccm	standard cubic centimeters per minute
SAM	self-assembled monolayer
SEM	scanning electron microscopy
SIMS	secondary ion mass spectroscopy
TGA	thermogravimetric analysis
thd	2,2,6,6-tetramethyl-3,5-heptanedionato
TMA	trimethylaluminum
TOF-ERDA	time-of-flight elastic recoil detection analysis
XPS	x-ray photoelectron spectroscopy
XRD	x-ray diffraction
XRR	x-ray reflection

1 Introduction

Thin films are thin coatings between a few nanometers up to a micrometer in thickness on a supporting material called as a substrate. They are essential building blocks in manufacturing modern devices in electronics and nanotechnology. Thin films can be made using various methods, most of which are either chemical or physical in nature.

Atomic layer deposition (ALD) was developed in the 1970s to deposit thin films chemically from a vapor phase. The films grow uniformly and conformally over large and complex areas with precise control on film thickness and excellent repeatability. These properties make ALD one of the most promising thin film deposition methods for microelectronics and nanotechnology. The importance of ALD is ever increasing as the dimensions of devices are continuously shrinking and their designs becoming more complex. This has led into a growing commercial interest in ALD grown materials and an industrially driven necessity to research and develop new ALD processes and ALD grown materials.

The first ALD grown noble metal thin films were reported in 2003 (Ref. 1) and since then the process development has been expanding because of the importance of these materials in microelectronics, catalysis and nanotechnology applications. Noble metal films have been grown by ALD mostly using combustion type reactions between noble metal precursors and molecular oxygen (O_2). The research has focused primarily on applying the deposited materials in various fields and in examining new precursors for the industrially most viable materials.

The main objective for this doctoral thesis work was to examine ALD noble metal oxide thin film growth using ozone (O_3) that is much more reactive than O_2. Noble metal oxides in general are not viewed as important as noble metals; however they can be interesting materials with intriguing combinations of properties. Primary example of this is iridium oxide which is conductive and biocompatible, and thus a candidate material for biological applications and implantable devices. Although noble metals are commonly grown by ALD, the process development for noble metal oxides has been limited. To address this,

fundamental research on capabilities of growing noble metal oxide films by ALD was examined over the course of the thesis study.

The ALD noble metal oxide growth was achieved with ozone only at deposition temperatures lower than those commonly used to deposit ALD noble metals with O_2. The noble metals are catalytic materials which resist oxidation. This means that the noble metal oxides can be reduced easily to noble metals. Indeed, the ALD noble metal oxide growth was converted to noble metal growth by adding molecular hydrogen (H_2) pulses that enabled the ALD of noble metal thin films at lower temperatures than required with O_2. In an effort to widen the selection of the ALD grown noble metals, an ALD osmium process was also introduced using the conventional O_2 chemistry.

This doctoral thesis gives a literature survey on the noble metal and noble metal oxide thin film materials grown by ALD. First, the thesis introduces how the films nucleate and grow in the oxygen-, ozone-, and reductant-based processes. Then the current status of ALD of noble metals and noble metal oxides is presented through the applied precursors. This survey includes also the processes developed during this thesis research to put them into a proper context. Particularly, the reported growth temperatures and impurity contents of the films are tabulated. Finally, the ALD processes developed during the thesis research are highlighted in more detail and the ozone-based ALD processes are compared in terms of the deposition temperature with the most common oxygen-based ALD processes.

2 Background

2.1 Noble metals

Noble metals consist from “several metallic elements that have outstanding resistance to oxidation, even at high temperatures”.[2] They are metals that “resist chemical action, do not corrode, and are not easily attacked by acids”.[3] According to the generally accepted definition the noble metals include ruthenium, osmium, rhodium, iridium, palladium, platinum, silver, and gold (Figure 1). Also rhenium, in some classifications,[2] is grouped as a noble metal because of some of its noble metal like properties. The definition of a noble metal is thus somewhat flexible. Some properties of the noble metals are presented in Table 1.

H																	He
Li	Be											B	C	N	O	F	Ne
Na	Mg											Al	Si	P	S	Cl	Ar
K	Ca	Sc	Ti	V	Cr	Mn	Fe	Co	Ni	Cu	Zn	Ga	Ge	As	Se	Br	Kr
Rb	Sr	Y	Zr	Nb	Mo	Tc	Ru	Rh	Pd	Ag	Cd	In	Sn	Sb	Te	I	Xe
Cs	Ba	57–71	Hf	Ta	W	Re	Os	Ir	Pt	Au	Hg	Tl	Pb	Bi	Po	At	Rn
Fr	Ra	89–103	Rf	Db	Sg	Bh	Hs	Mt	Ds	Rg	Cn	Uut	Fl	Uup	Lv	Uus	Uuo

Figure 1. Noble metals in the periodic table of elements. The elements in lanthanide (57–71) and actinide (89–103) groups have been omitted for clarity.

Table 1. Selected properties of the noble metals.[4]

Metal	Crystal system[5]	Density ($g\ cm^{-3}$)	Resistivity (0 °C) (μΩ cm)	Melting point (°C)
Ru	hexagonal	12.1	7.1	2333
Os	hexagonal	22.6	8.1	3033
Rh	cubic	12.4	4.3	1963
Ir	cubic	22.6	4.7	2446
Pd	cubic	12.0	9.8	1555
Pt	cubic	21.5	9.6	1768
Ag	cubic, hexagonal	10.5	1.5	962
Au	cubic	19.3	2.1	1064
Re	hexagonal	20.8	17.2	3185

The core of the noble metals, namely Ru, Os, Rh, Ir, Pd, and Pt, is also called as platinum group metals. The Encyclopaedia Britannica Online states that "the chemical behaviour of these metals is paradoxical in that they are highly resistant to attack by most chemical reagents yet, employed as catalysts, readily accelerate or control the rate of many oxidation, reduction, and hydrogenation reactions."[2] Thus these materials are catalytically very active.

2.2 Noble metal oxides

Although the noble metals are primarily known for their superior ability to resist oxidation, noble metals can be oxidized and relatively stable noble metal oxides formed. Selected properties of the noble metal oxides are summarized in Table 2. The noble metal oxides decompose, however, quite easily upon heating. Ru and Os form high oxidation state oxides (RuO_4 and OsO_4) in strongly oxidizing conditions, but these are volatile and dangerous. A curiosity among noble metal oxides is ReO_3, which has a lower resistivity than the corresponding Re metal (Table 1) and has been noted to exhibit metallic conductivity comparable even to highly conductive Ag.[6]

Table 2. Selected properties of the most common noble metal oxides.[4]

	Metal oxide	Metal valence	Density (g cm^{-3})	Melting point (°C)^{a}	Resistivity[7–13] (μΩ cm)	Crystal system[5,13]
Ru	RuO_2	+4	7.1	1300 dec.	35, 50	tetragonal
	RuO_4	+8	3.3	25 (b.p. 40)		
Os	OsO_2	+4	11.4	500 dec.	15, 60	tetragonal
	OsO_4	+8	5.1	41 (b.p. 131)		
Rh	Rh_2O_3	+3	8.2	1100 dec.	5×10^{6}	orthorhombic, trigonal
	RhO_2	+4	7.2		100	tetragonal
Ir	Ir_2O_3	+3		1000 dec.		
	IrO_2	+4	11.7	1100 dec.	$35^{[011]}$, $49^{[001]}$, 60	tetragonal
Pd	PdO	+2	8.3	750 dec.		tetragonal
Pt	PtO	+2	14.1	325 dec.		tetragonal
	PtO_2	+4	11.8	450	1×10^{12}	orthorhombic
Ag	Ag_2O	+1	7.2	~200 dec.		cubic
	AgO	+2	7.5	>100 dec.		monoclinic
	Ag_2O_2	+2	7.4	> 100		monoclinic
Au	Au_2O_3	+3		~150 dec.		orthorhombic
Re	ReO_2	+4	11.4	900 dec.	100	orthorhombic
	Re_2O_5	+5	~7			
	ReO_3	+6	6.9	400 dec.	9	cubic, hexagonal
	Re_2O_7	+7	6.1	327 (b.p. 360)		

a The boiling points of volatile higher oxidation state noble metal oxides of Ru, Os, and Re have been included in parenthesis.

2.3 Atomic layer deposition (ALD)

Atomic layer deposition (ALD)[14–16] is a thin film deposition technique using sequential and self-limiting chemical surface reactions of gaseous precursors. ALD is considered a modification of a chemical vapor deposition (CVD) method. In CVD the precursors are led into a reaction chamber simultaneously while ALD relies on the separation of the precursor pulses and the consecutive chemical reactions occurring on the surface. The ALD precursors react with the surface in a self-limiting and alternating manner, which results in a stepwise increase of matter on the surface, and by the repetition of the reaction cycle the film thickness is controlled accurately. An ALD precursor should be thermally stable to meet the self-limiting saturative behavior on a surface. By contrast CVD often includes thermal precursor decomposition in a gas phase or on a heated surface.

The following steps are performed in a full ALD cycle consisting of two precursors (Figure 2). The surface (substrate or film) is exposed to the first precursor which saturates the surface. The excess precursor and volatile by-products are purged from the reactor. The adsorbed layer of the first precursor is then exposed to and reacted with the second precursor. The volatile by-products and excess of the second precursor are purged from the reactor. By repeating these saturative steps, the film growth is self-limiting, the film thickness is controlled precisely, and the grown film is uniform and conformal. The stepwise deposition allows also tuning the film composition by various mixing possibilities. This unique control and combination of advantageous properties makes ALD an interesting and important method to grow thin films.

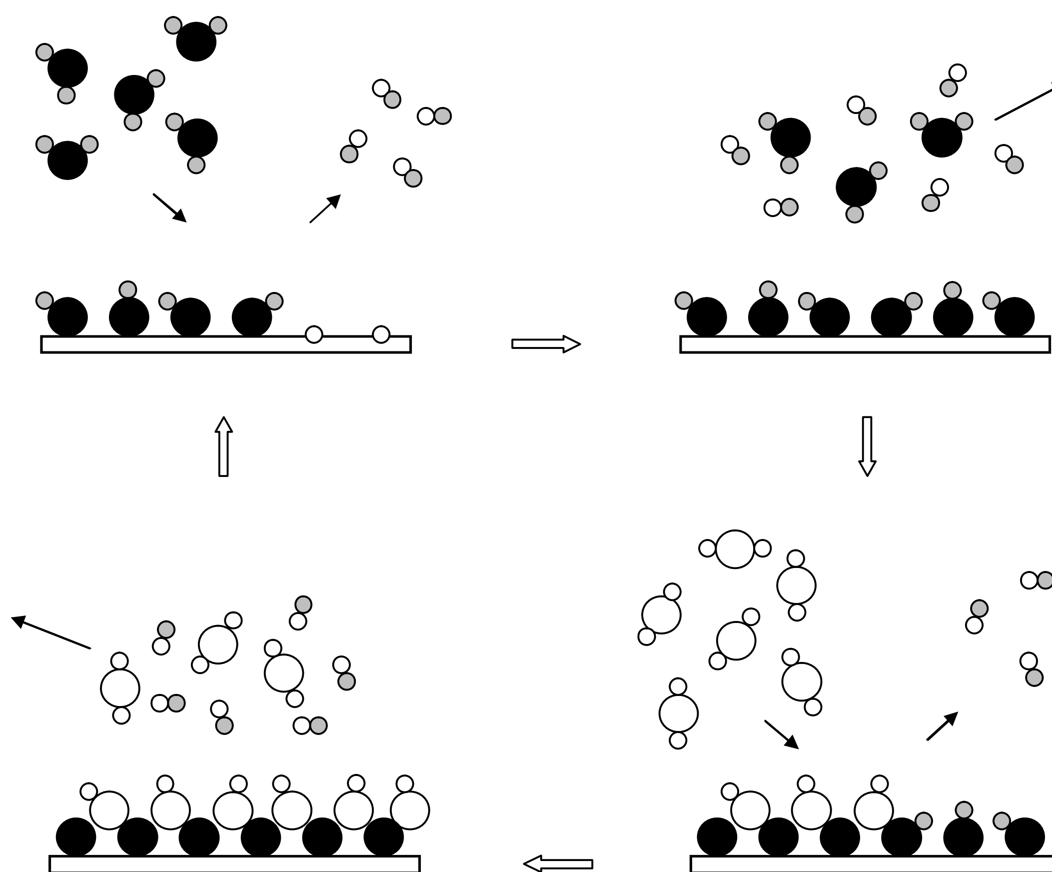

Figure 2. Simplified scheme of the ALD reaction sequence consisting of two precursors.

A large number of thin film materials can be grown by ALD.[17–19] These include oxides, sulphides, selenides, tellurides, nitrides, and fluorides but also some metals, most notably W, Cu, and noble metals. Industrial application areas and interests for ALD have been reviewed by Ritala and Niinistö.[20] Challenges related to industrial applicability of ALD have been discussed by Haukka.[21] The use of ALD for energy and environmental applications has been explored in recent reviews.[22,23] Noble metal containing materials can be used in various applications areas, such as in catalysis, semiconductors, electronics, fuel cells and batteries.[24] The rarity and particularly the cost of the noble metals make the use of thin films and nanoparticles even more crucial.

2.3.1 Thermal and plasma enhanced ALD

ALD is divided into two main subclasses depending on the activation of the reactions: thermal ALD and plasma enhanced ALD (PEALD). These vary from each other depending on how the reactants are activated to remove ligands from the adsorbed metal precursor.[21] In thermal ALD heat provides sufficient energy to facilitate the desired chemical reactions on the surface. In PEALD highly reactive species are generated from the reactant by a plasma discharge to enable growth at lower temperatures. Typical plasma source gases include H_2, NH_3, N_2, and O_2.

In thermal ALD the gaseous precursors are fed into the reactor in their molecular forms. Although all the precursors in a deposition cycle can incorporate metallic constituents to the films like in the halide–alkoxide ALD processes,[25] most often the metal precursors in thermal ALD are combined with various reactants such as H_2O, O_3, O_2, H_2S and NH_3.[17] Some reactants, like O_3, may form radical species; thus the difference of thermal ALD to the PEALD is the lack of plasma discharge despite the possible similarities in the reactant behavior.[26]

PEALD is divided further into various subclasses depending on the interaction between a plasma discharge and a substrate: direct plasma ALD, remote plasma ALD, and radical enhanced ALD.[27,28] These differ by the flux and the type of reactive species reaching the substrate. In the direct plasma ALD the substrate is positioned very close to the plasma discharge and therefore the fluxes can be very high as ions, electrons, radicals, and

photons are formed near the substrate. In the radical enhanced ALD, the substrate is located far away from the plasma generation zone and only a significantly reduced flux of radicals reaches the substrate. In the remote plasma ALD the substrate is closer to the plasma source so that plasma is present above the substrate. Thus the flux of radicals reaching the substrate is much higher than in the radical enhanced ALD while the fluxes of ions and electrons are much lower compared to the direct plasma ALD. Although the three PEALD configurations are distinct from each other, all these are referenced commonly as PEALD in this thesis. For a thorough and up-to-date summary on PEALD technology with its benefits and drawbacks, the review article by Profijt et al.[27] is highly recommended.

It is important to emphasize that the context in which the term "ALD" is used defines its meaning. ALD stands for the technique by definition, but it is also used to refer more specifically to the thermal ALD unless otherwise noted. This thesis adopts also the convention of shortening the term thermal ALD to ALD.

3 ALD of noble metals and their oxides

Thermal ALD processes for noble metals can be divided into three classes based on the reactant applied (Figure 3). The most common are O_2-based noble metal processes where deposition temperatures of 200 °C and above have been required for the film growth. Several noble metals (Ru, Os, Rh, Ir, and Pt) have been grown with O_2. Also Pd films have been deposited but with limited success. In contrast, conventional reducing agents H_2 and formalin have been successfully used in the thermal ALD of Pd (Figure 3). With these processes Pd films have been deposited below 200 °C and even as low as at 80 °C but start of the film growth can be problematic.

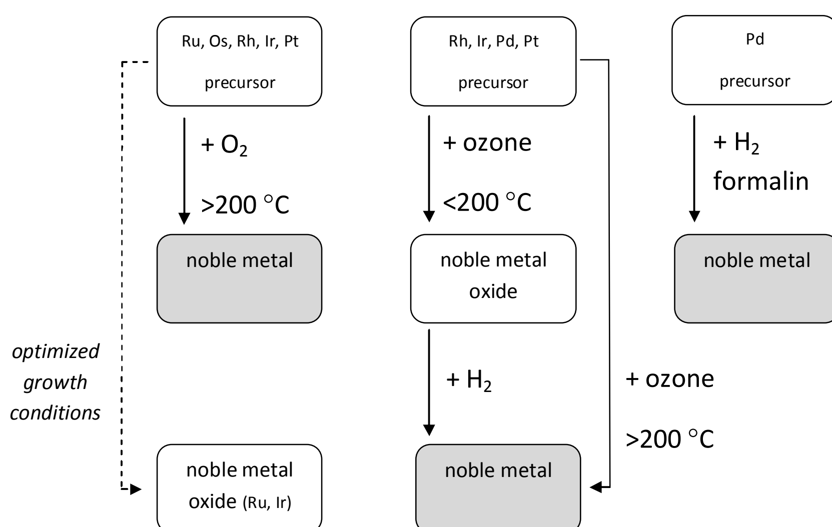

Figure 3. Simplified flowchart of the main thermal ALD processes for noble metals and their oxides.

Noble metals have been grown by thermal ALD also via noble metal oxides at deposition temperatures below 200 °C (Figure 3). Rh, Ir, and Pt metal films were deposited using ozone followed by H_2 in every growth cycle. The success in Pd growth via palladium oxide has been limited. At temperatures above 200 °C the ozone-based processes deposit metallic films also directly, without having to use H_2. In addition, ozone has been shown to be suitable for ALD of Ru as well.

Thermal ALD of noble metal oxides with ozone has been shown for Rh, Ir, Pd, and Pt (Figure 3). Rh_2O_3, IrO_2, PdO, and PtO_x films were grown only at temperatures below 200 °C. Noble metal oxides of RuO_2 and IrO_2 have been deposited also with O_2 but only at temperatures above 200 °C and using carefully optimized growth parameters.

PEALD processes for noble metals use NH_3, H_2, N_2, and O_2 plasmas (Figure 4). The films have been grown at wide deposition temperature range including very low temperatures (≥100 °C), but most often temperatures above 200 °C have been reported. The reductive NH_3 and H_2 plasmas have been mostly preferred in noble metal growth. Ag films have been grown by PEALD whereas thermal ALD of Ag films has not been successful to date.

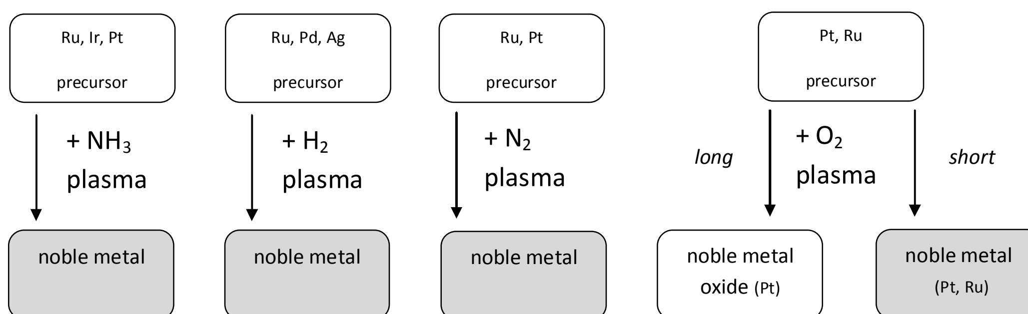

Figure 4. Simplified flowchart of the PEALD processes for noble metals and their oxides.

PEALD of noble metal oxides has been reported only for PtO_2 (Figure 4). PtO_2 films were grown with O_2 plasma at a deposition temperature range between 100 and 300 °C. Pt metal films have been grown using shorter/lower O_2 plasma exposures than required for the platinum oxide growth. O_2 plasma was used also for Ru metal film growth at 325 °C where the plasma exposure was kept short and the plasma flux low to avoid etching of the film and the formation of RuO_2.

This chapter surveys noble metal and noble metal oxide processes developed by both thermal ALD and PEALD approaches. First reaction pathways in thermal noble metal ALD processes (Figure 3) are presented through studies on reaction mechanisms (3.1). These consist of thermal ALD processes using O_2 (3.1.1), ozone (3.1.2), and conventional

reducing agents (3.1.3). Mechanistic studies on PEALD processes using O_2, NH_3, and N_2 plasmas are also introduced shortly (3.1.4). Then nucleation in thermal ALD and PEALD is briefly addressed (3.2). The rest of Chapter 3 (3.3–3.12) summarizes the developed noble metal and noble metal oxide ALD processes covering both thermal ALD and PEALD. The processes are categorized by the applied noble metal precursors and the emphasis is on the growth temperatures.

3.1 Reaction mechanisms in ALD processes of noble metals and their oxides

Reaction mechanism studies on the noble metal and noble metal oxide ALD processes provide fundamental understanding of the ALD chemistry. The reaction mechanism during the steady-state film growth has to be separated from the initial nucleation mechanism, i.e. the start of the film growth on the substrate surface. Nucleation is examined in its own chapter (3.2). In this chapter the steady-state reaction mechanisms in the main type ALD noble metal and noble metal oxide processes are summarized.

3.1.1 Oxygen-based processes

ALD noble metal processes use mostly molecular oxygen, O_2, as the reactant (Figure 5). Importantly, those noble metals that have been deposited by ALD are able to dissociate molecular oxygen catalytically in these combustion-type processes, thus making oxygen reactive. Molecular oxygen chemisorbs on the noble metal surface as atomic oxygen,[29,30] and some oxygen atoms may also diffuse into the subsurface region at least in the case of Ru.[29,30] During the noble metal precursor pulse a reaction takes place between the metal precursor and the adsorbed oxygen atoms resulting in a noble metal surface with some ligands or their fragments still remaining on the surface.[29,30] The following oxygen pulse combusts the remaining ligands and fragments, and surface oxygen atoms are replenished.[29,30]

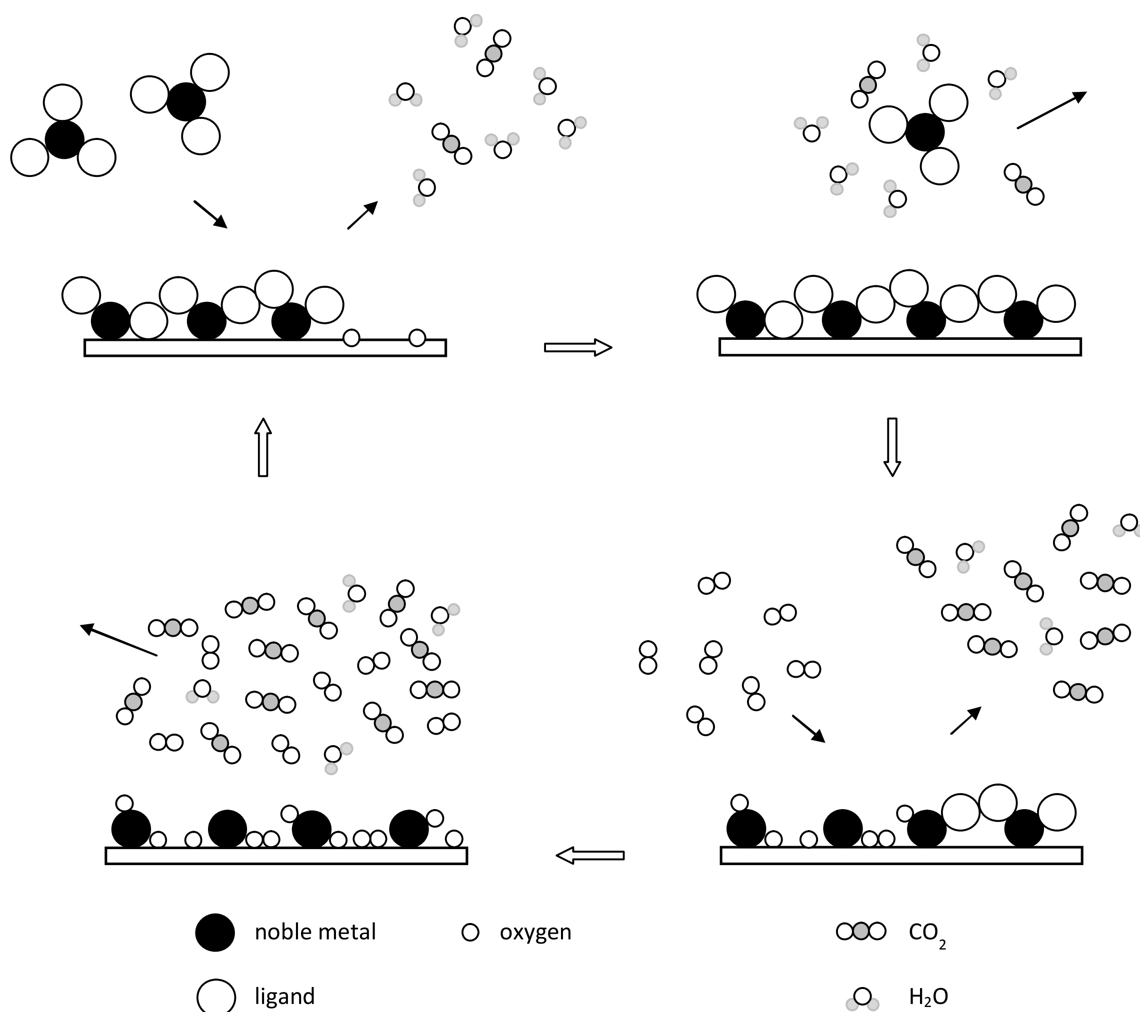

Figure 5. Simplified reactions in an oxygen-based ALD noble metal process. The surface suboxide has been omitted for clarity.

The two main reaction by-products are H_2O and CO_2 which are released during both the oxygen and noble metal precursor pulses.[29–31] Different ligands in the noble metal precursors lead to differences in reaction pathways, and thus additional reaction by-products may form.[29,31,32] As an example a β-diketonate, $Ru(thd)_3$, produces also H_2 and CO as the reaction by-products.[32] H_2 is liberated during the $Ru(thd)_3$ pulse and in a smaller degree during the following purge period while some CO is formed during the O_2 pulse.[32] $Ru(Cp)(CO)_2Et$ adsorption on the surface leads to the formation of CO and H_2 as well as CO_2 and H_2O.[33] H_2O is released only during the $Ru(Cp)(CO)_2Et$ pulse, not during the oxygen pulse when CO_2 and CO are formed.[33] The formation of CO can not be ruled out

in the metallocene, $RuCp_2$, based ALD Ru process either, especially during the $RuCp_2$ pulse under oxygen deficient conditions.[29]

In the $MeCpPtMe_3$–O_2 ALD process for Pt, methane (CH_4) forms as a by-product during the $MeCpPtMe_3$ pulse in amounts higher or comparable to CO_2.[31,34] The ratio of CH_4 to CO_2 increases with longer $MeCpPtMe_3$ pulses, which was assumed to result from the excess $MeCpPtMe_3$ reacting with the reaction products, such as H_2O directly or –OH surface species.[31] The reaction mechanism studies on the ALD Pt process have not revealed CO by-product but it should be noted that already at very low Pt nanoparticle loading levels, Pt exhibits near 100 % conversion of CO to CO_2 at temperatures between 150 and 250 °C.[35]

The formation of CH_4 and CO reaction by-products in the $MeCpPtMe_3$–O_2 process can be explained alternatively by dehydrogenation reactions during the noble metal precursor pulse, in particular after the oxygen has become consumed from the surface.[36] Hydrogen atoms become available on the catalytic Pt surface once dehydrogenation reactions of $MeCpPtMe_3$ ligands occur and hydrogenate some methyl (Me) ligands to CH_4. Also other reaction products, e.g. ethane, cyclopentene, cyclopentane, and benzene may be formed and the adsorbed hydrogen atoms can recombine to H_2. Upon the decrease of surface oxygen concentration CO starts to form because of the incomplete combustion.[36] In the $MeCpPtMe_3$–O_2 process the dominant reaction pathway during the $MeCpPtMe_3$ pulse is still the ligand combustion by the surface oxygen to CO_2. But as $MeCpPtMe_3$ decomposes on the catalytic Pt surface by the dehydrogenation reactions, a carbonaceous layer forms that restricts further adsorption and decomposition of $MeCpPtMe_3$.[36] Thus the carbonaceous layer saturates the surface by poisoning and is eliminated only by combustion during the following O_2 pulse. Deposition temperatures higher than 200 °C are needed to remove the carbonaceous layer by molecular oxygen efficiently while stronger oxidizing agents, such as O_2 plasma and ozone, are effective at lower temperatures.[36] During the O_2 pulse the combustion of carbonaceous layer is instantaneous above 250 °C whereas the rate of combustion decreases with decreasing temperature down to 100 °C where no Pt growth occurs.[37] The dissociation of O_2 on the surface and the combustion of the carbonaceous layer are thus determined by the extent of fragmentation of the ligands by dehydrogenation reactions in the carbonaceous layer.[37] Also the

$Ru(Cp)(CO)_2Et–O_2$ ALD Ru process has shown dehydrogenation reactions during the Ru precursor pulse and the formation of carbonaceous surface layer which consists of about 30 % of the carbon atoms in the precursor.[33]

The solvent used in liquid injection ALD (LIALD) to dissolve the noble metal precursor can play a role in the reaction mechanism as in the ALD of Ru using molecular oxygen and $Ru(thd)_3$ dissolved in ethylcyclohexane (ECH).[38,39] During the noble metal precursor pulse both $Ru(thd)_3$ and ECH react with the surface oxygen atoms.[38] Because ECH oxidizes more easily, a lower concentration of $Ru(thd)_3$ dissolved in ECH results in a lower Ru film growth rate.[38] This means that the effect of the solvent can not be ignored in the deposition of noble metals by LIALD.

It has also been suggested that large O_2 flows lead to a formation of a large number of subsurface oxygen atoms.[40] This can result in incomplete oxygen consumption during the following Ru precursor pulse and the growth of RuO_2. Also, the number of subsurface oxygen atoms becomes larger at higher growth temperatures, which may lead to the formation of a ruthenium oxide phase.[40] Although ALD proceeds through saturative chemical reactions on the surface, the deposition parameters, such as temperature, precursor dose and partial pressure, may nevertheless have an impact on the film growth.

3.1.2 Ozone-based processes

$Ir(acac)_3–O_3–H_2$ and $Ir(acac)_3–O_3$ pulsing sequences have been examined with a quadrupole mass spectrometer (QMS) and a quartz crystal microbalance (QCM) to reveal the reaction mechanisms in the ozone-based ALD processes of Ir and IrO_2.[30] With these processes the Ir and IrO_2 film growth is achieved at lower temperatures (165–200 °C) compared to the corresponding oxygen-based ALD Ir process (225–375 °C).[I,IV,41] An important distinction between the ozone-based processes and the $Ir(acac)_3–O_2$ process is that in the former $Ir(acac)_3$ adsorbs on the surface stoichiometrically (molecularly or dissociatively) rather than reactively.[30] Figure 6 visualizes the difference between the reactive and stoichiometric adsorption of the noble metal precursor in the oxygen- and ozone-based processes.

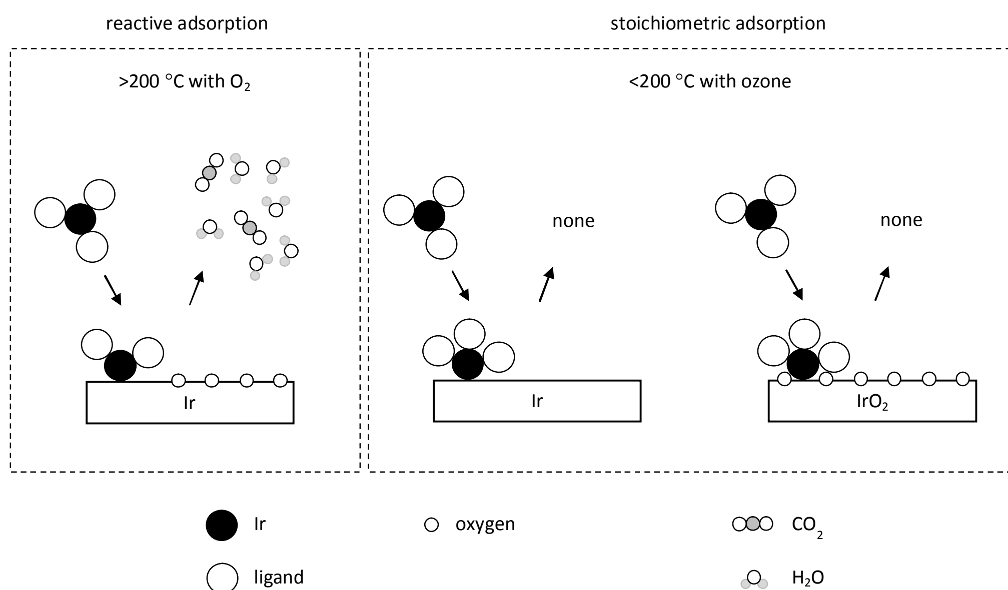

Figure 6. Adsorption of $Ir(acac)_3$ precursor on a surface in oxygen and ozone-based ALD processes.

The only byproducts detected in the ozone-based processes at 195 °C are CO_2 and H_2O similar to the corresponding oxygen-based process.[30] In the $Ir(acac)_3$–O_3–H_2 ALD process of Ir CO_2 is detected only during the O_3 pulse while H_2O is detected during both the O_3 and the H_2 pulses. In comparison, in the ALD IrO_2 process [$Ir(acac)_3$–O_3] the byproducts are released only during the O_3 pulse. The oxygen atoms in the IrO_2 are thus not oxidative toward the acac ligands at 195 °C and are thereby different from the reactive oxygen atoms on the Ir surface above 225 °C in the $Ir(acac)_3$–O_2 process.[30] Therefore, at low deposition temperatures (<200 °C) iridium oxide forms instead of an iridium metal film.

3.1.3 Reductant-based processes

The reductive noble metal ALD chemistry, i.e. using a true reducing agent, has so far been limited to ALD growth of Pd. The reaction mechanism in ALD of Pd using $Pd(hfac)_2$ and formalin (37% solution of formaldehyde, HCOH, in water with 10–15% methanol) has been examined by QCM.[42] $Pd(hfac)_2$ reacts with the H-terminated Pd surface and releases some of its ligands as Hhfac. The following HCOH pulse reacts with the hfac-terminated Pd surface and decomposes into atomic H and CO. The resulting atomic H reacts with the

Pd-hfac species to release the remaining hfac ligands from the surface and regenerates the H-terminated starting surface for the next Pd(hfac)$_2$ pulse. Thus the role of the HCOH is to serve as a H atom source in the process.[42]

There is a similarity between the reductive Pd(hfac)$_2$–formalin and the oxidative oxygen-based ALD noble metal processes: in the reductive process atomic H is needed to release part of the ligands during the metal precursor pulse while in the oxidative process atomic O combusts the ligands partly on the surface (Figure 7). Likewise, the remaining ligands are eliminated during the reactant pulse by dissociating the reactant to an atomic form on the catalytic surface, and some reactant remains on the surface in the atomic form to react with the following noble metal precursor pulse. However, the reductive pathway proceeds by eliminating the ligands intact in protonated form instead of combusting them to smaller molecules (CO_2 and H_2O) in the oxygen-based processes. The reductive pathway seems to be unique to Pd and has so far been demonstrated to proceed only with a fluorinated metal precursor.

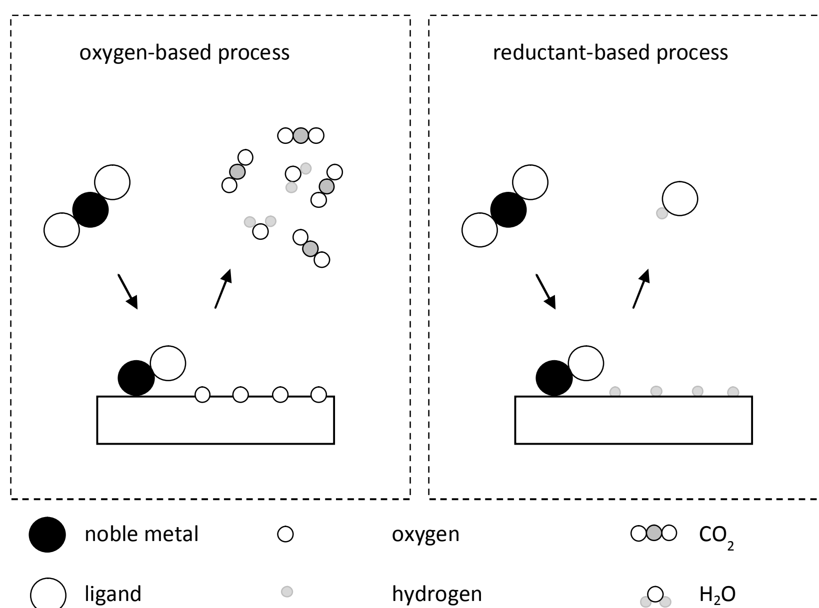

Figure 7. Adsorption of noble metal precursors on surfaces in oxygen and reductant-based ALD processes.

3.1.4 Plasma-based processes

Reaction mechanisms in PEALD noble metal processes have not yet been examined in detail. This is most likely because of the complexity of the overall reactions occurring during the plasma pulse and the difficulty in analyzing them. Still, some insight on reaction mechanism in the plasma-based processes has been obtained recently using in-situ mass spectrometry and optical emission spectroscopy.[43]

The $MeCpPtMe_3$–O_2 plasma PEALD process was examined at 250 °C. Because oxygen atoms are present in the O_2 plasma the reaction mechanism was expected to follow the combustion-type reactions similar to the thermal ALD $MeCpPtMe_3$–O_2 process.[43] This means that oxygen atoms are left on the surface after the O_2 plasma pulse and react with the $MeCpPtMe_3$ during the following noble metal precursor pulse (Figure 8). Also dehydrogenation reactions take place during the $MeCpPtMe_3$ pulse and the detected reaction byproducts are CO_2, H_2O, and CH_4 similar to the thermal $MeCpPtMe_3$–O_2 process. Likewise, CO_2 and H_2O byproducts are formed during the O_2 plasma pulse.[43]

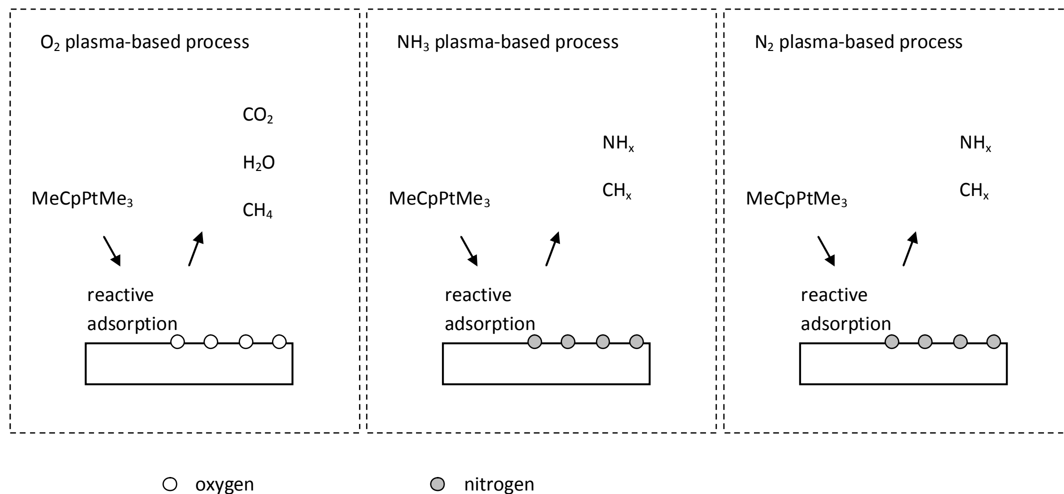

Figure 8. Adsorption of $MeCpPtMe_3$ precursor on a surface in O_2, NH_3, and N_2 plasma-based PEALD processes at 250 °C.

Longrie et al.[43] have examined also the $MeCpPtMe_3$–NH_3 plasma and $MeCpPtMe_3$–N_2 plasma PEALD processes at 250 °C and some conclusions on the reaction mechanisms were drawn from in-situ mass spectrometry measurements. During the plasma pulse

radical plasma species eliminate the precursor ligands, and NH_x and CH_x byproducts are detected. Notably nitrogen atoms are bound to the surface after the NH_3 and N_2 plasma pulses and react with $MeCpPtMe_3$ during the following noble metal precursor pulse (Figure 8). The adsorbed nitrogen atoms are not, however, stably bound on the Pt surface and can also desorb from the surface.[43] As a consequence, when the pumping time (purge) was increased from 15 to 45 s, the growth rates in the $MeCpPtMe_3$–NH_3 plasma and $MeCpPtMe_3$–N_2 plasma processes decreased drastically from 0.4 and 0.3 Å/cycle to 0.2 Å/cycle and almost zero, respectively.[43] It should be emphasized that the similar increase in purges did not influence the growth rate in the $MeCpPtMe_3$–O_2 plasma process at the same temperature.[43] This means that the oxygen atoms on the Pt surface are more stable compared to the nitrogen atoms.

3.2 Nucleation in ALD of noble metals and their oxides

In most ALD processes, like those of metal oxides, uniform film growth starts already after the first few deposition cycles. The processes exhibit either negligible or very short nucleation delays when the starting surface contains suitable functional groups as reactive sites for either of the precursors used. Thus the nucleation and continuous film growth is quite trivial when a compatible surface offers proper surface species for the precursor to react with.

In the ALD of noble metals, by contrast, the start of the film growth, nucleation to be more precise, is more problematic and therefore a fundamental issue. The formation of the noble metal nuclei is crucial for the growth of the noble metal film and for the resulting film properties, such as morphology and surface roughness. In general, the start of the film growth is affected by a nucleation delay which has been found pronouncedly present especially in the oxygen-based ALD Ru and Os processes. In some ALD Ru processes, for example, long nucleation delays up to hundreds of cycles have been observed while the ALD Os process[VIII] has shown a nucleation delay of about 350 cycles. It should be emphasized that with a few exceptions all the noble metal ALD processes, in some degree, show delayed nucleation.

The growth of ALD noble metals starts with a formation of nanoparticles as nuclei. During the following growth cycles these nanoparticles grow in size and additional nuclei appear on the surface. The nanoparticles then coalesce to islands and finally form a continuous film on which the growth continues at a constant growth per cycle rate during the following steady-state growth. The initial nucleation density of the noble metal plays a critical role in the formation of metallic films as a high nucleation density results in a low nucleation delay and ensures faster formation of a continuous noble metal layer with smoother surface than obtained with low nucleation density.

Reaction mechanisms during the nucleation differ from those during the steady-state growth. During the steady-state growth similar reactions occur between the precursors and the species on the film surface in every ALD cycle. By contrast, the initial nucleation of noble metal on various surfaces is a complex and poorly understood issue. The common oxygen-based ALD noble metal processes, for example, rely on the noble metal surface to dissociate molecular oxygen catalytically to atomic oxygen for the growth to proceed. The problem during the initial nucleation period is thus how the noble metal precursor can react with the surface when atomic oxygen is not available for partial ligand combustion and, vice versa, how molecular oxygen dissociates into reactive surface atomic oxygen without catalytically active noble metal. It has been suggested that the first metallic nuclei are most likely formed by some minor decomposition of the noble metal precursor and these nuclei then catalyze further the growth of the noble metal.[17]

Nucleation can be improved using precursors that have active adsorption properties towards the surface as in the ALD Ru growth using 2,4-(dimethylpentadienyl) (ethylcyclopentadienyl)Ru [(EtCp)Ru(DMPD)] precursor.[44] In general, the functionalization of the precursors and their ligands can improve the nucleation properties and thus decrease the nucleation delay. For example, the cyclopentadienyl ligand is considered highly stable and when one of the cyclopentadienyl ligands (EtCp) from a metallocene is opened, as in the (EtCp)Ru(DMPD), the precursor becomes more reactive towards surface sites.[21] Also feeding the noble metal precursor twice in one cycle can be used to increase the nucleation density by enhancing the surface saturation by the absorbed precursor.[45]

As for the reactant, longer air/oxygen pulses decrease the nucleation delay by enhancing the growth during the initial cycles.[46] The O_2 pressure also affects the ALD noble metal nucleation. Using pure oxygen instead of air decreases the low temperature limit of the ALD process and increases the nucleation density thus resulting in smoother films with improved adhesion properties.[47] Low O_2 pressure (0.02 Torr) has been shown to result in extremely long Pt nucleation delays on Al_2O_3 but on Pt surfaces ALD Pt films can still be readily grown.[48] Hence, the growth of ALD Pt can be inhibited even on ALD Al_2O_3 at 300 °C when the O_2 pressure is carefully chosen.[48] The use of short $MeCpPtMe_3$ pulses in the unsaturated growth regime has been shown to lead to discontinuous Pt islands as the growth occurs preferentially on the pre-existing Pt islands.[49] $MeCpPtMe_3$ overexposures, on the other hand, can be used to control the Pt nanoparticle size on silica gel particles in a fluidized bed reactor at 320 °C, where partial thermal decomposition of $MeCpPtMe_3$ may occur.[50]

Several other factors such as growth temperature,[44,46,51] substrate,[47,51–60] precursor selection,[44,61] and ALD process parameters have also been found to affect the delay in nucleation. Various surface pretreatments, such as UV-ozone, oxygen plasma, argon plasma, and acid treatments, can improve or alter the nucleation of the ALD noble metals.[62–67] For example, surface carbon contamination can limit the adsorption of the noble metal precursor.[66] On carbon nanotubes the Ar and O_2 plasma treatments have been found to either prohibit ALD Pt growth (Ar plasma) or to result in worse film uniformity compared to the non-treated sample,[68] whereas on TiN the in-situ Ar plasma treatment decreases the nucleation delay in ALD Ru growth.[69] On carbon nanotubes trimethylaluminum (TMA) exposures, on the other hand, lead to an improvement in uniformity of Pt coverage.[68]

The nucleation and growth of noble metals by ALD can be prevented completely with polymer mask layers like poly(methyl methacrylate) (PMMA) and poly(vinyl pyrrolidone) (PVP),[70,71] and with SAMs (self-assembled monolayers) of octadecyltrimethoxysilane (ODS) and octadecyltrichlorosilane (OTS).[72–75] Patterning surfaces with these layers which protect the surface against ALD film growth leads to a selective-area ALD.[76] On the other hand, as the nucleation of noble metals is often limited on some surfaces, film growth can be also activated on selected areas by patterning with layers which promote

film nucleation,[76] like RuO_x for selective-area ALD of Ru.[77] In this case the oxygen in RuO_x is reactive towards $RuCp_2$ allowing Ru ALD at 250 °C where no growth occurs on Si.

Nucleation is crucial also for making noble metal catalysts by ALD as e.g. dispersion, density and size of the noble metal particles affect the activity of the catalysts.[78–83] Pretreatment of the substrate with acetylacetone (Hacac) before noble metal precursors, e.g. $Ir(acac)_3$ and $Pt(acac)_2$, leads to a reduction of the nucleation density, i.e. the noble metal content, in the catalyst.[84–86] The effectiveness of Hacac in blocking the growth is however influenced by the underlying substrate.[86] The size of the metal precursor molecule, and hence steric effects, also determine the catalyst loading on the substrate.[85,86] Recent progress in the growth of noble metal catalysts by ALD has been reviewed by Lu et al.[87]

The effect of the underlying surface on the Pd nucleation and growth in the $Pd(hfac)_2$–formalin reductive ALD chemistry has been studied.[88] The nucleation difficulties in ALD of Pd are linked to surface poisoning by the reaction byproducts,[89,90] where Hhfac formed from $Pd(hfac)_2$ readsorbs to the Al_2O_3 surface and forms passivating Al(hfac) and Al(tfa) surface species that are difficult to remove by the following formalin pulse.[90] TMA was shown to be useful in removing the surface poisoning and enhancing nucleation on Al_2O_3 surfaces.[89] A number of approaches for accelerating the nucleation of ALD Pd have been examined, including ozone treatment, performing the formalin exposures at a higher temperature (300 °C), longer formalin exposures, longer N_2 purging times, and combinations of these.[88] Only longer formalin exposures enhanced significantly Pd nucleation rate which was suggested to originate from the removal of the hfac ligands bound to the Al_2O_3 substrate.[88] In a fluidized bed reactor at 200 °C, in addition, a prolonged $Pd(hfac)_2$ exposure can further increase the Pd content on Al_2O_3;[91] however long, 6–14 min, $Pd(hfac)_2$ pulses and up to 20 deposition cycles were used to deposit Pd nanoparticles by ALD.

The nucleation differs also between the oxygen-based thermal ALD and NH_3 plasma based PEALD processes as exemplified with $Ru(EtCp)_2$ and $RuCp_2$ precursors.[92,93] The PEALD Ru has shown minimal nucleation delay on Si and SiO_2 surfaces while thermal

ALD results in a lack of a film on Si and unreliable growth on SiO_2.[93] The radicals formed in the NH_3 plasma are able to remove ligands from the adsorbed metal precursor which leads to an improved nucleation and almost substrate independent constant growth rate in contrast to the O_2-based ALD.[93] Interestingly, NH_3 and H_2 plasmas may still result in large differences in nucleation delay: e.g. PEALD of Ru using $Ru(EtCp)_2$ and NH_3 plasma at 330 °C has shown very large nucleation delays of over 500 cycles on TiN compared to $Ru(EtCp)_2$–H_2 plasma (~120 cycles).[94,95] On SiO_2 the nucleation delay with the $Ru(EtCp)_2$–NH_3 plasma is considerably shorter than on TiN while with the $Ru(EtCp)_2$–H_2 plasma the nucleation delay somewhat increases.[95] In contrast, the (MeCp)Ru(Py)–NH_3 plasma and (MeCp)Ru(Py)–H_2 plasma Ru PEALD processes have both shown delays less than 10 cycles on TiN.[94,95] Also the nucleation in the Pt PEALD process with O_2 plasma has been examined on Al_2O_3.[96] The PEALD Pt did not nucleate and grow immediately on Al_2O_3 as linear steady state growth was achieved only after 50 cycles.[96] These examples show that although PEALD processes have relatively short nucleation delays, nucleation can still be an issue also in the PEALD of noble metals.

3.3 Ruthenium

Ruthenium is one of the most attractive noble metals in respect of cost and physical properties; therefore a substantial number of ALD Ru precursors has been introduced and explored (Figure 9). Molecular O_2 is used most often as the other reactant in thermal ALD while PEALD Ru processes rely on the use of NH_3 and H_2 plasmas. In thermal ALD molecular H_2 and NH_3 reactants have been applied in lesser extent with precursors which are very reactive or have quite low thermal stability. Table 3 summarizes the ALD and PEALD Ru processes with their deposition temperatures and growth rates. The reported film impurities are found in Table 4.

Table 3. ALD and PEALD Ru processes reported in the literature.

Metal precursor		$T_{vap.}$ (°C)	Reactant	$T_{dep.}$ (°C)	Growth rate (Å $cycle^{-1}$)	Ref.
$RuCp_2$		50	O_2 (air)	275–400	$0.1^{275°C}$, $0.3^{300°C}$, $0.4^{325-375°C}$, $0.5^{400°C}$	51
$RuCp_2$		60	O_2	225–275	$0.1^{225°C}$, $0.3^{250°C}$, $0.4^{275°C}$	47
$RuCp_2$		80	O_2	245	0.2–0.3	108
$RuCp_2$			O_2 (air)	250	0.2	77
$RuCp_2$			O_2	270	0.5	217
$RuCp_2$		50	O_2	275	1	58
$RuCp_2$		80	O_2	310–350	1	58,74
$RuCp_2$		85	O_2	300,350	$1.2^{300°C}$	93,112
$RuCp_2$	PEALD	85	NH_3 plasma	300	0.9	93
$Ru(EtCp)_2$		80	O_2	270	0.7, 1.5	109,116
$Ru(EtCp)_2$		80	O_2	270	1.0	111
$Ru(EtCp)_2$			O_2	300	0.4	110
$Ru(EtCp)_2$		80	O_2	300	0.5	59
$Ru(EtCp)_2$		65	O_2	300	1.8	40,93
$Ru(EtCp)_2$			ozone	225–275	$0.9^{225°C}$, $1.1^{250°C}$, $1.2^{275°C}$	113
$Ru(EtCp)_2$	PEALD	80	NH_3 plasma	100–270	0.2	118
$Ru(EtCp)_2$	PEALD	80	NH_3 plasma	270	0.4	92,115,116
$Ru(EtCp)_2$	PEALD	90	NH_3 plasma	270		119
$Ru(EtCp)_2$	PEALD	90	NH_3 plasma	290,300	0.3–0.4	45
$Ru(EtCp)_2$	PEALD	65	NH_3 plasma	300	0.8	93
$Ru(EtCp)_2$	PEALD	50	NH_3 plasma	330	0.2	94,95
$Ru(EtCp)_2$	PEALD	60	NH_3 plasma	350	0.5	117
$Ru(EtCp)_2$	PEALD	75	H_2 plasma	200	0.3	120
$Ru(EtCp)_2$	PEALD	50	H_2 plasma	330	0.2	94,95
$Ru(EtCp)_2$	PEALD	75	H_2/N_2 plasma	200	0.4	120
$Ru(EtCp)_2$	PEALD	80	H_2/N_2 plasma	200	0.4	104
(EtCp)Ru(MeCp)		45	O_2	250–325	$0.2–0.3^{250°C}$, $0.4–0.5^{275-300°C}$	53
$(Me_2NEtCp)RuCp$		75–80	O_2 (air)	325–500	$0.2^{325-350°C}$, $0.4^{375°C}$, $0.5^{400-450°C}$, $0.8^{500°C}$	46
(EtCp)Ru(DMPD)			O_2	250	0.4	66
(EtCp)Ru(DMPD) in ECH			O_2	210–290	$0.2^{210°C}$, $0.3–0.4^{230°C}$, $0.4–0.5^{250°C}$, $0.3–0.5^{290°C}$	122
(EtCp)Ru(DMPD) in ECH		200	O_2	230–280	$0.4^{225-250°C}$, $0.5^{280°C}$	61
(EtCp)Ru(DMPD) in ECH			O_2	250	0.3	69
(EtCp)Ru(DMPD) in ECH		230	O_2	280	0.5	121
$Ru(DMPD)_2$		82	O_2	325	0.6	124
$Ru(DMPD)_2$	PEALD	82	N_2 plasma	325	0.3	124

(EtCp)Ru(Py)		55	O_2	275–350	$0.3–0.5^{275°C}$, $0.2–0.4^{300°C}$, $0.4–0.6^{325°C}$, $0.5–0.6^{350°C}$	125
(MeCp)Ru(Py)			O_2	NA	0.4–0.6	126
(MeCp)Ru(Py)		80	NH_3 plasma	330	0.4	94,95
(MeCp)Ru(Py)		80	H_2 plasma	330	0.3	94,95
$Ru(Me_2Py)_2$		55–60	O_2	250–325	$0.2^{250°C}$, $0.6^{300°C}$	127
$Ru(Cp)(CO)_2Et$		85	O_2	200–325	$0.8–0.9^{300°C}$	128
$Ru(Cp)(CO)_2Et$		90	O_2	325	1.0	33
$Ru(Cp)(CO)_2Et$		90	O_2	325	1.0	130
$Ru(Cp)(CO)_2Et$	PEALD	90	O_2 plasma	325	1.1	130
$Ru(thd)_3$		100	O_2 (air)	325–450	$0.3^{325°C}$, $0.4^{350–400°C}$, $0.5^{450°C}$	32
$Ru(thd)_3$		100	O_2	250, 325	$0.2^{250°C}$, $0.4^{325°C}$	47
$Ru(thd)_3$ in ECH			O_2	330, 380	$0.3^{380°C}$	38,39
$Ru(od)_3$/n-butylacetate solution		200	O_2	275–450	$0.6^{275–300°C}$, $0.8^{325–375°C}$, $1.0^{400°C}$, $1.8^{425°C}$, $2.0^{450°C}$	138
(^{i}Pr-Me-Be)Ru(CHD)		120	O_2	185–310	$0.6^{185°C}$, $0.8^{200°C}$, $0.9^{225–270°C}$, $1.3^{310°C}$	140
(^{i}Pr-Me-Be)Ru(CHD)		100	O_2	220	0.9–1.0	139
(^{i}Pr-Me-Be)Ru(CHD)		120	O_2	225	0.8	105
(^{i}Pr-Me-Be)Ru(CHD)		100	O_2	140–350	0.9^{NA}	141
(Et-Be)Ru(CHD)		100	O_2	140–350	0.9^{NA}	141
(Et-Be)Ru(Et-CHD)		100	O_2	140–350	$0.4^{225°C}$	141
(^{i}Pr-Me-Be)Ru(CHD)	PEALD	100	NH_3 plasma	140–400	$0.6^{140°C}$, $0.8^{185°C}$, $0.9^{225–400°C}$	142
(^{i}Pr-Me-Be)Ru(CHD)	PEALD	100	NH_3 plasma	270	1.0	144
(^{i}Pr-Me-Be)Ru(CHD)	PEALD	100	H_2/N_2 plasma	270	0.6	143
$Ru(Me\text{-}Me_2\text{-}CHD)_2$		60	O_2	200–325	$0.1^{200°C}$, $0.3^{235°C}$, $0.5^{250–310°C}$, $0.2^{325°C}$	145
$Ru(Me\text{-}Me_2\text{-}CHD)_2$		60	O_2	NA	0.5	146
$Ru(CO)_3$(CHD)			NH_3	200	3.5–4	147
$Ru(^tBu\text{-}Me\text{-}amd)_2(CO)_2$		140	O_2	300–400	$0.5^{300°C}$, $1.0^{325°C}$, $1.5^{350°C}$, $1.7^{400°C}$	149
$Ru(^tBu\text{-}Me\text{-}amd)_2(CO)_2$		130	NH_3	200–300	$0.08^{250°C; 0.06 CVD}$, $0.3^{280°C; 0.15 CVD}$, $0.7^{300 °C; 0.4 CVD}$	150
ToRuS		3	5 % H_2	230		152
ToRuS		RT	H_2	100–200	$1.3^{100–175°C}$, $1.4^{200–225°C}$, $1.5^{250°C}$	153
ToRuS		25	H_2	>150, >200	1.8^{NA}	151
ToRuS	PEALD	RT	H_2 plasma	100, 200	1.1	153

Abbreviation NA denotes “not available”.

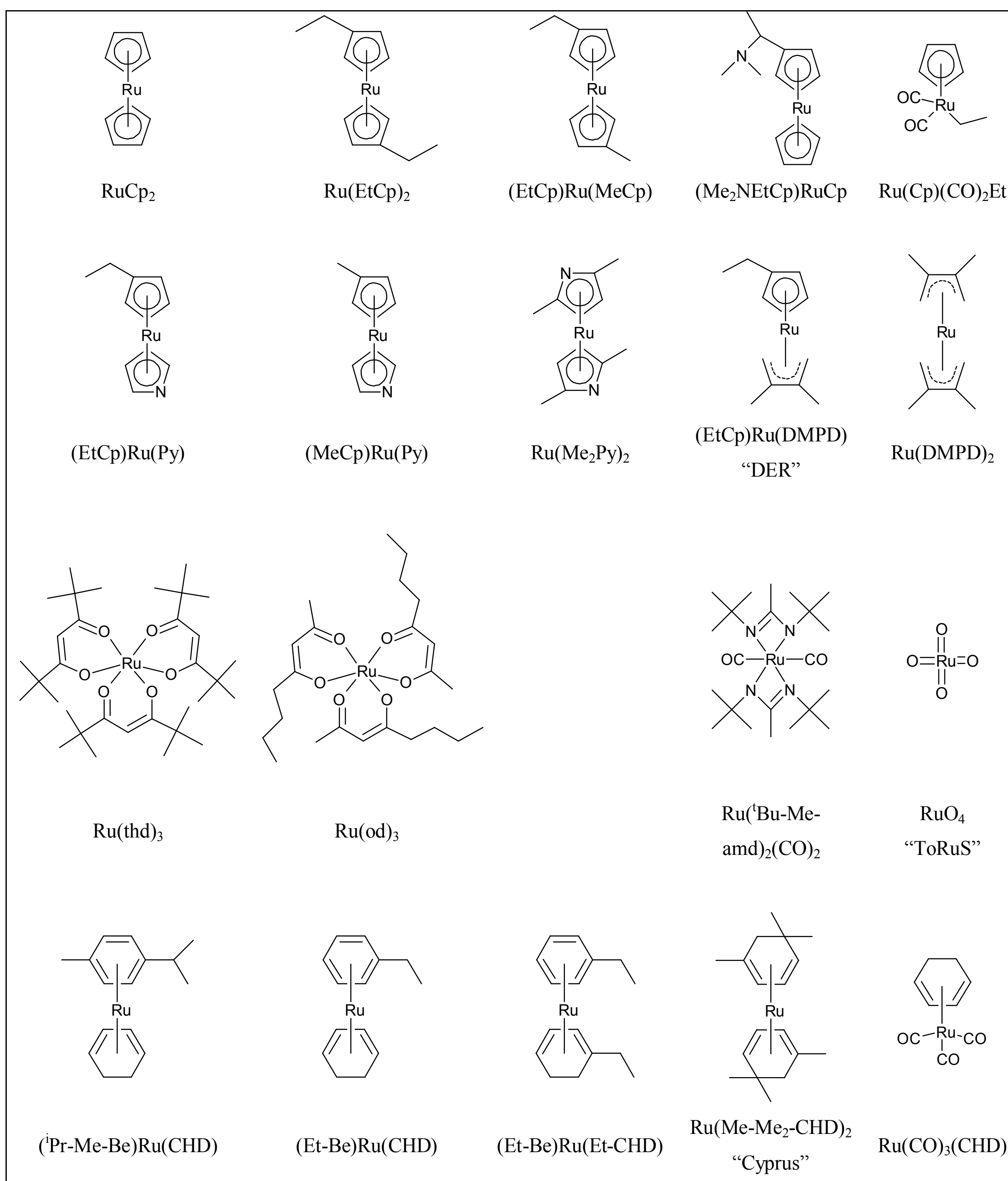

Figure 9. Ruthenium precursors reported for ALD and PEALD Ru processes.

Table 4. Impurity contents of ALD and PEALD Ru processes.

Cycle sequence	$T_{dep.}$ (°C)	Impurity contents (at.%)	Method	Ref.
$Ru(Cp)_2$–O_2 (air)	300	O <1.5, C <0.3, H <0.4	TOF-ERDA	51
	350	O <0.4, C <0.2, H <0.2	TOF-ERDA	51
	400	O <0.5, C <0.3, H <0.2	TOF-ERDA	51
$Ru(Cp)_2$–O_2	245	O in surface and in film	AES	108
$RuCp_2$–NH_3 plasma	300	C <XPS limit, N <XPS limit	XPS	93
$Ru(EtCp)_2$–O_2	270	O <2, C <2	TOF-ERDA, AES	109
$Ru(EtCp)_2$–ozone	275	O <1	AES	113
$Ru(EtCp)_2$–NH_3 plasma	270	C, O, N <TOF-ERDA limit	TOF-ERDA	115
$Ru(EtCp)_2$–NH_3 plasma	270	O $1.4^{\text{plasma power 150W}}$, O 1.8^{100W},O 16.6^{20W}	RBS	119
$Ru(EtCp)_2$–NH_3 plasma	270	O ~2, C <XPS limit, N <XPS limit	XPS	118
$Ru(EtCp)_2$–NH_3 plasma	300	C <XPS limit, N <XPS limit	XPS	93
(EtCp)Ru(DMPD) in ECH–O_2	250, 280	O <AES limit	AES	61
(EtCp)Ru(DMPD) in ECH–O_2	280	negligible O and C	XPS	121
$Ru(DMPD)_2$–O_2	325	O <1, C <0.2, N <0.2	SIMS	124
$Ru(DMPD)_2$–N_2 plasma	325	O <1, C <0.5, N <0.5	SIMS	124
(EtCp)Ru(Py)–O_2	275	O <2, C 0.6, H 2, N 0.5	TOF-ERDA	125
(MeCp)Ru(Py)–O_2	NA	O 10, C <1.3, H <2	ERDA	126
$Ru(Me_2Py)_2$–O_2	275	O 3.6, C 1.6, H 3, N 1.2	TOF-ERDA	127
$Ru(thd)_3$–O_2 (air)	350	O 4.1, C 1.2, H 2.2	TOF-ERDA	32
$Ru(thd)_3$ in ECH–O_2	380	O <1	SIMS	38
(^{i}Pr-Me-Be)Ru(CHD)–O_2	220	O ~4	XPS	139
(^{i}Pr-Me-Be)Ru(CHD)–O_2	225	O <SIMS limit, C ~1.8	SIMS	105
(^{i}Pr-Me-Be)Ru(CHD)–O_2	270	O <SIMS limit, C <SIMS limit	SIMS	140
(^{i}Pr-Me-Be)Ru(CHD)–O_2	310	O <SIMS limit, C ~2.4	SIMS	140
(^{i}Pr-Me-Be)Ru(CHD)–NH_3 plasma	225	O <AES limit, N <AES limit	AES	142
(^{i}Pr-Me-Be)Ru(CHD)–H_2/N_2 plasma	270	C 1.5, N <0.5	RBS	143
Ru(^{t}Bu-Me-amd)$_2$(CO)$_2$–O_2	NA	O 0.3, C 0.3	APM	149
Ru(^{t}Bu-Me-amd)$_2$(CO)$_2$–NH_3	300	O ~0.2%, C ~0.05%	SIMS	150
Ru(^{t}Bu-Me-amd)$_2$(CO)$_2$–NH_3	NA	O, C, N <RBS limit	RBS	150
ToRuS– 5% H_2	230	O 1–2	AES	152
ToRuS–H_2	100, 200	O 3, C 0.5–1, H <1, N <1	ERDA	153
ToRuS–H_2	250	O <AES limit, C <AES limit	AES	151

Thermal ALD and PEALD Ru thin films have been examined for many applications. The use of Ru as adhesion, seed and diffusion barrier layers for Cu metallization has been studied extensively.[97–102] Ruthenium is also an interesting electrode material for DRAM capacitor structures.[103] Nanolaminate and mixture films containing Ru have been considered for Cu metallization[104,105] and for gate electrode applications.[106] The wide applicability of Ru does not entirely originate from the good properties of Ru itself but also from the good electrical conductivity of the ruthenium oxide (RuO_2).

Most of the ALD Ru processes are classified here into groups depending on ligands in precursors. The first group consists of metallocenes which are ferrocene ($FeCp_2$) type of compounds having a “sandwich” structure with two parallel cyclopentadienyl rings.[107] In this thesis also compounds having only a cyclopentadienyl ligand and compounds with five-membered pyrrolyl rings have been put into this category as derivatives of metallocene precursors used in ALD. The second group is reserved for β-diketonate precursors. Those which do not fall into these two groups, such as cyclohexadienyl and benzene containing compounds, amidinates, and a tetroxide RuO_4, are presented in the chapter designated as the other precursors.

3.3.1 Metallocene precursors

The most widely studied and applied ALD Ru precursors are metallocenes and their derivatives (Figure 9). Several of these cyclopentadienyl-based Ru precursors have been used with molecular O_2 as a reactant.

The first ALD noble metal process was reported by Aaltonen et al.[51] who deposited Ru films from ruthenocene ($RuCp_2$) and O_2 (air). The Ru films were successfully deposited on Al_2O_3 and TiO_2 films between 275 and 400 °C. Without the Al_2O_3 and TiO_2 nucleation layers the Ru films were non-uniform.[51] On an Ir starting surface the films grew at as low temperature as 225 °C.[47] In general, Ru nucleates more efficiently on catalytically active noble metal starting surfaces than on oxides (Al_2O_3, SiO_2).[47,108]

$Ru(EtCp)_2$ and O_2 have been applied to deposit Ru films at 270 °C on TiN surfaces[109] and at 300 °C on Al_2O_3 coated porous anodic Al_2O_3,[110] SiO_2,[59] SiN_X,[59] and NH_3 plasma treated

SiO_2[59]. $Ru(EtCp)_2$ is a liquid[109] in comparison to solid $RuCp_2$ and is therefore more extensively used. Though most papers report growth of Ru only, ruthenium oxide formation has been observed in some papers when specific combinations of deposition parameters have been applied (Chapter 3.4).[40,109,111,112]

Interestingly, ozone has been used as a reactant for ALD of Ru from $Ru(EtCp)_2$,[113] though ozone can easily etch Ru to volatile RuO_4.[114] Ru films were grown at 225–275 °C on ZrO_2 using ozone concentrations lower than 100 g/m^3 while higher concentrations (100–200 g/m^3) led to RuO_x and RuO_2.[113] Shorter nucleation delays, smoother films and better adhesion were listed as benefits of using ozone while similar resistivities, impurity concentrations and densities were obtained as with the O_2-based chemistry.[113] Furthermore, the Ru film on ZrO_2 did not show blistering or delamination as compared to the film grown with the O_2-based ALD process.[113]

(EtCp)Ru(MeCp) and O_2 have been applied to grow Ru films at 250–325 °C on TiO_2, Al_2O_3, HfO_2, ZrO_2, HF-etched Si, and SiO_2.[53] At 250 °C long O_2 pulses were required to deposit continuous Ru layers while at higher temperatures reactions proceeded faster.[53] Ru films have, in some cases, indicated possible blistering or partial delamination from substrates which was suggested to be affected by film thicknesses, substrates, deposition temperatures, and post-growth treatments.[53] An amino-derived metallocene, [1-(dimethylamino)ethyl]ruthenocene [$(Me_2NEtCp)RuCp$], required high temperatures (325–500 °C) to grow Ru with O_2 (air) on in-situ grown Al_2O_3 and uniform films were obtained only at 375 °C and above.[46]

For PEALD of Ru, $Ru(EtCp)_2$ has been used with NH_3 plasma on starting surfaces such as TiN,[92,115–117] TaN,[45,93,118] Si,[45,93,117,119] and SiO_2[93]. The films were deposited between 270 and 350 °C (Table 3).[45,93,115–119] The $Ru(EtCp)_2$–NH_3 plasma process works at far lower temperatures (≥100 °C) as well;[118] however the 7 nm film deposited at 100 °C was almost amorphous, far more resistive (80 μΩcm), and rougher (1.8 nm) than the film grown at 270 °C (14 μΩcm, 0.6 nm) with a similar thickness.[118] Additionally, the Ru film deposited at 200 °C on in-situ grown TaN was still weakly nanocrystalline and had substantial resistivity (60–70 μΩcm) compared to the film deposited at 270 °C.[118] This indicates why

temperatures of 270 °C and above are preferred in PEALD of Ru from $Ru(EtCp)_2$ and NH_3 plasma. H_2 plasma has been also used to deposit Ru films at 200 °C from $Ru(EtCp)_2$ and the choice of plasma gas, H_2/N_2 or pure H_2, can affect whether RuN_x or Ru is grown.[120] Additionally, the H_2/N_2 plasma and $Ru(EtCp)_2$ have been shown to deposit crystalline Ru films with low resistivity (13 μΩcm) already at 200 °C.[104]

Surface roughnesses of PEALD Ru films grown from $Ru(EtCp)_2$ and NH_3 plasma at 270–300 °C are generally substantially lower than those of thermal ALD Ru films grown with O_2.[93,115] The PEALD Ru films have been reported to be denser[115,116] and show negligible nucleation delays on various surfaces including TaN_x, Si, and SiO_2 in contrast to thermal ALD Ru films.[93] However, thin PEALD Ru films have also been reported[118] to grow slower on TaN (~0.2 Å/cycle) than on Si (0.3 Å/cycle) which indicates differences in nucleation on different materials. Thus it is not surprising that nucleation delays of about 50 cycles on TiN and 80 cycles on Si have been observed.[117]

For successful PEALD of Ru, highly reactive radicals such as N or NH_2 from NH_3 plasma should be present.[93] This means that high enough plasma power is essential to grow high quality PEALD Ru films.[93] The PEALD plasma power influences the impurity contents too: high plasma powers result in low carbon impurities (1.8 at.% at 100 W and 1.4 at.% at 150 W) while low plasma power (20 W) can lead to substantial carbon contamination (16.6 at.%).[119] Also longer low power plasma pulses (20 s, 20 W) are required to achieve comparable saturation in film thickness per cycle as with higher plasma power (5 s, 100 W).[116] In general, the extra energy supplied by plasma drives the rearrangement of Ru atoms from the preferential (101) orientation towards the thermodynamically most stable (002) orientation in the PEALD Ru films.[115,116]

The growth rates of the $Ru(EtCp)_2$–NH_3 plasma and $Ru(EtCp)_2$–O_2 processes differ substantially with the growth rate being lower in PEALD (0.4 Å/cycle) than in the thermal oxygen-based ALD (1.5 Å/cycle).[116] In PEALD the number of atoms deposited in a cycle has been observed to be less than 40 % compared to the oxygen-based ALD.[116] The adsorbed oxygen atoms in oxygen-based ALD are reactive towards the Ru precursor and combust part of the precursor ligands. The adsorbed oxygen is lacking in NH_3 plasma PEALD which explains the lower number of Ru atoms deposited per cycle and, hence,

lower growth rate.[116] Indeed, in oxygen-based ALD of Ru inclusion of a H_2 plasma step after the oxygen pulse has been reported to decrease the growth rate drastically to a similar level as in PEALD of Ru using NH_3 plasma.[116] Thus, the adsorbed oxygen atoms left on the surface after the O_2 pulse are consumed by the H_2 plasma and are not available to react with the $Ru(EtCp)_2$.

An interesting modification of the $Ru(EtCp)_2$ precursor is the (dimethylpentadienyl)(ethylcyclopentadienyl)Ru [(EtCp)Ru(DMPD)], in which a non-cyclic pentadienyl-ligand is used to enhance the nucleation properties of the precursor.[21] (EtCp)Ru(DMPD) dissolved in ethylcyclohexane (ECH) and O_2 have been used to deposit Ru films at 230–290 °C on Si, SiO_2, TiO_2, TiN and noble metal surfaces.[44,54,61,69,121,122] Ru films were grown also at 210 °C on Au and Pt surfaces.[122] Negligible Ru nucleation delays were reported on Si, SiO_2, TiO_2, TiN surfaces;[61,121] however lower Ru nucleation density and larger grain size was suggested on SiO_2.[61] In another study,[69] substantial nucleation delay (~100 cycles) was observed on TiN and this was reduced to about 60 cycles after in-situ Ar plasma pretreatment.

Also both cyclopentadienyl ligands have been switched to the linear dienyl DMPD-ligands. The resulting $Ru(DMPD)_2$ is solid at room temperature and thermally less stable than the liquid (EtCp)Ru(DMPD).[123] It has been applied to both thermal ALD and PEALD at 325 °C.[124] In PEALD notably N_2 plasma was used as the reactant while thermal ALD relied on the usual O_2.[124] Lower film growth rates and smoother films were obtained with the PEALD $Ru(DMPD)_2$–N_2 plasma process as compared with the thermal $Ru(DMPD)_2$–O_2 process on in-situ grown TaN.[124] This is similar as observed earlier with $Ru(EtCp)_2$.

Several precursors where one or both cyclopentadienyl ligands have been substituted with pyrrolyl (Py) rings have been also examined for Ru ALD. One of these is (EtCp)Ru(Py) which was used with O_2 to deposit Ru films at 275–350 °C on HF-etched Si (Si-H), SiO_2, ZrO_2, and TiN substrates.[125] The film growth was not efficient and uniform at 250 °C, but Ru growth was achieved at as low temperature as 275 °C on SiO_2 and Si-H.[125] ZrO_2 promoted the Ru nucleation most efficiently, but the films also roughened quickly.[125]

Although slightly faster growth rate was achieved on Si-H than on SiO_2, the nucleation was suspected to be slower and less homogeneous.[125] Roughening of the Ru film was dependent on the starting surface as the films grown on SiO_2 were mostly smooth and light-mirroring metallic layers whereas the films on TiN and especially on ZrO_2 were milky, i.e. light-scattering, and thus rough.[125]

A similar pyrrolyl containing precursor, (MeCp)Ru(Py), deposited either Ru or RuO_2 depending on the length of the O_2 pulse (1 s vs. 4 s, respectively).[126] (MeCp)Ru(Py) was applied also with NH_3 and H_2 plasmas at 330 °C.[94,95] Both PEALD processes showed similar growth characteristics and minimal nucleation delays of less than 10 cycles on TiN.[94,95] Notably, NH_3 and H_2 gases were introduced into the reaction chamber also during the (MeCp)Ru(Py) pulse and the following purge whereas the purge period after the plasma step was omitted.[94,95] Furthermore, Ru precursor with two methyl substituted pyrrolyl rings, $Ru(Me_2Py)_2$, was used with O_2 to deposit Ru films between 250 and 325 °C.[127] The Ru films were grown on Al_2O_3, TiO_2, HfO_2, SiO_2, and H terminated Si surfaces where the SiO_2 and Si-H surfaces showed Ru nucleation problems at higher temperatures (320–325 °C).[127]

Ru thin films have been deposited also from cyclopentadienyl ethylruthenium dicarbonyl, $Ru(Cp)(CO)_2Et$, and O_2.[128,129] Thermal decomposition of $Ru(Cp)(CO)_2Et$ was concluded to occur at 325 °C and with typical ALD exposure times (5 s) the surface reactions did not reach completion until precursor decomposition at above 300 °C.[128] In another study[129] the film grown from $Ru(Cp)(CO)_2Et$ and O_2 consisted of both Ru and RuO_2. It was noted with ex-situ XPS measurements that the film growth starts as Ru, but after 24 cycles the RuO_2 component increased.[129] Interestingly, the growth was found linear on hydrogen passivated Si(111) already after the first two cycles.[129]

Ru growth by ALD and PEALD has been compared using $Ru(Cp)(CO)_2Et$ and either molecular O_2 or O_2 plasma at 325 °C.[130] No CVD-like growth was observed when only $Ru(Cp)(CO)_2Et$ was pulsed into the reactor but the authors suspected that the precursor is close to the onset of decomposition at 325 °C.[130] The growth rates of the $Ru(Cp)(CO_2Et)$–O_2 (1.0 Å/cycle) and $Ru(Cp)(CO_2Et)$–O_2 plasma (1.1 Å/cycle) processes were similar.[130] The films deposited by thermal ALD were slightly denser compared to the PEALD films;

however PEALD led to faster nucleation on TiN surface (~45 cycles) compared to thermal ALD (~85 cycles).[130] Both processes deposited very rough films as the surface roughnesses of 15 nm thick films were 5 nm (ALD) and 10 nm (PEALD).[130] Short plasma exposures (800 ms) were used in PEALD to ensure that RuO_2 did not form while the use of relatively high plasma power resulted in a lack of film growth.[130] Likewise, when the Ru films were exposed after the deposition to O_2 plasma slight etching was observed.[130]

Besides for Ru thin film deposition, ruthenium cyclopentadienyl containing precursors have been examined also for ALD of Ru nanoparticles on various surfaces, such as SiO_2,[131] porous SiOC:H template,[132] Al_2O_3,[133,134] and Al_2O_3 coated carbon and silica aerogels.[135] With PEALD Ru nanoparticles have been deposited on SiO_2 using NH_3 plasma.[131,136] Furthermore, NH_3 plasma PEALD and O_2-based ALD processes can also be combined to control the size and density of the Ru nanoparticles, where the PEALD provides the high nucleation density while thermal ALD is used for tuning the size of the nanoparticles.[131] ALD has also been used for deposition of mixed metal Ru-Pt nanoparticles on Al_2O_3 by controlling the ratio of the corresponding metal deposition cycles.[137]

3.3.2 β-Diketonate precursors

The development of β-diketonate Ru precursors has not been as extensive as the cyclopentadienyl-based precursors. $Ru(thd)_3$ and $Ru(od)_3$ were published shortly after the $RuCp_2$–O_2 ALD Ru process, however other β-diketonates have not been reported since. The β-diketonate precursors have Ru in a nominal oxidation state of +3 instead of +2 as in the metallocene precursors. The lower oxidation state may be one of the reasons why metallocenes are preferred above β-diketonates in the O_2-based combustion ALD processes. The reported β-diketonates seem to need similar growth temperatures as the metallocenes and result in comparable growth rates (Table 3). Correlation between the metal precursors and the amounts of impurities in the Ru films is hard to make but it seems that the β-diketonates lead to similar or slightly higher impurity contents than the metallocenes (Table 4).

$Ru(thd)_3$ and molecular O_2 have been used to deposit Ru on Al_2O_3 between 325 and 450 °C, where 450 °C is close to the onset of the $Ru(thd)_3$ decomposition.[32] Only very thin films were obtained on Al_2O_3 at 300 °C,[32] while films grew on Ir surface at a substantially lower temperature of 250 °C.[47] The ALD Ru growth rate and the grain size increased with increasing deposition temperature while the appearance of the films changed from specular (350 °C) to slightly milky (400 °C) at higher temperatures because of the increased film roughness.[32] The impurity contents in the films grown from $Ru(thd)_3$ were higher than in the films grown from $RuCp_2$ at the same temperature (Table 4).[32,51] Also much higher air flow rate (40 sccm vs. 2 sccm) was required to deposit films with $Ru(thd)_3$.[32,51]

$Ru(thd)_3$ has been dissolved in ECH for LIALD to deposit Ru films with oxygen at 330 and 380 °C.[38,39] The reported nucleation delays were 70 ± 30 cycles.[38] The number of Ru solution injections in an ALD cycle increased the film thickness to a certain saturation value which depended also on the concentration of the $Ru(thd)_3$.[38,39] This was explained to result from the ECH solvent which during the Ru solution injection step competes with $Ru(thd)_3$ to react with adsorbed oxygen on the surface.[38,39] Furthermore, the growth rate decreased with both increasing O_2 flow rate and O_2 feeding time too.[38,39] Over 6 s O_2 feeding times with high O_2 flow rates (500 sccm) did not result in film growth at all[38] or resulted in a mixture of Ru and RuO_2.[39] Also $Ru(od)_3$ dissolved in n-butylacetate (0.1 M) has been used with O_2 for LIALD of Ru films on SiO_2/Si wafers between 275 and 450 °C and on carbon nanotube array templates at 300 °C.[138] Although the process window of ALD was reported to be 325–375 °C, the Ru growth rate on SiO_2 at 275 °C was still about 0.6 Å/cycle.[138]

3.3.3 Other precursors

Besides metallocene-derived Cp-compounds and β-diketonates, also other types of Ru precursors have been used, some of which are unconventional and innovative. It was mentioned in Chapter 3.3.1 how metallocenes have been modified to more reactive and less stable compounds by changing one or both Cp-rings to other ligands, i.e. from $Ru(EtCp)_2$ to (EtCp)Ru(DMPD) and $Ru(DMPD)_2$ (Figure 9). Further examples in this chapter illustrate how the ALD noble metal precursor design and synthesis is progressing

from the β-diketonates (+3) and metallocenes (+2) towards the zero oxidation state precursors. However, even a very high oxidation state (+8) precursor RuO_4 is not unfamiliar to the ALD noble metal chemistry.

A zero oxidation state Ru precursor, (η6-1-isopropyl-4-methylbenzene)(η4-cyclohexa-1,3-diene)ruthenium(0) [(^{i}Pr-Me-Be)Ru(CHD)], and O_2 were used for ALD of Ru films at 220 °C.[139] The nucleation delay was negligible on TiN and very short (~11 cycles) on SiO_2.[139] A continuous 3.5 nm thick Ru film was confirmed already after 50 ALD cycles by transmission electron microscopy.[139] The same precursor was used with O_2 also at 185–310 °C on thermally-grown SiO_2.[140] Although the Ru growth rate was about 0.6 Å/cycle at 185 °C, the resulting porous film had a low density (6.3 g/cm^3) and very high (>3000 μΩcm) resistivity.[140] The growth rate increased to about 0.8 Å/cycle and the film resistivity decreased to about 100 μΩcm at 200 °C.[140] The ALD temperature window with a growth rate of about 0.9 Å/cycle was observed between 225 and 270 °C while partial precursor decomposition occurred at 310 °C.[140]

In addition to (^{i}Pr-Me-Be)Ru(CHD), similar zero oxidation state precursors, (Et-Be)Ru(CHD) [ethylbenzene-cyclohexadiene Ru(0)] and (Et-Be)Ru(Et-CHD) [ethylbenzene-ethyl-cyclohexadiene Ru(0)] have been applied with O_2 for ALD of Ru films between 140 and 350 °C.[141] On thermally grown SiO_2 the Ru films showed very short incubation periods (3 and 5 cycles); thus a continuous Ru film was obtained after only 60 cycles at 225 °C using the (Et-Be)Ru(Et-CHD)–O_2 ALD process.[141]

(^{i}Pr-Me-Be)Ru(CHD) has been used with a direct NH_3 plasma for PEALD of Ru between 140 and 400 °C on TiN surfaces.[142] A very wide ALD temperature window between 225 and 400 °C was found with a growth rate of 0.9 Å/cycle.[142] Also H_2 plasma enabled the PEALD of Ru at 225 °C while thermal ALD of Ru with molecular H_2 and NH_3 was not successful.[142] PEALD of Ru was also examined with a N_2/H_2 plasma at 270 °C.[143] The PEALD processes using either NH_3 or N_2/H_2 plasmas exhibited negligible nucleation delays on TiN and SiO_2.[142,143] Nanocrystalline Ru films having high nitrogen contents (about 20 at.% N) were achieved with high N_2/H_2 plasma gas ratios at 270 °C.[143]

Combined with PEALD SiN_x in various ratios, the PEALD Ru process with NH_3 plasma was applied to deposit Ru-Si-N for Cu diffusion barriers.[144]

Another innovative precursor is Ru(Me-Me_2-CHD)$_2$ [bis(2,6,6-trimethyl-cyclohexadienyl)ruthenium] which is commercially known as Cyprus. Ru(Me-Me_2-CHD)$_2$ has been used with molecular O_2 to deposit Ru films by ALD,[145,146] and also RuO_2 when the O_2 partial pressure was increased.[145] Nucleation delays at 270 °C were the shortest on CVD SiO_2, followed by ALD TiO_2 and H-terminated Si surfaces, and were on all these materials less than 50 cycles.[145] Surprisingly, a long nucleation delay of 250 cycles was observed on the ALD Al_2O_3 starting surface.[145] Also, on TiO_2 surface the about 23 nm thick Ru film exhibited in SEM some very large grainlike objects (diameters ~50–200 nm) not observed on other substrates.[145] The authors did not specify these large grainlike structures in detail, though based on XRD it was assumed that those grains oriented towards the (101) direction.[145]

A Ru precursor having CO ligands has been also examined. Ru(CO)$_3$(CHD) and NH_3 gas were used to grow Ru films at 200 °C on Si by a process called a modified ALD system.[147] The thermal stability of Ru(CO)$_3$(C_6H_8) is low as the precursor decomposes already at temperatures above 100 °C.[147] As a consequence, the flow rate of Ru precursor governed the film properties, such as thicknesses, uniformities, and oxygen impurities.[147] Though the process was not true ALD, Ru films with good uniformity, linear growth, and negligible oxygen contents were deposited on 8-inch (200 mm) wafers.[147]

An amidinate precursor, Ru(^{t}Bu-Me-amd)$_2$(CO)$_2$, has been explored for ALD. It is a solid compound which sublimes completely in TGA.[148] ALD was attempted between 300 and 400 °C using the precursor and molecular O_2.[149] The Ru film growth rate was about 1 Å/cycle at 325 °C, but films were also obtained without using O_2 (0.3 Å/cycle).[149] This shows that the process contains a substantial CVD component and thus Ru(^{t}Bu-Me-amd)$_2$(CO)$_2$ seems to decompose thermally at those temperatures. It was also observed that the appearance of the Ru films changed to milky with visible flakes peeling off when higher O_2 exposures were used at 325 °C.[149]

The same Ru(^{t}Bu-Me-amd)$_2$(CO)$_2$ precursor was also applied with a reducing agent, NH_3, to grow Ru films on WN surface.[150] Again, ALD of Ru was explored but the precursor could also be used as a single-source precursor in pulsed CVD mode (0.4 Å/cycle; 300 °C).[150] It should be emphasized that substantial CVD growth was noted already above 200 °C in pulsed CVD of Ru precursor only while there was little or no deposition below 200 °C.[150]

One of the most exceptional noble metal precursors introduced to ALD is RuO_4 diluted in an unspecified solvent. Pure RuO_4 melts at slightly above room temperature (25 °C) and evaporates at 40 °C.[4] It is also highly toxic and may even explode.[4] But the RuO_4-solvent mixture is a liquid which is claimed to be non-toxic, non-flammable, and non-corrosive.[151] This has been commercialized as ToRuS, Total Ruthenium Solution.[151] The solvent has not been specified but it is supposedly a blend of organic solvents some of which have been fluorinated.[152] Ru films were obtained from ToRuS and molecular H_2 by ALD above 150 °C, while films with excellent characteristics were noted to be grown above 200 °C.[151] Ru films were also deposited using ToRuS and 5 % H_2 in N_2 at 230 °C by pulsed CVD in which the precursor pulses were alternated and separated by Ar purges.[152] The phase of the deposited film was either RuO_2 (1–10 s) or Ru (>15 s) depending on the feeding time of H_2/N_2 gas.[152] ALD mode was also studied at 230 °C but it was concluded that ALD does not occur because Ru layer density increased linearly with increasing RuO_4 feeding time.[152] In another study,[153] Ru and RuO_2 films were deposited using ToRuS and molecular H_2, and low temperatures between 100 and 250 °C were explored. The Ru film growth showed ALD behavior at a low temperature (100 °C) but became CVD already at 200 °C because of the RuO_4 decomposition.[153] Also PEALD Ru films were grown using H_2 plasma at 100 and 200 °C with similar growth rates (1.1 Å/cycle) at both temperatures.[153]

3.4 Ruthenium oxide

ALD of RuO_2 is strongly related to the deposition of ALD of Ru metal with molecular O_2 as the reactant. This was already briefly noted in the previous chapter on ALD of Ru. Key parameters determining whether RuO_2 or Ru is formed are deposition temperature,

precursor doses, and oxygen partial pressure. It should be emphasized that these parameters are not independent from each other as RuO_2 formation is observed only when an optimized combination of parameters is applied. The reported ruthenium oxide processes and their properties are collected to Tables 5–7.

Table 5. ALD RuO_x and RuO_2 processes reported in the literature.

Metal precursor		$T_{vap.}$ (°C)	Reactant	$T_{dep.}$ (°C)	Growth rate (Å $cycle^{-1}$)	Ref.
$Ru(EtCp)_2$		80	O_2	270	1.5–1.7	109
$Ru(EtCp)_2$		80	O_2	270	1.7	111
$Ru(EtCp)_2$		80	O_2	280	0.3	163
$Ru(EtCp)_2$		65	O_2	300, 350	up to 7 (300 °C)	40
$Ru(EtCp)_2$	mod.	135	O_2 (also in pulses and purges)	265	1.4	164
$RuCp_2$		85	O_2	300	3.2	112
(EtCp)Ru(DMPD) in ECH	mod.		O_2 (also in Ru prec. pulse)	250	NA	165
(MeCp)Ru(Py)			O_2	NA	0.7–0.8	126
$Ru(thd)_2(cod)$ in pyridine			O_2	290	6.6	162
$Ru(Me\text{-}Me_2\text{-}CHD)_2$		60	O_2	NA	NA	145
RuO_4 in solvent		3	5 % H_2	230	2.4	152

abbreviation mod. indicates a modified ALD system ; NA = not available

Table 6. Impurity contents of ALD RuO_2 processes.

Cycle sequence	$T_{dep.}$ (°C)	At. composition (at.%)	Impurity contents (at.%)	Method	Ref.
(MeCp)Ru(Py)–O_2	NA	Ru 34, O 57	C 0.1, H 1.4	ERDA	126
$Ru(thd)_2(cod)$ in pyridine–O_2	290	Ru, O	C low, some N	SIMS	162
RuO_4 in organic solvent–H_2	230	Ru, O ~60		AES	152

Table 7. Roughness and resistivity values reported for the ALD RuO_2 processes.

Cycle sequence	$T_{dep.}$ (°C)	Thickness (nm)	Roughness (nm)	Resistivity (μΩ cm)	Ref.
$Ru(EtCp)_2$–O_2	270	90	4.2	70	111
$Ru(EtCp)_2$–O_2	270			70	109
$Ru(EtCp)_2$–O_2	350			75	40
$Ru(EtCp)_2$–O_2	280	30	5		163
$Ru(EtCp)_2$–O_2	300			~120	40
$Ru(EtCp)_2$–O_2 (O_2 in pulses and purges)	265	40	2.0	130	164
$RuCp_2$–O_2	300	70		200	112
$RuCp_2$–O_2	300	100		270	112
(MeCp)Ru(Py)–O_2		10	1.0–1.2	~100	126
$Ru(thd)_2(cod)$ in pyridine–O_2	290	17	1.1	160	162
Ru(Me-Me_2-CHD)$_2$–O_2				~300	145
RuO_4 in organic solvent–H_2	230	7.2–21.6	0.2	~250	152

The $Ru(EtCp)_2$–O_2 chemistry is the most studied for ALD of RuO_2. The resulting film, either Ru or RuO_2, has been controlled by the ratio of the $Ru(EtCp)_2$ pulse time to the oxygen partial pressure during the oxygen pulse,[109,111] by the O_2 flow rate,[40] and by the total pressure of the ALD system[111] when a specific deposition temperature is used. Thus the phase change from Ru to RuO_2 can be achieved by controlling the growth temperature as well.[40] The formation of the RuO_2 phase has been found to be dependent also on the Ru precursor.[40]

RuO_2 films have been grown by ALD at 270 °C with short $Ru(EtCp)_2$ pulses (2–3 s) and specific $O_2/(Ar + O_2)$ ratios (25–33 %).[111] In another study[40] phase change from Ru to RuO_2 was achieved by controlling the O_2 flow rate. An increase of the O_2 flow rate from 10 to 12 sccm led from Ru to mixed Ru and RuO_2 phases while RuO_2 only was observed with large O_2 flow rates (67 sccm).[40] Also an elevation of the deposition temperature from 300 to 350 °C can lead to a RuO_2 film growth.[40]

The $RuCp_2$–O_2 process has also been shown to produce RuO_2 under certain conditions similar to the $Ru(EtCp)_2$–O_2 process, but to a lesser extent;[112] large O_2 flow rate resulted in nanocrystalline Ru grains mixed with amorphous RuO_x while long O_2 exposures with

small O_2 flow led to dense Ru only. The oxygen partial pressure, not the length of the oxygen exposure, determines the amount of subsurface oxygen atoms.[112] When the number of subsurface oxygen atoms increases with increasing growth temperature formation of ruthenium oxide becomes feasible at high enough oxygen pressures. As an example, an increase of the O_2 flow rate from 3 to 20 sccm has been shown to increase the growth rates and resistivities from 1.2 Å/cycle and about 20 μΩcm to 3.2 Å/cycle and 270 μΩcm, respectively.[112]

RuO_2 deposited from $Ru(EtCp)_2$ and molecular O_2 by ALD has been considered and studied for some applications. As an example, $SrRuO_3$ has interest in DRAM devices as a conductive seed layer that is structurally compatible with $SrTiO_3$ high-k material.[154,155] A $SrRuO_3$ seed layer has been formed by annealing a stack of ALD grown RuO_2 and SrO under O_2 ambient.[154,155] Additionally, RuO_2–Al_2O_3 thin films have been grown in various ratios by thermal ALD Ru(EtCp)–O_2 and PEALD TMA–O_2 plasma processes at 230 °C, and examined as heating resistors for thermal inkjet printheads.[156] $Ru(EtCp)_2$ has been also applied to deposit RuO_x nanocrystals for memory capacitors.[157–160] Light harvesting and emission properties of about 10–20 nm RuO_2 nanoparticles grown at 350 °C from $Ru(EtCp)_2$ and O_2 on ZnO nanorods have been examined.[161]

In addition to the $Ru(EtCp)_2$–O_2 and $RuCp_2$–O_2 processes for RuO_2, a cyclopentadienyl precursor with a pyrrolyl ring, (MeCp)Ru(Py), has been shown to produce RuO_2 with long O_2 pulses.[126] As an example, 4 s O_2 pulses led to RuO_2 films while Ru metal films were grown with 1 s pulses.[126] The increase of the O_2 pulse length in the (MeCp)Ru(Py)–O_2 process has therefore a similar RuO_2 producing effect as the increment of O_2 flow rate (dose) in the $Ru(EtCp)_2$–O_2 process[40].

A modified β-diketonate precursor $Ru(thd)_2(cod)$ has been shown to deposit RuO_2 films by LIALD.[162] $Ru(thd)_2(cod)$ dissolved in pyridine and molecular O_2 were used to grow films at 290 °C on Si(100).[162] Fully conformal growth of RuO_2 films on trenches (aspect ratio 3) was achieved but the conformality decreased progressively in higher aspect ratio structures (40 % in aspect ratio of 12).[162] In LIALD the solvent can limit the formation of RuO_2 as was noted using $Ru(thd)_3$ dissolved in ECH.[39] Also $Ru(Me\text{-}Me_2\text{-}CHD)_2$ has been observed to deposit RuO_2 instead of Ru when O_2 partial pressure is increased.[145] These

examples suggest that although RuO_2 growth has not been verified with all Ru precursors, the deposition should be feasible with metallocenes, β-diketonates as well as other precursors alike. However, the nucleation in oxygen-based ALD of RuO_2 may be similarly dependent on the applied Ru precursor as the nucleation in the oxygen-based ALD of Ru. For example, the ALD RuO_2 process using $Ru(EtCp)_2$ and molecular O_2 has shown to suffer from prolonged nucleation on Si substrates.[163]

More unconventional approaches have been used as well to grow RuO_2 films. Oxygen mixed with argon was used also during noble metal precursor pulse and for purging to deposit RuO_2 from $Ru(EtCp)_2$ and O_2 at 265 °C.[164] Although no saturated growth rate was obtained with increasing $Ru(EtCp)_2$ pulse lengths (1–5 s), the RuO_2 process was still found to proceed mainly by the ALD-type growth mechanism.[164] Background O_2 flow has been employed also during the Ru precursor pulse [(EtCp)Ru(DMPD) dissolved in ECH] to suppress the reduction of RuO_2 to Ru at 250 °C.[165] Introduction of both O_2 reactant and Ru precursor at the same time into the reaction chamber would however lead to reactions more typical to CVD than ALD.

Also ozone has been used as a reactant for ALD of ruthenium oxide films from $Ru(EtCp)_2$.[113] The RuO_x and RuO_2 films were grown at 275 °C using ozone concentrations between 100 and 200 g/m^3.[113] At higher ozone concentrations (>200 g/m^3) etching became dominating and thus no film was grown at all.[113]

RuO_2 films have also been grown from RuO_4, which was dissolved in a blend of organic solvents, and molecular H_2 as a reactant.[152,153] At 230 °C RuO_4 showed thermal decomposition and the RuO_2 films were grown from RuO_4 and 5 % H_2 in N_2 by more like pulsed CVD rather than ALD.[152] The RuO_2 films were grown using short H_2/N_2 gas feeding times (1–10 s) whereas Ru was obtained with longer H_2/N_2 feeding times (>15 s).[152] RuO_2 film growth was also examined in the ALD mode at a slightly lower temperature of 200 °C.[153] However, RuO_2 films were obtained even without any H_2 pulses and with a high growth rate (0.8 Å/cycle);[153] thus it was concluded that saturative RuO_4 surface behavior was lacking at 200 °C and the RuO_4–solvent mixture behaved as a CVD chemical.[153]

3.5 Osmium

Osmium is a challenging metal because of its hardness, brittleness, low vapor pressure, and very high melting point. Os can also oxidize easily to either OsO_2 or to the dangerous volatile OsO_4.[4] These characteristics are indicative for the limited interest in Os metal and film deposition.

Ru and Os thin films have been previously been deposited by CVD using $RuCp_2$ and $OsCp_2$, respectively, with oxygen as a co-reactant.[166] Motivated by the similarities between the CVD Ru and Os processes, an ALD Os process[VIII] was developed using $OsCp_2$ and O_2 similar to the existing $RuCp_2$–O_2 ALD Ru process[51]. The Os films were grown between 325 and 375 °C on in-situ grown Al_2O_3.[VIII] The details of the ALD Os process are presented in its own chapter (5.6) under the Results and discussion section and in publication [VIII]. This is the first report of Os film deposition by ALD while no ALD osmium oxide processes have been reported. An ozone-based process would not be desirable as Os may easily oxidize to the volatile and deadly OsO_4 instead of OsO_2 even at room temperature.[4] However the approaches used for ALD of RuO_2 should be feasible for ALD of OsO_2 as well.

3.6 Rhodium and rhodium oxide

ALD Rh processes are one of the least examined among the ALD noble metal processes. The process development has been based solely on a single β-diketonate precursor, $Rh(acac)_3$. The published ALD Rh metal and oxide processes with deposition temperatures, growth rates and impurity contents are shown in Tables 8 and 9. The surface roughnesses and resistivities obtained with these processes are collected to Table 10.

Table 8. ALD Rh metal and oxide processes.

Metal precursor	$T_{vap.}$ (°C)	Reactant	$T_{dep.}$ (°C)	Growth rate (Å $cycle^{-1}$)	Ref.
Rh metal					
$Rh(acac)_3$	150	O_2	200–300	$0.6–0.8^{250°C}$	167
$Rh(acac)_3$	150	O_2	225–325	$0.5^{225°C}$, $0.9–1.2^{275–310°C}$, $1.9^{325°C}$	168
$Rh(acac)_3$	150	ozone–H_2	160–180	0.2–0.3	VII
Rh oxide					
$Rh(acac)_3$	150	ozone	160–180	0.2–0.3	III

Table 9. Impurity contents of ALD Rh metal and oxide processes.

Cycle sequence	$T_{dep.}$ (°C)	At. composition (at.%)	Impurity contents (at.%)	Method	Ref.
Rh metal					
$Rh(acac)_3$–O_2	250	Rh, O <2.3	C <1.6, H <0.1	TOF-ERDA	167
$Rh(acac)_3$–O_2	300	Rh, O present (not quantified)	C <XPS limit	XPS	168
$Rh(acac)_3$–ozone–H_2	160	Rh ~94, O 3	C 0.6, H 3	TOF-ERDA	VII
$Rh(acac)_3$–ozone–H_2	180	Rh ~98, O 0.7	C 0.3, H 1.5	TOF-ERDA	VII
Rh oxide					
$Rh(acac)_3$–ozone	160	Rh 36, O 57	C 1.2, H 6.4	ERDA	III
$Rh(acac)_3$–ozone	170	Rh 36, O 57	C 1.4, H 5.9	ERDA	III
$Rh(acac)_3$–ozone	180	Rh 37, O 57	C 0.5, H 5.5	ERDA	III

Table 10. Roughness and resistivity values reported for the ALD Rh metal and oxide processes.

Cycle sequence	$T_{dep.}$ (°C)	Thickness (nm)	Roughness (nm)	Resistivity (µΩ cm)	Ref.
Rh metal					
$Rh(acac)_3$–O_2	250	15		24	167
$Rh(acac)_3$–O_2	250	25		10	167
$Rh(acac)_3$–O_2	250	40		10	167
$Rh(acac)_3$–O_2	250	~140		8	167
$Rh(acac)_3$–O_2	300	NA		~10	168
$Rh(acac)_3$–ozone–H_2	160	19	1.7	11	VII
$Rh(acac)_3$–ozone–H_2	170	23	1.1	11	VII
$Rh(acac)_3$–ozone–H_2	180	27	1.3	10	VII
Rh oxide					
$Rh(acac)_3$–ozone	160, 170	~80	$0.7^{160°C}$, $1.4^{170°C}$	6000–8000	III, *a*
$Rh(acac)_3$–ozone	180	~80	0.5	5000–6000	III, *a*
$Rh(acac)_3$–ozone	170	~40,60		11000	III

a unpublished surface roughness data

Rh metal films have been deposited using $Rh(acac)_3$ and molecular O_2 on in-situ grown Al_2O_3 mostly at 250 °C.[167] The low-temperature limit for the $Rh(acac)_3$–O_2 process was reported to be 200 °C while thermal self-decomposition of $Rh(acac)_3$ was observed already at 300 °C.[167] Growth rate of Rh films was about 0.8 Å/cycle with 1–10 s O_2 pulses at 250 °C whereas the growth rate increased from 0.6 to 0.8 Å/cycle with 1 to 10 s $Rh(acac)_3$ pulses and showed saturation only at the longest pulses.[167] Some explanations suggested for the need to use long $Rh(acac)_3$ pulses to obtain saturated growth rate included the low vapor pressure of $Rh(acac)_3$, thermal self-decomposition of $Rh(acac)_3$, and its adsorption and desorption behavior.[167]

The same $Rh(acac)_3$–O_2 ALD Rh process has been applied also in a homebuilt hot-wall quartz tube reactor between 225 and 325 °C.[168] The deposition results on CVD HfO_2 and thermally grown SiO_2 were noted to be consistent with the previous results.[167,168] Selective area ALD of Rh was accomplished by using patterned photoresists which prevented Rh growth.[168] Nucleation of Rh was inhibited also on the oxide surfaces (SiO_2 and HfO_2) when hexamethyldisilazane had been used to promote adhesion of the photoresist to these surfaces.[168]

The ozone-based chemistries were applied with the $Rh(acac)_3$ precursor to deposit Rh_2O_3 and Rh metal films with Rh(acac)–O_3 and Rh(acac)–O_3–H_2 processes, respectively, at low temperatures between 160 and 180 °C.[III,VII] The details of these processes are presented in the Results and discussion section and in publications [III] and [VII].

3.7 Iridium

Various Ir precursors have been presented in the literature for ALD and PEALD Ir processes (Figure 10). The thermal ALD Ir processes are based on either oxidative (combustion) chemistry, reductive chemistry, or a combination of these two. The combustion processes using molecular O_2 are the most common also for the Ir ALD. In PEALD of Ir both reductive NH_3 plasma and mixed H_2 and O_2 plasma have been used. The ALD Ir processes with some key properties are listed in Tables 11–13.

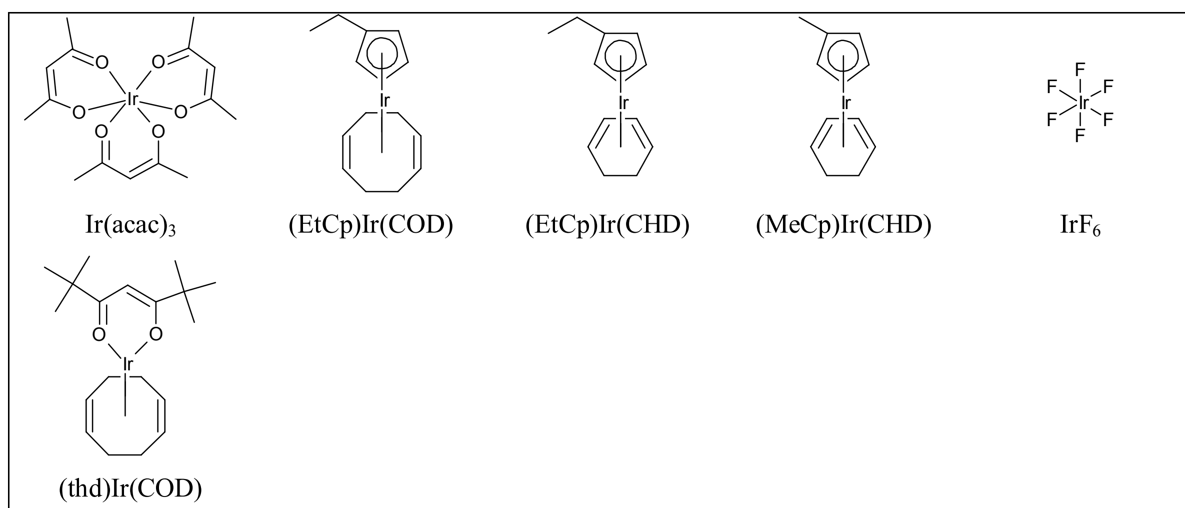

Figure 10. Iridium precursors reported for ALD and PEALD Ir processes.

Table 11. ALD and PEALD Ir processes reported in the literature.

Metal precursor		$T_{vap.}$ (°C)	Reactant	$T_{dep.}$ (°C)	Growth rate (Å $cycle^{-1}$)	Ref.
$Ir(acac)_3$		150	O_2 (air)	225–400	$0.2^{225°C}$, $0.3^{250°C}$, $0.4^{275°C}$, $0.4–0.5^{300°C}$, $0.5–0.6^{325–400°C}$	41
$Ir(acac)_3$			O_2	225	0.2	72,73
$Ir(acac)_3$			O_2	250	0.3	180
$Ir(acac)_3$		150	O_2	250	0.5	179
$Ir(acac)_3$		170	O_2	300	0.5	182
$Ir(acac)_3$		160	O_2	300	0.5	34
$Ir(acac)_3$		200	O_2	350	0.8	181
$Ir(acac)_3$		155	ozone–H_2	165–200	0.2	IV
(EtCp)Ir(COD)		100	O_2	240–420	$0.2^{240°C}$, $0.3^{270°C}$, $0.4^{300–420°C}$	55, 185
(EtCp)Ir(COD)		85	O_2	230–290	$\sim1.5^{290°C}$	186
(EtCp)Ir(COD)		85	O_2	270	1.5	187
(EtCp)Ir(COD)	PEALD	85	NH_3 plasma	270	0.4	187, 188
(EtCp)Ir(COD)	PEALD	85	NH_3 plasma	290	0.6	190
(EtCp)Ir(COD)	$PEALD^{mod.}$		H_2 plasma	240–420	$0.2^{240°C}$, $0.4^{270°C}$, $0.5^{300°C}$, $0.6^{330–360°C}$, $0.8^{390°C}$, $0.9^{420°C}$	191
(EtCp)Ir(CHD)	PEALD		mixed O_2+H_2 plasma	400–450	0.5–0.6	192
(EtCp)Ir(CHD) in ECH	PEALD		mixed O_2+H_2 plasma	360	0.5	193
(MeCp)Ir(CHD)		45–50	O_2	225–350	$0.2–0.3^{225–300°C}$, $0.3^{350°C}$	V
(MeCp)Ir(CHD)		45	ozone–H_2	120–180	0.2–0.3	VI
IrF_6		RT	molecular H_2	375–550	around $1^{temp. NA}$	194

abbreviation mod. indicates a modified ALD system what was called as a cyclic CVD-like hybrid ALD

Table 12. Impurity contents of ALD and PEALD Ir processes.

Cycle sequence	$T_{dep.}$ (°C)	Atomic composition (at.%)	Impurity contents (at.%)	Method	Ref.
$Ir(acac)_3$–O_2 (air)	225–350	Ir, O <0.5	C <0.3, H 1.0	TOF-ERDA	41
$Ir(acac)_3$–ozone–H_2	165–200	Ir 91–94, O 4–7	C 0.3–0.6, H 1–2	TOF-ERDA	IV
(EtCp)Ir(COD)–NH_3 plasma	270	Ir	C <3, N <3	AES	188
(MeCp)Ir(CHD)–O_2	225–250	Ir 90–91, O 6–7	C ≤0.8, H 2–3	TOF-ERDA	V
(MeCp)Ir(CHD)–O_2	275–300	Ir 95, O 3	C 0.6, H 1–2	TOF-ERDA	V
(MeCp)Ir(CHD)–O_2	350	Ir 96, O 3	C 0.3, H <1	TOF-ERDA	V
(MeCp)Ir(CHD)–ozone–H_2	120	Ir 81, O 12	C 1.2, H 6	TOF-ERDA	VI
(MeCp)Ir(CHD)–ozone–H_2	160	Ir 90, O 6	C 0.2, H 3.1	TOF-ERDA	VI

Table 13. Roughness and resistivity values reported for the ALD Ir processes.

Cycle sequence	$T_{dep.}$ (°C)	Thickness (nm)	Roughness (nm)	Resistivity (μΩ cm)	Ref.
$Ir(acac)_3$–O_2 (air)	300	9	0.5	18	41
$Ir(acac)_3$–O_2 (air)	225–400	~70	$1.6^{300°C}$	<12, $\sim10^{350°C}$	41
$Ir(acac)_3$–ozone–H_2	165–200	~60	1.1–1.4	11–12	IV
$Ir(acac)_3$–ozone–H_2	185	~20		16–17	IV
(EtCp)Ir(COD)–O_2	290	NA		9	186
(EtCp)Ir(COD)–NH_3 plasma	270	30	2	21	188
(EtCp)Ir(COD)–NH_3 plasma	270	>50		10	188
(EtCp)Ir(COD)–NH_3 plasma	290	3	0.4		190
(EtCp)Ir(COD)–NH_3 plasma	290	50		8.3	190
(EtCp)Ir(COD)–(mixed H_2+O_2 plasma)	400	16		16	192
(EtCp)Ir(COD)–(mixed H_2+O_2 plasma)	425	19		11	192
(EtCp)Ir(COD)–(mixed H_2+O_2 plasma)	450	14		13	192
(MeCp)Ir(CHD)–O_2	300	10		17–18	V
(MeCp)Ir(CHD)–O_2	300	16		14	V
(MeCp)Ir(CHD)–O_2	300	32		12	V
(MeCp)Ir(CHD)–O_2	225–350	40–60	$6.0^{225°C}$, $4.0^{250°C}$, $1.2^{275°C}$, $1.8^{300°C}$, $2.7^{350°C}$	8–10	V
(MeCp)Ir(CHD)–ozone–H_2	120	39	0.5	14–16	VI
(MeCp)Ir(CHD)–ozone–H_2	160	48	0.6	12–13	VI
(MeCp)Ir(CHD)–ozone–H_2	120–180	20–25	0.4	16–21	VI

The most widely applied ALD Ir process is $Ir(acac)_3$–O_2, initially reported by Aaltonen et al.,[41] who successfully achieved Ir growth between 225 and 400 °C. Lower deposition temperatures (200 °C) did not result in film growth.[41] The growth rate increased at higher deposition temperatures while partial thermal self-decomposition of $Ir(acac)_3$ was observed at 400 °C.[41] The resistivity of the films decreased between 300 and 375 °C because of the increased crystallinity of the films at higher growth temperatures.[41]

The $Ir(acac)_3$–O_2 ALD Ir process has been examined for deposition of barrier layers for copper in damascene processing.[169–171] It has been also applied in the fabrication of x-ray diffractive optics, such as Fresnel zone plates.[172–175] For UV applications, iridium wire grid polarizers[176,177] and inductive grid filters[178] have been demonstrated. Thin Ir coatings on photonic crystals can be used to modify the optical properties for near-IR wavelengths.[179] The ALD Ir on TiO_2 and Al_2O_3 coated cellulose[180] and Al_2O_3 coated fiber matrix[181] can be used for catalytic applications.

Selective area ALD has been achieved at 225 °C with the $Ir(acac)_3$–O_2 process using patterned ODS (octadecyltrimethoxysilane) and OTS (octadecyltrichlorosilane) SAM layers as masks.[72,73] The $Ir(acac)_3$–O_2 Ir films can be converted to IrO_x using potential cycling in 0.1 M H_2SO_4 and the resulting activated IrO_x films be used for pH sensing applications.[182] Also nanostructured Ir/Pt films with various stoichiometries have been presented.[183] The contents of Ir and Pt can be adjusted by using various ratios of ALD cycles for Ir and Pt.[34,183]

$Ir(acac)_3$ has however quite limited volatility whereas (EtCp)Ir(COD) and (MeCp)Ir(CHD) are higher volatility alternatives. The reported source temperatures for (EtCp)Ir(COD) (85–100 °C) and (MeCp)Ir(CHD) (45–50 °C) are considerable lower than the 150–200 °C needed for $Ir(acac)_3$ (Table 11). In addition, (EtCp)Ir(COD) is a liquid at room temperature[184] and (MeCp)Ir(CHD) melts at its source temperature[V] in contrast to solid $Ir(acac)_3$.

(EtCp)Ir(COD) has been used with molecular O_2 to deposit Ir films.[55,185–188] The films were grown in a large deposition temperature range between 230 and 420 °C.[55,185,186] The onset of Ir film growth with the (EtCp)Ir(COD)–O_2 process should be close to 230 °C as in another study[185] Ir growth was not observed below 240 °C. Using (EtCp)Ir(COD) and O_2 precursors the phase of the film (IrO_2/Ir) was controlled by the oxygen partial pressure and the deposition temperature between 230 and 290 °C.[186] This is similar to the oxygen-based ALD Ru and RuO_2 processes as shown previously. However, the most oxygen-based Ir processes have been reported to deposit only Ir metal films while IrO_x and IrO_2 growth with high O_2 partial pressures has been observed only with the (EtCp)Ir(COD)–O_2 process.[55,186] Oxidation of about 20 nm thick Ru and Ir films has been previously

compared at elevated temperatures under O_2 atmosphere and it was observed that the oxidation of Ir started at considerably higher temperatures (above 500 °C) than that of Ru (above 250 °C).[189] The higher stability of Ir under O_2 obviously explains why noble metal oxide formation in oxygen-based Ir processes is not as commonly reported as in ALD of Ru.

Surface roughnesses of the Ir films grown on Si with the (EtCp)Ir(COD)–O_2 ALD process have been found to be deposition temperature dependent, where 330−360 °C proved to be optimal for growing smooth films for the Cu diffusion barrier application.[185] In another study,[55] the smoothest and the most uniform Ir film was deposited on ALD TaN among the Si, SiO_2 and ALD TaN substrates. In this thesis, (MeCp)Ir(CHD) and O_2 were used to grow Ir films between 225 and 350 °C on ALD grown Al_2O_3.[V] The surface roughnesses of the Ir films grown with the (MeCp)Ir(CHD)–O_2 process were the highest when deposited at 225–250 °C and decreased strongly with increasing deposition temperature.[V] The similarities between the (EtCp)Ir(COD) and (MeCp)Ir(CHD) precursors might also explain the similar tendency for increased roughness at lower deposition temperatures.

PEALD Ir films have been deposited using (EtCp)Ir(COD) and NH_3 plasma at 270[187,188] and 290 °C[190]. The growth rate saturated at 270 °C to about 0.4 Å/cycle, which was substantially lower than the growth rate in the corresponding O_2-based ALD Ir process (1.5 Å/cycle).[187] The authors explained the higher growth rate in the O_2-based ALD process by the “secondary adsorption of oxygen” which simply means that the adsorbed oxygen atoms react with the precursor during the noble metal precursor pulse. (EtCp)Ir(COD) has been used also together with H_2 plasma to deposit Ir between 240 and 420 °C but the authors call this cyclic CVD-like hybrid ALD as H_2 gas was supplied also during the (EtCp)Ir(COD) pulse.[191]

In general, the PEALD Ir films are smoother than the films deposited by the O_2-based thermal ALD processes.[187,188] Furthermore, the PEALD Ir films have stronger (111) preferred orientation than the Ir films deposited by the O_2-based thermal ALD which is related to the extra energy delivered from the NH_3 plasma to the surface.[188] The momentum provided by NH_3 plasma species bombarding the surface rearranges the

deposited Ir atoms to the most stable (111) plane in the fcc structure. Too high energy (>150 W plasma power) can, however, lead to the agglomeration and non-uniform films.[188] The resistivity of the 30 nm thick PEALD Ir film grown at 270 °C was reported to be relatively high (about 21 μΩcm).[188] In contrast, in another study[190] a 50 nm thick PEALD Ir film grown at 290 °C had a resistivity of only 8.3 μΩcm.

Mixed hydrogen and oxygen plasma has been used for PEALD of Ir films as electrodes for ferroelectric random access memories (FRAMs).[192,193] The films were grown from (EtCp)Ir(CHD) at relatively high temperatures of 360 and 400–450 °C.[192,193] Similar to (EtCp)Ir(COD), also (EtCp)Ir(CHD) is a liquid at room temperature but it is more volatile.[184] When the PEALD Ir films were deposited at 400 °C and higher temperatures on an oxide coated trench patterns peeling of Ir films was reported.[192] Adhesion improved when TiAlN was applied between the substrate and the 20 nm thick PEALD Ir film. Similar peeling and adhesion problems were not reported when a lower deposition temperature (360 °C) and ECH solvent for (EtCp)Ir(CHD) were used in liquid injection PEALD.[193]

Thermal noble metal ALD processes using conventional reducing agents are scarce, but an example is the deposition of Ir thin films from IrF_6 and molecular H_2 between 375 and 550 °C.[194] No film growth took place below 375 °C and films with good uniformity were obtained at 400 °C and above. AES showed that these films were pure without any detected fluorine. The tape tests proved good adhesion of Ir films to SiO_2 and HfO_2.[194]

By combining consecutive oxidative and reductive chemistries, $Ir(acac)_3$–O_3–H_2 and (MeCp)Ir(CHD)–O_3–H_2 sequences were developed for the Ir deposition.[IV,VI] The Results and discussion section and publications [IV] and [VI] summarize these processes in detail.

In addition to the Ir precursors reported in Table 11, (thd)Ir(COD) has been applied to ALD for depositing 1–3 nm Ir nanoparticles for catalysis.[80] The (thd)Ir(COD) source temperature was 120–140 °C and the growth temperatures were between 120 and 250 °C.[80]

3.8 Iridium oxide

Ir precursors used for ALD and PEALD of iridium oxide thin films and nanodots are shown in Figure 11. These are similar to the precursors used for Ir ALD. The ALD iridium oxide thin films have been grown using either molecular oxygen[186] or ozone[I,VI] as an oxidant (Table 14). The film properties are collected to Tables 15 and 16.

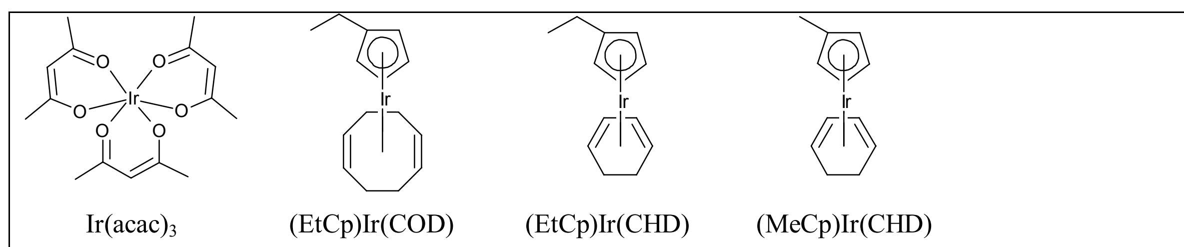

Figure 11. Iridium precursors reported for ALD iridium oxide processes.

Table 14. ALD iridium oxide processes reported in the literature.

Metal precursor	$T_{vap.}$ (°C)	Reactant	$T_{dep.}$ (°C)	Growth rate (Å $cycle^{-1}$)	Ref.
$Ir(acac)_3$	155	ozone	165–200	$0.2^{165°C}$, $0.4^{185°C}$	I
(EtCp)Ir(COD)	85	O_2	230–290	$4.7^{290°C}$	186
(MeCp)Ir(CHD)	45	ozone	100–180	$0.3^{100–120°C}$, $0.4^{140°C}$, $0.5^{160°C}$, $\sim0.6^{180°C}$	VI
(EtCp)Ir(CHD) in PEALD ECH		mixture (O_2+H_2) plasma	250	nanodots	196

Table 15. Impurity contents of ALD iridium oxide processes.

Cycle sequence	$T_{dep.}$ (°C)	At. composition (at.%)	Impurity contents (at.%)	Method	Ref.
$Ir(acac)_3$–ozone	165–175	Ir 30–31, O 64–65	C <1, H 4–4.5	ERDA	I
$Ir(acac)_3$–ozone	185	Ir 32, O 65	C <0.5, H 3.5	ERDA	I
$Ir(acac)_3$–ozone	200	Ir 37, O 60	C <0.5, H 3.2	ERDA	I
(EtCp)Ir(COD)–O_2	230		C <AES limit	AES	186
(MeCp)Ir(CHD)–ozone	120	Ir 20, O 46	C 8, H 18, (Al 7)	TOF-ERDA	VI
(MeCp)Ir(CHD)–ozone	160	Ir 31, O 62	C 2.2, H 5	TOF-ERDA	VI

Table 16. Roughness and resistivity values reported for the ALD iridium oxide processes.

Cycle sequence	$T_{dep.}$ (°C)	Thickness (nm)	Roughness (nm)	Resistivity (μΩ cm)	Ref.
$Ir(acac)_3$–ozone	185	~40		170–200	I
$Ir(acac)_3$–ozone	165	34	1.0		*a*
$Ir(acac)_3$–ozone	165	68	1.4		*a*
$Ir(acac)_3$–ozone	175	60	2.1		*a*
$Ir(acac)_3$–ozone	185	68	2.8		*a*
(EtCp)Ir(COD)–O_2	290	NA		120	186
(MeCp)Ir(CHD)–ozone	100,120	32	0.3		VI
(MeCp)Ir(CHD)–ozone	140	43	1.9		VI
(MeCp)Ir(CHD)–ozone	160	51	3.0	~200	VI
(MeCp)Ir(CHD)–ozone	180	57	4.0		VI

a unpublished surface roughness data

In a study with (EtCp)Ir(COD) and molecular O_2, the phase of the film being deposited (IrO_2/Ir) could be controlled by the oxygen partial pressure and the deposition temperature between 230 and 290 °C.[186] This is similar to the RuO_2 ALD as described earlier. However, a thin Ir layer formed at the interface between the IrO_2 film and SiO_2 in the (EtCp)Ir(COD)–O_2 ALD IrO_2 process at the examined temperature range.[186] The interfacial Ir layer was eliminated only by decreasing the deposition temperature to 230 °C while increasing the deposition pressure (3 Torr) and oxygen partial pressure [O_2/(O_2+Ar) ratio 100 %]. Thus a critical oxygen pressure was reached for the transition from Ir to IrO_2.[186] The growth rate of the (EtCp)Ir(COD)–O_2 IrO_2 process at 290 °C was about 4.7 Å/cycle, which was noted to be about three times higher than the growth rate of Ir films (1.5 Å/cycle) at the same temperature.[186]

(EtCp)Ir(COD) has also been used with O_2 to grow IrO_2-TiO_2 by mixing with the titanium isopropoxide–NH_3 ALD cycles for TiO_2.[195] The resistivity of the IrO_2-TiO_2 was controlled from 1500 to 357 μΩcm by tuning the IrO_2:TiO_2 ratio. These mixed films could be suitable as heating resistor materials for non-passivated thermal inkjet printheads.[195] In addition, (EtCp)Ir(CHD) and a mixture of oxygen and hydrogen plasma have been used for PEALD of IrO_2 nanodots for charge-trap flash-memory devices.[196]

With ozone-based chemistry, iridium oxide films were obtained between 165 and 200 °C when $Ir(acac)_3$ was used as the Ir precursor.[I] The films grown above 200 °C were metallic

while the low temperature limit (165 °C) of the ALD process was set by the $Ir(acac)_3$ sublimation temperature (155 °C). The (MeCp)Ir(CHD) precursor sublimes at a substantially lower temperature (45 °C) and thus iridium oxide films could be deposited at as low temperatures as 100 °C.[VI] The iridium oxide films deposited by the (MeCp)Ir(CHD)–O_3 process at 100 and 120 °C were x-ray amorphous with considerably lower film density compared to the crystalline IrO_2 films grown at higher temperatures.[VI]

The IrO_2 films grown with the $Ir(acac)_3$–O_3 process have been applied for pH sensors as pH sensitive layers on native oxide covered Ti conductor.[197] Also Ti microelectrode arrays were coated with biocompatible IrO_2 and examined for stem cell research.[198] $Ir(acac)_3$–O_3 process has also been used in making IrO_2 nanotubes.[199] The IrO_2 film was first deposited directly on PVP fiber at 165 °C and then the sample was calcined at 500 °C to combust PVP fiber support and form hollow IrO_2 nanotubes.[199]

An alternative method for obtaining iridium oxide would be the oxidation of the ALD Ir films by potential cycling in 0.1 M H_2SO_4.[182] The oxidation of Ir to IrO_x is associated with a significant volume expansion. Such films on anodized Al_2O_3 templates were used for pH sensing and a further study on using IrO_x in neural stimulation applications was expected.[182] In addition, surfaces of PEALD Ir films were oxidized by treating with O_2 plasma and annealing to enhance the dielectric constant of TiO_2 grown on top for DRAM capacitors.[200] The enhancement was expected to be related to the structural compatibility between IrO_2 and TiO_2.[200] ALD grown Ir film can be oxidized to IrO_2 also by annealing under O_2.[189] The oxidation of about 20 nm thick Ir film to tetragonal IrO_2 started above 500 °C and was complete above 850 °C.[189]

3.9 Palladium and palladium oxide

ALD Pd processes have been based solely on a single Pd precursor, namely $Pd(hfac)_2$, though suitability of some other precursors has also been examined (Figure 12). Different from the other ALD noble metal processes the Pd processes rely mostly on true reducing agents rather than on the most common molecular oxygen. Glyoxylic acid, molecular H_2, and most commonly formalin have been used to deposit Pd films. PEALD of Pd with H_2

plasma has also been widely explored. The developed Pd metal and oxide ALD and PEALD processes and their properties are listed in Tables 17–19.

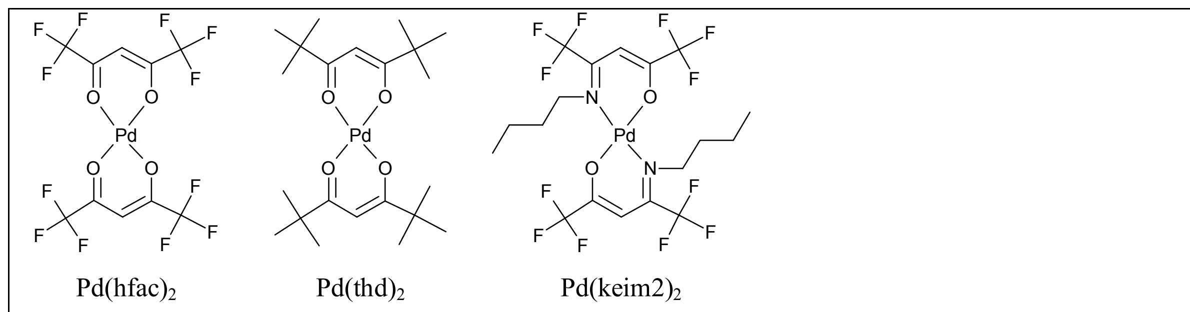

Figure 12. Palladium precursors reported for ALD and PEALD of Pd and PdO.

Table 17. ALD and PEALD processes of Pd and PdO reported in the literature.

Metal precursor		$T_{vap.}$ (°C)	Reactant	$T_{dep.}$ (°C)	Growth rate (Å $cycle^{-1}$)	Ref.
Pd metal						
$Pd(hfac)_2$		60	glyoxylic acid	210	seed layer	201
$Pd(hfac)_2$		50	H_2	80, 130	$0.2–0.3^{80°C}$, $0.1^{130°C}$	201
$Pd(hfac)_2$		48	H_2	80	0.2–0.3	202
$Pd(hfac)_2$		50	H_2	100	0.2	203
$Pd(hfac)_2$		50	formalin	200	0.2–0.3	42
$Pd(hfac)_2$			formalin	200	0.2–0.3	88
$Pd(hfac)_2$	PEALD	48	H_2 plasma	80	0.5	202
$Pd(hfac)_2$	PEALD	48	H_2 plasma	80	0.1–0.3	206
$Pd(hfac)_2$	PEALD	46	H_2 plasma	80	0.3	210
$Pd(hfac)_2$	PEALD	46	H_2 plasma	80	0.1–0.2	207
$Pd(hfac)_2$	PEALD	48	H_2 plasma	85	0.3	208,209
$Pd(hfac)_2$	PEALD	48	H_2/N_2 plasma	80	0.3–0.4	211
$Pd(hfac)_2$	PEALD	50	H_2 plasma	100	0.2	203
$Pd(keim2)_2$		60	O_2	250–275	$0.6^{250°C}$	47
$Pd(thd)_2$		130	O_2	250–275	non-uniform films	56
$Pd(thd)_2$			O_2 (air)	180	nanoparticles	82
$Pd(thd)_2$		120	ozone–H_2	130–160	non-uniform films	VII
Pd oxide						
$Pd(thd)_2$		120	ozone	130–160	$0.1^{130°C}$, $0.2^{140–160°C}$	VII

Table 18. Impurity contents of ALD and PEALD of Pd and PdO films.

Cycle sequence	$T_{dep.}$ (°C)	Elemental contents (at.%)	Method	Ref.
Pd metal				
$Pd(hfac)_2$–formalin	200	no impurities in thicker films, F < det. limit on 42 nm film	XPS	42
$Pd(hfac)_2$–formalin	200	O, F < det. limit	AES	90
$Pd(hfac)_2$–H_2 plasma	85	negligible F	XPS	208
$Pd(keim2)_2$–O_2	250	O 1.0, C 0.5, H 0.3, F 0.1, N 0.1	TOF-ERDA	47
$Pd(thd)_2$–ozone–H_2	130	O 0.3, C 0.2, H <0.2	TOF-ERDA	VII
$Pd(thd)_2$–ozone–H_2	150	O ~3.5, C ~0.4, H ~1.6	TOF-ERDA	VII
Pd oxide				
$Pd(thd)_2$–ozone	130	Pd 39, O 49, C 0.4, H 7	TOF-ERDA	VII
$Pd(thd)_2$–ozone	150	Pd 47, O 48, C <0.2, H 3	TOF-ERDA	VII

Table 19. Roughness and resistivity values reported for the ALD and PEALD processes of Pd and PdO.

Cycle sequence	$T_{dep.}$ (°C)	Thickness (nm)	Roughness (nm)	Resistivity (μΩ cm)	Ref.
Pd metal					
$Pd(hfac)_2$–formalin	200	42	4.2	14	42
$Pd(hfac)_2$–formalin	200	4		37	42
$Pd(hfac)_2$–H_2 plasma	80	2	$2.1^{\text{on Si}}$		206
$Pd(hfac)_2$–H_2 plasma	80	4	$0.4^{\text{on W}}$		206
$Pd(hfac)_2$–H_2 plasma	80	3	0.1		210
$Pd(hfac)_2$–H_2 plasma	80	3	0.5		207
Pd oxide					
$Pd(thd)_2$–ozone	130	23	0.9	~300 000	VII
$Pd(thd)_2$–ozone	140	42	1.8	21 000	VII
$Pd(thd)_2$–ozone	150	42	1.3	21 000	VII
$Pd(thd)_2$–ozone	160	43	2.8	27 000	VII

Glyoxylic acid was used as a reducing agent for $Pd(hfac)_2$ in making a Pd seed layer on tetrasulfide SAM at 210 °C where the glyoxylic acid becomes unstable and dissociates to CO_2 and H_2CO.[201] After depositing the seed layer, the growth was continued with molecular H_2 instead of glyoxylic acid and by decreasing the deposition temperature from 210 to 80 °C. Pd films were also deposited on Ir surfaces using H_2 at 80 and 130 °C.[201] In another study,[202] very thin Pd films (2–3 nm) were grown using $Pd(hfac)_2$ and H_2 at 80 °C

on air-exposed Ta (TaO_x) while only a chemisorbed $Pd(hfac)_2$ layer formed on SiO_2. ALD growth of Pd from $Pd(hfac)_2$ and H_2 has also been initiated at 100 °C on EBID (electron beam induced deposition) grown Pt[219] and ALD grown Pt nanoparticles[203].

Also formalin has been used successfully in Pd thin film deposition from $Pd(hfac)_2$.[42] Formalin consists of 37 % formaldehyde (HCOH) in water with additional 10–15 % methanol (CH_3OH) to inhibit the formation of polymerized paraformaldehyde. The nucleation of Pd using formalin was effective only at 200 °C, not at 100 °C. The thermal stability of $Pd(hfac)_2$ (230 °C) restricted the use of higher temperatures. $Pd(hfac)_2$ and formaldehyde were used at 200 °C also to coat porous anodic aluminum oxide substrates with conformal 2 nm thick Pd films for hydrogen sensing applications.[204,205]

Elam et al.[42] have examined the nucleation of Pd on Al_2O_3 surfaces using H_2, methanol, ethanol, isopropanol [$(CH_3)_2CHOH$], acetone [$(CH_3)_2CO$], TMA [$Al(CH_3)_3$], and formalin. Several oxidation agents, such as hydrogen peroxide, H_2O, oxygen, and ozone were also tested in order to grow PdO films to be then reduced by H_2 to the metallic form. Only formalin was found to effectively nucleate ALD Pd on Al_2O_3. H_2 did not nucleate Pd growth on Al_2O_3 even after several hundred $Pd(hfac)_2$–H_2 cycles between 100 and 200 °C. However, once Pd nucleated with formalin, either formalin or H_2 could be used for subsequent Pd ALD growth at 100 and 200 °C with identical growth rates. Films thicker than 20 nm were noted to be partially removed from the substrates in the tape test.

H_2 plasma has been used to grow Pd films by PEALD from $Pd(hfac)_2$. Films were deposited on iridium,[206,207] tungsten,[206,207] silicon,[206] SiO_2,[202] and TaO_x[202] surfaces at 80 °C, and on TaN[208–210] at 80–85 °C. The nucleation of PEALD Pd varied on different substrates, but the nucleation delays were estimated to be less than 100 cycles on Ir, W, and Si surfaces.[206] Pd films were deposited at 80 °C using $Pd(hfac)_2$ and H_2/N_2 plasma on air-exposed, annealed poly(p-xylylene) (PPX, Parylene-N) and air-exposed Si.[211] The H_2/N_2 plasma creates on the PPX reactive $–NH_2$ surface groups that enable the chemisorption of the precursor which, in turn, enables the growth.[211] The mixture of hydrogen and nitrogen was optimized to ensure enough free hydrogen atoms arriving at the surface for ligand removal and Pd reduction, while at the same time keeping the

hydrogen atom flux low enough to minimize the degradation of the PPX. All attempts to deposit Pd on PPX using only H_2 plasma resulted in the complete etching of the PPX film.

In the $Pd(hfac)_2$–H_2 plasma PEALD process the reactive atomic hydrogen from the plasma serves as the reducing agent during the initial Pd monolayer growth.[206] Depending on the substrate, the H_2 plasma either enables deposition (i.e. oxide-terminated W and Si) or enhances deposition by providing reactive H species to the surface for scavenging organic ligands and for reducing the Pd^{2+}. Once a uniform catalytic Pd has been deposited on the surface, the deposition rate per cycle stabilizes since the fresh Pd surface dissociates also H_2 molecules.

The PEALD $Pd(hfac)_2$–H_2 plasma process has been used to grow Pd nucleation layers between TaN barrier and Cu in the interconnect technology.[208–210,212] PEALD of Pd has been applied also on Ir and W surfaces before Cu metallization.[207,212] Both electroless deposition[207,210,212] and direct electroplating[208,209] were used to deposit Cu on the PEALD grown Pd. The PEALD $Pd(hfac)_2$–H_2 plasma process has also been used to deposit Pd nanoparticles which were then selectively coated with ALD grown Pt for synthesis of supported bimetallic core/shell nanoparticles.[203]

Oxygen-based Pd ALD processes using either an β-ketoiminato, $Pd(keim2)_2$, or $Pd(thd)_2$ have been examined with limited success.[47,56] Pd films were grown with the $Pd(keim2)_2$–O_2 process at 250 and 275 °C on Al_2O_3,[47,56] but thermal self-composition of $Pd(keim2)_2$ as well as increasing growth rate with increasing $Pd(keim2)_2$ pulse length were observed at 250 °C.[47] The adhesion of Pd films to Al_2O_3 was noted to be poor, but was improved when an Ir film was used as the starting surface.[47] The increase of the O_2 flow rate from 20 to 40 sccm at 275 °C led to milky-like films with very rough surfaces.[47] Regardless these limitations of $Pd(keim2)_2$, the Pd films grown at 250 °C were uniform and had low impurity contents.[47,56]

$Pd(thd)_2$ was examined with O_2 at 250–275 °C but the resulting films were non-uniform.[56] $Pd(thd)_2$ was suggested to possibly etch the as-deposited Pd film at those temperatures. Pd nanoparticles have been grown at a lower temperature (180 °C) on porous carbon with

extended $Pd(thd)_2$ exposures (4 × 6 h) followed by removal of the ligands by synthetic air at 180 °C.[82] The resulting catalyst consisted of metallic palladium but contained also palladium oxide (PdO_2) according to XPS and XRD.[82]

$Pd(thd)_2$ has also been also applied in the consecutive oxidation and reduction scheme at low temperatures.[VII] Pd films were deposited between 130 and 160 °C using the $Pd(thd)_2$–O_3–H_2 process on in-situ grown Al_2O_3. Non-uniform films with considerably high growth rates were grown which was suggested to result from the formation of Pd-hydride.[VII] Similarly, PdO films were deposited from $Pd(thd)_2$ and O_3 between 130 and 160 °C on in-situ grown Al_2O_3 but without the non-uniformity issues met in the Pd metal growth.[VII] Both the $Pd(thd)_2$–O_3 and $Pd(thd)_2$–O_3–H_2 processes are discussed in the Results and discussion section as well as in the reference [VII].

It should be noted that several oxidation agents have been previously screened for PdO deposition from $Pd(hfac)_2$, such as H_2O_2, H_2O, O_2 and ozone.[42] However, no film growth on Al_2O_3 was achieved with any of these reactants.[42] The lack of a film growth with ozone shows a drastic difference between the fluorinated $Pd(hfac)_2$ and the non-fluorinated $Pd(thd)_2$ β-diketonates (Figure 12). More generally, no such O_2 or ozone -based ALD noble metal processes are known where the metal precursors would contain fluorine. The only exception is $Pd(keim2)_2$ which was already shown decomposing at the examined deposition temperature.[47]

3.10 Platinum and platinum oxide

Pt processes are the most important ALD noble metal processes together with the ALD Ru and Ir processes because of the wide applicability of Pt. Surprisingly enough, both thermal ALD and PEALD of Pt have relied nearly exclusively on a single platinum precursor, $MeCpPtMe_3$ (Figure 13 and Table 20). Some of the key properties of the films are presented in Tables 21 and 22.

Table 20. ALD and PEALD processes of Pt and PtO_x reported in the literature.

Metal precursor		$T_{vap.}$ (°C)	Reactant	$T_{dep.}$ (°C)	Growth rate (Å $cycle^{-1}$)	Ref.
Pt metal						
$MeCpPtMe_3$		RT	O_2	200–300	$0.3^{200°C}$, $0.4^{225°C}$, $0.5^{250–300°C}$	47
$MeCpPtMe_3$		70	O_2	200–300	$0.1^{200°C}$, $0.4^{225–250°C}$, $0.5^{300°C}$	225,226
$MeCpPtMe_3$		70	O_2	150–450	$0.1^{200°C}$, $0.4^{225–250°C}$, $0.5^{\geq 300°C}$	36
$MeCpPtMe_3$		65	O_2	245, 295	0.5	108
$MeCpPtMe_3$		RT	O_2 (air)	250, 300, 350	$0.5^{300°C}$	213
$MeCpPtMe_3$		48	O_2	250	0.5	68
$MeCpPtMe_3$			O_2	260–340	0.5^{NA}	60
$MeCpPtMe_3$			O_2	270	0.3	217
$MeCpPtMe_3$			O_2	270	0.4	221
$MeCpPtMe_3$		70	O_2	270, 300	0.4	215
$MeCpPtMe_3$		40	O_2	300	0.5	52
$MeCpPtMe_3$			O_2	300	0.4	49
$MeCpPtMe_3$			O_2	300	0.3–0.5	48
$MeCpPtMe_3$			O_2	300	0.4	219
$MeCpPtMe_3$		30	O_2	300	0.5	203
$MeCpPtMe_3$		50	O_2	300	0.5	183
$MeCpPtMe_3$			O_2	300	0.5	31
$MeCpPtMe_3$		40	O_2	300	0.6	34
$MeCpPtMe_3$		65	O_2 (air)	310	0.4	75
$MeCpPtMe_3$		60	O_2	330	0.4	218
$MeCpPtMe_3$		70	O_2–H_2	300	0.3	36
$MeCpPtMe_3$	PEALD	30	O_2 plasma	150–350	0.5	43
$MeCpPtMe_3$	PEALD	70	O_2 plasma	200, 300	0.5	225,226
$MeCpPtMe_3$	PEALD		O_2 plasma	200		96
$MeCpPtMe_3$	PEALD	70	O_2 plasma	300	0.5	96
$MeCpPtMe_3$	PEALD	70	O_2 plasma	300	0.5–1.1	36
$MeCpPtMe_3$	PEALD	30	NH_3 plasma	150–350	$0.2^{150°C}$, $0.3^{200°C}$, $0.4^{250–300°C}$, $0.5^{350°C}$	43
$MeCpPtMe_3$	PEALD	30	N_2 plasma	150–350	$0.1^{150°C}$, $0.2^{200°C}$, $0.3^{250–300°C}$, $0.4^{350°C}$	43
$MeCpPtMe_3$	PEALD	70	O_2 plasma–H_2	100	0.4	226
$Pt(acac)_2$		110	ozone–H_2	120–130	0.3	VII
$Pt(acac)_2$		110	ozone	140–200	$0.5^{140°C}$, $0.6^{150–170°C}$, $0.7^{200°C}$	II
Pt oxide						
$MeCpPtMe_3$	PEALD	70	O_2 plasma	100–300	$0.6^{100–200°C}$, $0.5^{300°C}$	225,226
$Pt(acac)_2$		110	ozone	120, 130	$0.3^{120°C}$, $0.5^{130°C}$	II

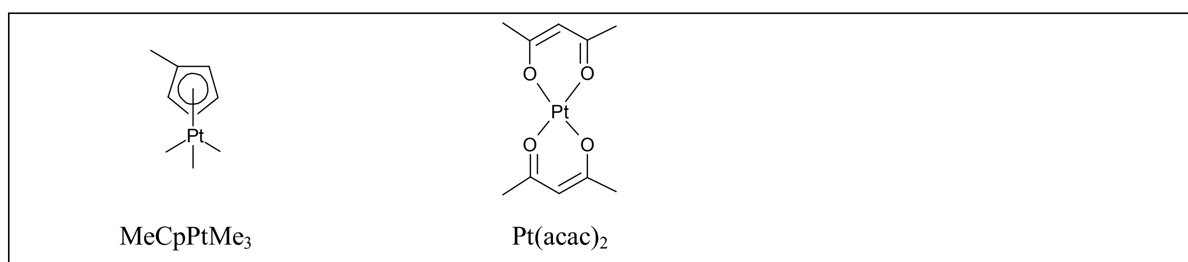

Figure 13. Platinum precursors reported in Pt metal and oxide processes by ALD and PEALD.

Table 21. Impurity contents of Pt and PtO_x films grown by ALD and PEALD.

Cycle sequence	$T_{dep.}$ (°C)	At. composition (at.%)	Impurity contents (at.%)	Method	Ref.
Pt metal					
$MeCpPtMe_3$–O_2 (air)	300	Pt	O 1–2, C 0.5–1, H 0.5–1	TOF-ERDA	213
$MeCpPtMe_3$–O_2	250, 300	Pt	O <0.3, C <0.3, H <0.3	TOF-ERDA	47
$MeCpPtMe_3$–O_2	200	Pt	O <0.5, C <0.5, H <0.5	TOF-ERDA	47
$MeCpPtMe_3$–O_2	245, 295	Pt	no contaminants (<0.1 det. limit)	XPS	108
$MeCpPtMe_3$–O_2 (air)	310	Pt	no contaminants (0.1% det. limit)	XPS	75
$MeCpPtMe_3$–O_2	300	Pt ~90	O 1, C ~2.5, Ta 5	AES	49
$MeCpPtMe_3$–O_2	300	Pt 98	O 2	XPS	219
$MeCpPtMe_3$–O_2	300	Pt	<1% for any impurities present	XPS	96
$MeCpPtMe_3$–O_2	300	Pt 100	O <5, C <5	RBS	225,226
$MeCpPtMe_3$–O_2 plasma	300	Pt 100	O <5, C <5	RBS	225,226
$MeCpPtMe_3$–O_2 plasma	150, 300	Pt	O, C, N <XPS det. limit	XPS	43
$MeCpPtMe_3$–NH_3 plasma	250, 300	Pt	O, C, N <XPS det. limit	XPS	43
$MeCpPtMe_3$–N_2 plasma	250, 300	Pt	O, C, N <XPS det. limit	XPS	43
$MeCpPtMe_3$–O_2 plasma–H_2	100	Pt	O <5, C <5	RBS	226
$Pt(acac)_2$–ozone–H_2	120–130	Pt >98	O <1, C <0.5, H <0.5	TOF-ERDA	VII
$Pt(acac)_2$–ozone	140–150	Pt 94	O 6, C <0.5, H <0.7	ERDA	II
$Pt(acac)_2$–ozone	200	Pt 91	O 8, C <0.5, H 0.4	ERDA	II
Pt oxide					
$MeCpPtMe_3$–O_2 plasma	300	Pt 31, O 69	C <5	RBS	225,226
$Pt(acac)_2$–ozone	120	Pt 37–39, O 48–49	C <0.5, H 13	ERDA	II
$Pt(acac)_2$–ozone	130	Pt 35, O 55	C <0.5, H 10	ERDA	II

Table 22. Roughness and resistivity values reported for the ALD and PEALD processes of Pt and PtO_x.

Cycle sequence	$T_{dep.}$ (°C)	Thickness (nm)	Roughness (nm)	Resistivity (μΩ cm)	Ref.
Pt metal					
$MeCpPtMe_3$–O_2 (air)	300	50	4.0		213
$MeCpPtMe_3$–O_2 (air)	300	110	17	12	213
$MeCpPtMe_3$–O_2 (air)	310	11.2	2.8		75
$MeCpPtMe_3$–O_2 (air)	310	18.3	1.8	41.9	75
$MeCpPtMe_3$–O_2 (air)	310	30.2	1.5	16.3	75
$MeCpPtMe_3$–O_2	200	30	0.8	17	47
$MeCpPtMe_3$–O_2	250	45	0.8		47
$MeCpPtMe_3$–O_2	300	50	1.2	13	47
$MeCpPtMe_3$–O_2	300	25	0.5		48
$MeCpPtMe_3$–O_2	245	1.2–15	1		108
$MeCpPtMe_3$–O_2	300	10		18	49
$MeCpPtMe_3$–O_2	300	12.7	0.8		49
$MeCpPtMe_3$–O_2	300	20		14	49
$MeCpPtMe_3$–O_2	300	39		13.1	49
$MeCpPtMe_3$–O_2	300	35		11	219
$MeCpPtMe_3$–O_2	270, 300	20	0.6–0.7	13.2	215
$MeCpPtMe_3$–O_2		10		37	60
$MeCpPtMe_3$–O_2		15–50		12–14	60
$MeCpPtMe_3$–O_2		≤50	0.6–0.9		60
$MeCpPtMe_3$–O_2	300	27	0.7	13	225,226
$MeCpPtMe_3$–O_2 plasma	300	29	0.4	15	225,226
$MeCpPtMe_3$–NH_3 plasma	250	48		12	43
$MeCpPtMe_3$–O_2 plasma–H_2	100	22		19	226
$Pt(acac)_2$–ozone–H_2	120	52	2.3	13–14	VII
$Pt(acac)_2$–ozone–H_2	130	54	2.0	12–13	VII
$Pt(acac)_2$–ozone	140	110		11	II
Pt oxide					
$MeCpPtMe_3$–O_2 plasma	300	27	0.4	$>1\times10^8$	225,226
$Pt(acac)_2$–ozone	130	50–60	0.5	$1.5–5\times10^6$	II,VII

Initially Pt films were grown by ALD with $MeCpPtMe_3$ and air at 300 °C.[213] $MeCpPtMe_3$ showed signs of thermal self-decomposition at 350 °C and to a much lesser extent also at 300 °C. Only very thin films grew at 250 °C with air[213] whereas pure O_2 decreased the low deposition temperature limit to 200 °C.[47,214] At even lower temperatures (<200 °C) the precursor ligands were not removed during the O_2 pulse causing a lack of Pt growth.[214] At 300 °C Pt films have been deposited at 300 °C with similar growth rates regardless which

reactant, air or pure O_2, is used.[47] Pure O_2 led, however, to smoother films with better adhesion properties.[47,213] When H_2 was added to the reaction sequence after the O_2 pulse, the growth rate decreased from 0.5–0.6 Å/cycle to 0.3 Å/cycle at 300 °C.[36] H_2 removes oxygen from the Pt surface and thus $MeCpPtMe_3$ upon adsorption does not undergo combustion reactions with surface oxygen.

ALD Pt films have been grown on various substrates, such as Al_2O_3,[213,215] ZrO_2,[215] SiO_2,[75,108,215,216] borosilicate glass,[213] native oxide covered Si,[60,213] Si,[60,216] GaN,[217] and in-situ grown TaN_x[49]. Shrestha et al.[60] reported that the nucleation and adhesion may be poor on bare Si surfaces, even on native oxide covered Si. On HF cleaned Si surfaces at 300 °C nucleation of Pt has been shown to be significantly retarded while Pt grows more readily on SiO_2.[216] Pt films have been deposited also on metals such as Ru, Au, and W.[108,218]

Mackus et al.[48,219] have grown Pt selectively at 300 °C by using low O_2 pressure (0.02 Torr) and EBID grown Pt seeds. The low O_2 pressure caused growth retardation on an oxide surface while growth initiated readily on the EBID Pt seeds. A 0.5 nm thick Pt seed layer was sufficient to initiate Pt ALD growth but such thin seeds resulted in a nucleation delay.[48] The selective ALD growth of Pt on EBID patterned seed layers is interesting for nanopatterning and making contacts as demonstrated by contacting multi-walled carbon nanotubes.[219] Low O_2 pressure (0.0075 Torr) has also been used to deposit Pt selectively on Pd nanoparticles to obtain supported core/shell bimetallic nanoparticles.[203]

Nanostructured Pt films have been deposited for glucose sensing applications.[183] ALD Pt nanoparticles were grown on WC for the oxygen reduction reaction catalysis[220] and on TiO_2 for photocatalysis.[214] ALD Pt has been grown as well onto carbon nanotube arrays and on yttria-stabilized zirconia for fuel cell applications.[68,75] Pt nanotubes have been also prepared using nanoporous anodic aluminum oxide templates.[60] Ordered nanopillar arrays were coated with Pt for MOSFET applications.[221]

Pt nanoparticles have been deposited from $MeCpPtMe_3$ and O_2 on materials such as plasma and acid treated carbon nanotubes,[63,64] acid treated carbon cloth,[64] carbon aerogels,[35] $SrTiO_3$ single crystal surfaces[52] and nanocubes,[222] silicon nanowires,[223] and

silica gel.[224] Ru-Pt nanoparticles were grown on Al_2O_3.[137] Also ALD films of Pt-Ru[108] and Pt-Ir[34,183] with varying compositions have been deposited.

PEALD Pt films have been grown using $MeCpPtMe_3$ and either O_2, NH_3, or N_2 plasmas at a temperature range between 150 and 350 °C.[43] The Pt films grown with $MeCpPtMe_3$–O_2 plasma process showed constant growth rate of 0.4–0.5 Å/cycle between 150 and 300 °C whereas the growth rates of the Pt films deposited with $MeCpPtMe_3$–NH_3 and $MeCpPtMe_3$–N_2 plasma processes increased with increasing deposition temperatures. On SiO_2, the N_2 and NH_3 plasma Pt processes did not show any nucleation delay while the $MeCpPtMe_3$–O_2 plasma process did not lead to any growth after 100 growth cycles and the delayed nucleation was associated to the relatively low O_2 pressures used.[43] The PEALD Pt films deposited with the O_2, NH_3, and N_2 plasma processes were pure and besides surface contamination did not contain any O, C, and N impurities according to the XPS measurements.[43]

Studies on ALD of platinum oxide have been much more limited than ALD of Pt metal. Platinum oxide films have been grown by both thermal ALD with ozone[II] and PEALD with oxygen plasma.[225,226] Knoops et al.[225,226] deposited PEALD PtO_2 films between 100 and 300 °C using $MeCpPtMe_3$ and O_2 plasma. At 200–300 °C the length of the O_2 plasma pulse determined whether Pt (0.5 s) or PtO_2 (5 s) was grown.[225,226] The outcome can depend also on the other deposition parameters and reactor design as also Pt metal has been grown with similar long plasma exposures.[43,96] Already 4–5 nm thick PEALD Pt films grown on Al_2O_3 with O_2 plasma were nearly continuous and conformal,[96] which indicated faster nucleation compared to the O_2-based thermal ALD chemistry. Formation of PtO_x nanoclusters has been suggested to enhance the nucleation and growth by providing more oxygen to react with the platinum precursor.[96]

Knoops et al.[226] have also shown that a H_2 exposure step after the O_2 plasma deposits Pt metal with good material properties at a very low growth temperature of 100 °C. The H_2 pulse was suggested to remove O and C impurities from the film. As an example, the PEALD Pt film grown from $MeCpPtMe_3$ and O_2 plasma at 200 °C had a resistivity of about 500 μΩcm while the PEALD Pt process with H_2 [$MeCpPtMe_3$–O_2 plasma–H_2 gas]

at 100 °C lower growth temperature resulted in more conductive film (resistivity 19 μΩcm).[226] When the PEALD Pt film grown at 200 °C was exposed to H_2 plasma after the deposition, the resistivity was lowered to only 61 μΩcm. This shows the benefit of using H_2 gas in every deposition cycle instead of reductive post-treatments.

Amorphous platinum oxide films have been grown by thermal ALD from $Pt(acac)_2$ and ozone but only at a narrow deposition temperature range between 120 and 130 °C.[II] At these temperatures the $Pt(acac)_2$–O_3–H_2 pulsing sequence resulted in metallic Pt films with good film purity.[VII] Metallic Pt films were also deposited using ozone at 140 °C and above.[II] These ALD processes are covered in detail later in the Results and discussion section and in references [II] and [VII].

3.11 Silver

A combination of low thermal stability and insufficient volatility of many Ag precursor candidates makes the development of ALD Ag processes particularly demanding. This is especially problematic when considering thermal ALD. Some Ag precursors (Figure 14) have been successfully applied for PEALD of Ag films. These precursors contain either phosphine adducts or fluorinated ligands, some even both. Notably, such ligands are not popular in other noble metal ALD processes as seen in the previous chapters. While PEALD with H_2 plasma has been needed to grow Ag films, thermal ALD has been limited to Ag nanoparticle growth only (Table 23). Tables 24 and 25 summarize the impurity contents, surface roughnesses, and resistivities reported for PEALD Ag films.

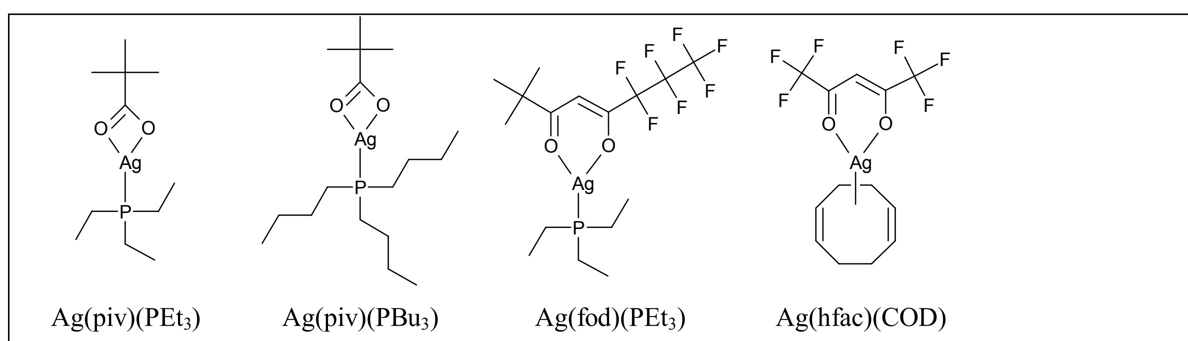

Figure 14. Silver precursors studied for PEALD and ALD Ag processes.

Table 23. PEALD and ALD Ag processes reported in the literature.

Metal precursor		$T_{vap.}$ (°C)	Reactant	$T_{dep.}$ (°C)	Growth rate (Å $cycle^{-1}$)	Ref.
$Ag(piv)(PEt_3)$	PEALD	125	H_2 plasma	140	1.2	227
$Ag(fod)(PEt_3)$	PEALD	106	H_2 plasma	120–150	$0.3^{120\,°C}$, $0.4^{>120\,°C}$	228
Ag(hfac)(COD)		50	propanol	110–150	nanoparticles	231

Table 24. Elemental compositions of PEALD Ag films.

Cycle sequence	$T_{dep.}$ (°C)	Elemental contents (at.%)	Method	Ref.
$Ag(piv)(PEt_3)$–H_2 plasma	140	Ag, O 10, C 1.0, H 5.0, P 4.0, (Si 4.0)	TOF-ERDA	227
$Ag(fod)(PEt_3)$–H_2 plasma	120	Ag 85, O 3, C 3, H 7, P 0.9, F 0.5, N 0.7	TOF-ERDA	228

Table 25. Roughness and resistivity values reported for the PEALD Ag processes.

Cycle sequence	$T_{dep.}$ (°C)	Thickness (nm)	Roughness (nm)	Resistivity (μΩ cm)	Ref.
$Ag(piv)(PEt_3)$–H_2 plasma	140	40		6	227
$Ag(fod)(PEt_3)$–H_2 plasma	120	17	4.8		228
$Ag(fod)(PEt_3)$–H_2 plasma	120	30	5.4		228
$Ag(fod)(PEt_3)$–H_2 plasma		22		6–8	228

PEALD was applied to deposit Ag films first with $Ag(piv)(PEt_3)$ [(2,2-dimethylpropionato) silver(I)triethylphosphine, $Ag(O_2C^tBu)(PEt_3)$] (Figure 14) and hydrogen radicals at 140 °C on glass and Si.[227] The onset of the thermal decomposition of the silver precursor was about 160 °C. A similar butyl phosphine compound, $Ag(piv)(PBu_3)$, resulted in visually dark, highly resistive films with slow growth.[227] Although both $Ag(piv)(PBu_3)$ and $Ag(piv)(PEt_3)$ left considerable (25–30 %) residues in normal-pressure TGA measurements, both compounds sublimed under vacuum without decomposition. The Ag films grown from $Ag(piv)(PEt_3)$ and H_2 plasma were very rough (XRR roughness >8 nm) and contained quite a high amount of impurities. Furthermore, the Ag films were speculated not to cover fully the substrate because about 4 at.% Si was found in TOF-ERDA (Table 24), most likely originating from the substrate. Despite the

high impurity contents and roughnesses a resistivity as low as 6 μΩcm was measured for about 40 nm thick Ag film. Attempts to deposit Ag by thermal ALD using molecular H_2 were not successful.[227]

Ag films have also been deposited using Ag(fod)(PEt_3) and H_2 plasma between 120 and 150 °C on soda lime glass and native silicon oxide surfaces.[228] In TGA Ag(fod)(PEt_3) left a residue of only 6 % while Ag(thd)(PEt_3), Ag(fod), Ag(piv), Ag(piv)(PEt_3), and Ag(hfac)(PMe_3) were found to decompose as concluded from the high residue masses that were close to the silver contents of the compounds.[228] With Ag(fod)(PEt_3) and H_2 plasma ALD-type saturative growth was achieved between 120 and 140 °C while the thickness non-uniformity increased at higher temperatures. This was noted to be indicative of thermal decomposition of the precursor. Up to 30 nm thick Ag films showed good adhesion by passing the Scotch tape test while Ag films thinner than 10 nm were non-continuous according to SEM. In the following study[229] the PEALD Ag process was examined on 60:1 aspect ratio trench structures but conformality was limited most likely because of a fast recombination of hydrogen radicals on a silver surface.

As an alternative silver precursor a homoleptic N,N′-dialkylacetamidinato compound was mentioned in a paper[230] where several new ALD metal processes for Fe, Co, Ni and Cu were presented using the corresponding metal acetamidinate precursors and molecular H_2. Unfortunately, no deposition data was reported for Ag films, although vapour pressure of the compound seems quite similar to the other metal acetamidinates.[230]

Although the deposition of Ag films by thermal ALD has proved to be difficult, the use of LIALD for growth of Ag nanoparticles has been demonstrated.[231] Ag(hfac)(COD) dissolved in toluene and propanol as the reducing agent were used at deposition temperatures between 110 and 150 °C on glass, amorphous SiN and carbon.[231] The nucleation density of Ag nanoparticles increased from $7 \cdot 10^9$ to $1.5 \cdot 10^{11}$ particles cm^{-2} when the deposition temperature was lowered from 150 to 110 °C.[231] The particle diameter increased with increasing number of deposition cycles and some secondary nucleation on existing particles was observed after 300 cycles.[231] However, no continuous films were obtained with Ag(hfac)(COD) and propanol in this study.[231] It should be also noted that there are no reports on ALD of silver oxide.

3.12 Gold, rhenium and their oxides

There are currently no reported thermal ALD processes for gold and its oxide. PEALD of Au has been attempted but with limited success.[232] In addition, thermal ALD or PEALD processes for Re metal and its various oxides have not been reported.

The unstability of possible Au precursors is a similar factor as in the case of ALD of Ag. It is expected that PEALD of Au similar to PEALD of Ag would be the probable approach for Au film growth. The importance of Au films and nanoparticles should guarantee PEALD processes to surface quite soon. An approach for PEALD and ALD processes would be using amidinates and guanidinates; at least a gold guanidinate $[Au(N^{i}Pr)_2NMe_2]_2$ sublimes at a low temperature (85 °C, 20 mTorr) with a 4 % residual mass left in TGA.[233] The suitability of these precursors has not been proven for PEALD and ALD. PEALD of Au has however been attempted with an unspecified Au precursor but achieving uniformity was reported to be challenging.[232]

Rhenium is at the border of refractory metals and noble metals, so deposition of Re metal could be more demanding compared to other noble metals when oxygen-based and ozone-based thermal ALD processes are considered. In contrast, ALD of rhenium oxides should be more feasible. In PEALD reductive and oxidative plasmas should readily deposit both metal and oxide films.

Thermal ALD has been used to grow tungsten from WF_6 and silanes,[234] so a similar approach would be attractive for ALD of Re as well. In fact, Klaus et. al.[234] speculated using Si_2H_6 reductant for MoF_6 and ReF_6 similar to WF_6. The ALD of molybdenum from MoF_6 and Si_2H_6 was proven a decade later,[235] which suggests that the fluorosilane elimination chemistry would be a good starting point for thermal ALD of Re metal as well. This approach would, however, require the use of dangerous silanes. Alternatively, H_2 could be a good candidate to be used with metal halides as demonstrated in ALD of Ir from IrF_6 and molecular H_2.[194] This would likely require much higher deposition temperatures than processes using more effective reducing agents, i.e. silanes.

4 Experimental

4.1 Film deposition

Noble metal and noble metal oxide thin films were deposited in a commercial hot-wall flow-type F-120 ALD reactor (ASM Microchemistry Ltd., Finland) operated under a nitrogen pressure of about 10 mbar. Nitrogen (99.9995 %) was produced with either NITROX UHPN 3000 or domnick hunter G2100E nitrogen generators, and N_2 gas was used as a carrier and purging gas. The ALD reactor was equipped with a quartz cassette holder which has room for two 5 × 5 cm^2 substrates.

The noble metal and noble metal oxide films were grown either on in-situ grown Al_2O_3 films, silicon (111) with native oxide on top, or soda lime glass surfaces. The in-situ grown Al_2O_3 was deposited mostly from trimethylaluminum (TMA) and deionized water whereas $AlCl_3$ (99 %, Alfa Aesar) and H_2O were used for the ALD Os process. Both TMA and H_2O were pulsed from external reservoirs held at room temperature and pulsed into the reactor through a needle valve and a solenoid valve. $AlCl_3$ was held inside the reactor at 80 °C and pulsed using inert gas valving. In each deposition two substrates (5 × 5 cm^2) were used, most often one soda lime glass and one Si(111).

The noble metal ALD precursors were sublimed from open boats held inside the reactor at temperatures listed in Table 26 and pulsed using inert gas valving. The noble metal oxide films were deposited using ozone which was produced with a Wedeco Ozomatic Modular 4 HC Lab ozone generator from oxygen (99.999 and 99.9999 %, Linde Gas and AGA). Ozone was pulsed into the reactor through a needle valve and a solenoid valve from the main ozone flow line. The estimated ozone concentration at the output of the generator in most cases was about 100 g/Nm^3 with a flow rate of 30 l/h. In the ozone based ALD noble metal processes the metal precursor was followed by separate ozone and hydrogen pulses with N_2 purges after all the precursors. The flow rate of H_2 (99.999 %, Aga) was adjusted by using a needle valve and a mass flow meter during continuous flow, and H_2 was pulsed into the reactor with a solenoid valve. The H_2 flow rate was usually set to a value of 15 or 20 sccm. Also noble metal ALD processes for Os and Ir were examined, in which

molecular O_2 was used. The flow rate of O_2 (99.9999 %, Linde Gas and Aga) for Os (5 sccm) and Ir (20 sccm) depositions was set similarly as for H_2.

Table 26. The noble metal precursors and their evaporation temperatures used in the ALD processes.

Precursor	$T_{vap.}$ (°C)	Manufacturers and purities
$OsCp_2$	80	Strem (99.9 %)
$Rh(acac)_3$	150	Volatec, ABCR (99 %)
$Ir(acac)_3$	155	Strem (98 %), ABCR (99.9 %)
(MeCp)Ir(CHD)	45–50	synthesized in-house
$Pd(thd)_2$	120	Volatec
$MeCpPtMe_3$	~RT	ABCR (99 %)
$Pt(acac)_2$	110	ABCR (99.9 %)

4.2 Film characterization

Film thicknesses were determined from X-ray reflectivity (XRR) patterns measured with a Bruker AXS D8 Advance diffractometer and modelled using Leptos software. Film thicknesses were also obtained from energy-dispersive X-ray spectroscopy (EDX) data measured using an Oxford INCA 350 microanalysis system connected to a Hitachi S-4800 field emission scanning electron microscope (FESEM). The EDX results were analyzed using a GMR electron probe thin film microanalysis program.[236]

Crystal structures of the films were identified from X-ray diffraction (XRD) patterns measured with a PANalytical X′Pert Pro and a Bruker AXS D8 Advance X-ray diffractometers using CuK_{α}-radiation. The measurements were usually carried out in a θ–2θ mode on samples grown on soda lime glass substrates with or without in-situ grown amorphous Al_2O_3 nucleation layer. Also grazing incidence XRD (GIXRD) measurements were performed on some samples, mostly noble metal oxides. Samples on Si(111) substrates were used for GIXRD.

Surface morphology of the films was examined by the FESEM, and atomic force microscope (AFM) using a Veeco Instruments Multimode V with Nanoscope V controller.

AFM samples were measured in a tapping mode in air using phosphorus-doped silicon probe (RTESP) delivered by Veeco Instruments to produce simultaneous topographical and phase images. Final AFM topography images were measured from $2 \times 2\ \mu m^2$ scanning areas with a scanning frequency of 0.5 Hz and no image processing except flattening was made. Film roughnesses were calculated as root-mean-square values (R_q).

Resistivities of the noble metal and noble metal oxide films were calculated from sheet resistances measured with a four-point probe technique and from the film thicknesses. Film adhesion to the starting surfaces was tested with a simplified Scotch tape test. Elemental compositions of the films were determined with elastic recoil detection analysis (ERDA) and time-of-flight ERDA (TOF-ERDA) at Helmholtz-Zentrum Dresden-Rossendorf (Germany), University of Jyväskylä (Finland), and University of Helsinki (Finland).[237]

5 Results and discussion

The main experimental results are summarized in this section. The detailed description of the experimental work and the results on the developed ALD processes can be found from the corresponding publications [I–VIII]. The developed ALD processes were put into a context of ALD of noble metals and their oxides already in Chapter 3. Also, the differences in reaction mechanisms between ozone and oxygen-based thermal ALD processes were discussed. In Chapter 5 the results on the ozone-based processes are compared to the existing oxygen-based processes with the corresponding noble metal precursors. Oxygen-based ALD processes for most noble metals were initially developed at the University of Helsinki using the same ALD reactor set-up which was also used for this thesis research. For more in-depth insight into the oxygen-based ALD noble metal processes, the Ph.D. thesis by Aaltonen[1] is highly recommended. Several of those oxygen-based ALD processes are either one of the few ALD processes developed for that particular noble metal or the most often applied ones. These include the ALD processes for Pt, Ir, and Rh metal films. The oxygen-based ALD processes presented by Aaltonen are therefore good references for the current ozone-based ALD processes.

5.1 Iridium oxide and metal

Several ALD processes were developed for iridium oxide and iridium metal. The iridium oxide films were deposited using ozone and either $Ir(acac)_3$ (Ref. I) or (MeCp)Ir(CHD) (Ref. VI) precursors. Iridium metal films were grown using the following combinations: $Ir(acac)_3$–O_3–H_2 (Ref. IV), (MeCp)Ir(CHD)–O_2 (Ref. V), and (MeCp)Ir(CHD)–O_3–H_2 (Ref. VI).

5.1.1 Film growth with $Ir(acac)_3$

$Ir(acac)_3$ is a well-established precursor to deposit iridium metal films by ALD with oxygen-based chemistry at temperatures starting from 225 °C.[41] The precursor is stable up to about 400 °C against thermal self-decomposition.[41] In MOCVD the onset temperatures have been reported to be 405 °C for decomposition in vacuum and 225 °C for reaction with oxygen.[238] In oxygen-based noble metal ALD growth, molecular O_2 is activated by a

dissociative chemisorption to reactive atomic oxygen on the metal surface. The dissociation of molecular O_2 most likely determines the threshold temperature for the processes to start. The onset temperature for the film growth in the $Ir(acac)_3$–O_2 ALD process is close to 225 °C.[41]

When O_2 was substituted with ozone [$Ir(acac)_3$–O_3], iridium oxide films were grown between 165 and 200 °C (Figure 15).[I] Ozone is more reactive than O_2 and dissociates easily to oxygen radicals and molecular oxygen. Knapas and Ritala[30] have shown that $Ir(acac)_3$ adsorbs stoichiometrically on the surface at these low temperatures and thus the surface oxygen atoms are not oxidative towards the acac ligands different from the $Ir(acac)_3$–O_2 process at higher temperatures. The IrO_2 growth rate in the $Ir(acac)_3$–O_3 process increased with increasing deposition temperature from less than 0.2 Å/cycle to roughly 0.4 Å/cycle between 165 and 200 °C (Figure 15).[I] The transition of the grown crystalline IrO_2 films to metallic Ir occurred above 200 °C which is in a good agreement with the onset deposition temperature in the oxygen-based ALD Ir process.[41]

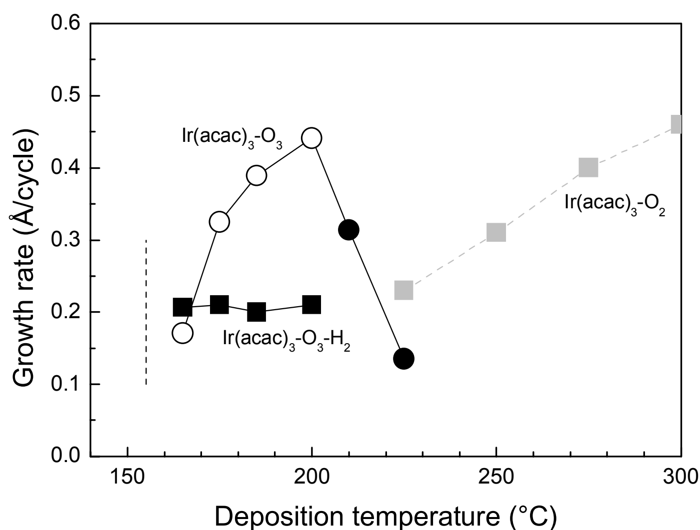

Figure 15. Growth rates of ALD processes using $Ir(acac)_3$ as a function of deposition temperature.[I,IV,41] Solid symbols denote Ir metal films while open symbols correspond to iridium oxide films. The growth rates of the $Ir(acac)_3$–O_2 process were adapted from Ref. 41. The dashed line marks the source temperature applied for $Ir(acac)_3$.

Iridium metal films were deposited between 165 and 200 °C by adding a H_2 pulse step to the IrO_2 deposition sequence: Ir(acac)$_3$–O_3–H_2.[IV] H_2 thus reduced the film after the oxidizing ozone pulse. The growth rate was about 0.2 Å/cycle at the studied temperature range (Figure 15) and did not exhibit similar strong deposition temperature dependence as the IrO_2 growth rate. The Ir growth rate of slightly above 0.2 Å/cycle in the Ir(acac)$_3$–O_2 process[41] at its onset deposition temperature (225 °C) agrees surprisingly well with the growth rate of the Ir(acac)$_3$–O_3–H_2 process (Figure 15).

Ir films were successfully deposited by the Ir(acac)$_3$–O_3–H_2 process on Al_2O_3 nucleation layers but also directly on bare soda lime glasses and native oxide covered silicon substrates.[IV] The film thickness depended linearly on the number of the deposition cycles at 185 °C but a slight nucleation delay was found.[IV] After 100 growth cycles at 185 °C, Ir was scattered discontinuously on the Al_2O_3 surface, and the about 5 nm thick film after 200 cycles still had tiny holes as observed by FESEM. The 7 nm thick film (300 cycles) seemed to be fully continuous according to FESEM although the resistivity of the film could not be measured reliably. The use of methanol at 185 °C did not reduce the oxide films as effectively as H_2.[IV]

5.1.2 Film growth with (MeCp)Ir(CHD)

The high sublimation temperature required for Ir(acac)$_3$ (155 °C) restricted the low temperature deposition limits to 165 °C in the Ir(acac)$_3$–O_3 and Ir(acac)$_3$–O_3–H_2 processes (Figure 15).[I,IV] Thus a new Ir precursor, (MeCp)Ir(CHD), was synthesized in-house.[V] For ALD, sufficient volatility of (MeCp)Ir(CHD) was obtained at source temperatures of 45–50 °C where the precursor also becomes a liquid.[V] The central ion is at +I valence state in (MeCp)Ir(CHD) similar to (EtCp)Ir(COD), but this differs from +III in the most commonly studied Ir(acac)$_3$.

The (MeCp)Ir(CHD)–O_2 ALD Ir process[V] was developed first while the low temperature processes for iridium oxide and iridium were achieved with (MeCp)Ir(CHD)–O_3 and (MeCp)Ir(CHD)–O_3–H_2 cycling sequences, respectively (Figure 16).[VI] With O_2, successful Ir film growth was obtained between 225 and 350 °C while only negligible growth was observed at 200 °C on Al_2O_3 surface. The low deposition temperature limit of

225 °C is in good agreement with the other oxygen-based Ir ALD processes: 225 °C was required in the Ir(acac)$_3$–O_2 process,[41] while the lowest reported deposition temperature for the (EtCp)Ir(COD)–O_2 process is 230 °C.[186]

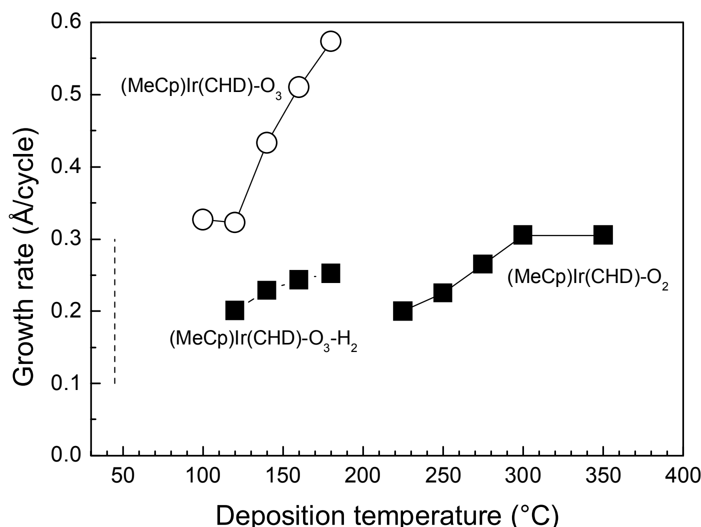

Figure 16. The growth rates of the ALD processes using (MeCp)Ir(CHD) as a function of deposition temperature.[V,VI] Solid symbols denote Ir metal films while open symbols correspond to iridium oxide films. The dashed line marks the source temperature applied for (MeCp)Ir(CHD).

In the (MeCp)Ir(CHD)–O_2 process the growth rate increased slightly from 0.2 Å/cycle to 0.3 Å/cycle at temperatures between 225 and 300 °C (Figure 16).[V] Although the growth rate seems to be constant between 300 and 350 °C, (MeCp)Ir(CHD) showed signs of thermal decomposition at 350 °C. The film uniformity at 350 °C was unaffected, even though slight decomposition of the precursor was observed in the hot end of the source tube. However, some scattered larger particles were found in the FESEM images, which are likely related to the slight precursor decomposition. Also at 300 °C some larger particles were seen but their density was lower than at 350 °C.

The films thinner than 10 nm deposited with the (MeCp)Ir(CHD)–O_2 process at 300 °C were too thin or discontinuous for conductivity measurements with the four-point probe.

After 100 cycles of (MeCp)Ir(CHD) and O_2, only separate Ir islands were formed on the Al_2O_3. These nuclei grew larger and into a contact with each other, though still leaving voids in the film after 200 cycles. The 9 nm thick film after 300 deposition cycles looked fully continuous and upon further cycles the grain size increased moderately according to FESEM.[V]

The iridium oxide films were grown using the ozone-based (MeCp)Ir(CHD)–O_3 ALD process between 100 and 180 °C (Figure 16).[VI] The film partially reduced to metallic iridium at 200 °C, which is close to the onset temperature of the oxygen-based Ir process. No film growth was observed at 80 °C, which indicates that 100 °C is close to the low temperature limit of the ozone-based process. The films deposited at 140 °C and above were crystalline whereas the films grown at lower temperatures were x-ray amorphous. The densities of the crystalline films were close to the IrO_2 bulk density (Figure 17). As the deposition temperature was decreased from 140 to 120 °C, the films became x-ray amorphous and the density decreased from about 11 g/cm^3 to less than 8 g/cm^3. The density was only about 5 g/cm^3 in the film grown at the lowest successful deposition temperature (100 °C).

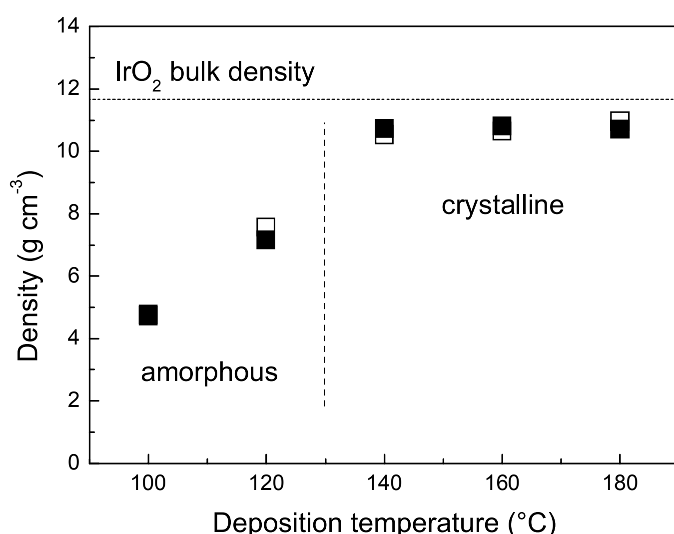

Figure 17. Densities of the iridium oxide films grown by the (MeCp)Ir(CHD)–O_3 process on Al_2O_3. The open and solid symbols denote films on Al_2O_3 coated soda lime glass and Si substrates, respectively. The film densities were determined with XRR.

The iridium metal films were grown with the (MeCp)Ir(CHD)–O_3–H_2 process between 120 and 180 °C (Figure 16).[VI] Unsuccessful deposition of Ir film at 100 °C is most likely related to the low density of the iridium oxide film grown at the same temperature (Figure 16). The growth rate of Ir increased with increasing deposition temperature from 0.2 Å/cycle to slightly above that. The growth rate at 180 °C was somewhat higher than the growth rate of Ir in the oxygen-based (MeCp)Ir(CHD)–O_2 process at its onset temperature (225 °C). The growth rates in the ozone-based ALD processes using (MeCp)Ir(CHD) are slightly higher than in the ozone-based ALD processes using $Ir(acac)_3$ at the corresponding deposition temperatures. However, this is reverse for the oxygen-based Ir ALD processes; i.e. $Ir(acac)_3$–O_2 process has higher growth rate than the (MeCp)Ir(CHD)–O_2 process.

5.1.3 Surface roughnesses

The surface roughnesses of the iridium oxide films grown by the (MeCp)Ir(CHD)–O_3 and $Ir(acac)_3$–O_3 processes were related to the deposition temperature so that rougher films were grown at higher temperatures (Figure 18). The iridium oxide films grown from $Ir(acac)_3$ were smoother in comparison to the films grown from (MeCp)Ir(CHD) (unpublished results). The surface roughnesses of about 35 and 70 nm thick iridium oxide films grown with $Ir(acac)_3$ and ozone at 165 °C were about 1.0 and 1.4 nm, respectively (unpublished results).

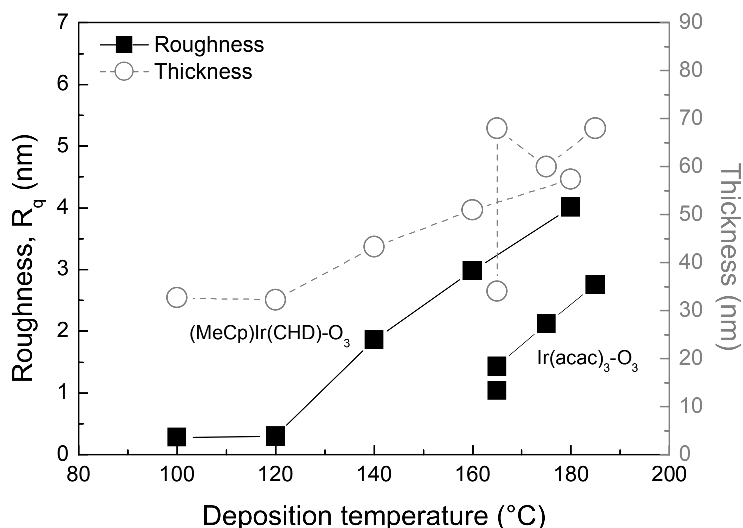

Figure 18. Thicknesses and roughnesses of iridium oxide thin films on Al_2O_3 as a function of deposition temperature. The ALD processes were (MeCp)Ir(CHD)–O_3[VI] and Ir(acac)$_3$–O_3 (unpublished results). The roughnesses were determined by AFM.

The Ir films grown with the O_3–H_2 chemistry did not have a similar strong relation of surface roughness to the deposition temperature as the ALD iridium oxide films (Figure 19). The about 70 nm and thinner films had surface roughnesses less than 1.5 nm. The (MeCp)Ir(CHD)–O_2 ALD process on the other hand resulted in Ir films having higher surface roughnesses (Figure 19). The surface roughnesses were the highest at the onset temperature of the oxygen-based process (225 °C) and then decreased with increasing deposition temperature. At 225 °C the surface roughness of the 40 nm thick film was 6.0 nm while at 275 °C the thicker (53 nm) film had a roughness of only 1.2 nm. The (MeCp)Ir(CHD)–O_2 process resulted only at 275 °C in surface roughnesses as low as the (MeCp)Ir(CHD)–O_3–H_2 Ir process at 70–150 °C lower temperatures.

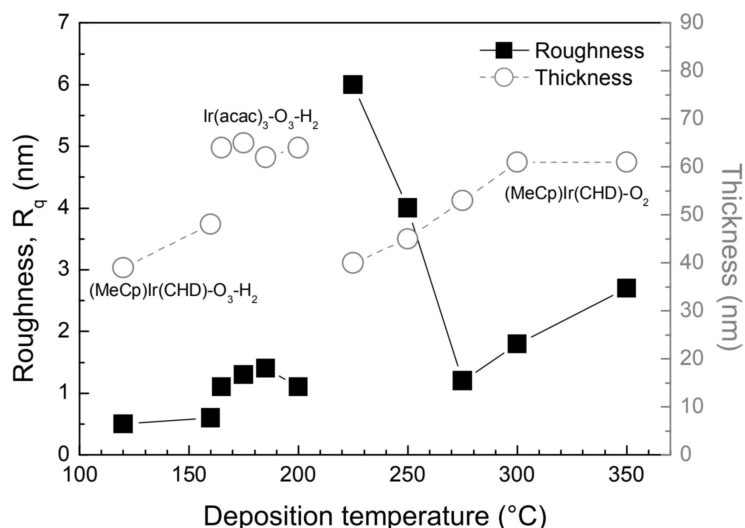

Figure 19. Roughnesses and thicknesses of iridium thin films as a function of deposition temperature. The applied ALD processes were (MeCp)Ir(CHD)–O_3–H_2, Ir(acac)$_3$–O_3–H_2, and (MeCp)Ir(CHD)–O_2.[IV,V,VI] The substrate was Si(111) with an Al_2O_3 nucleation layer. The roughnesses were determined by AFM.

In the (MeCp)Ir(CHD)–O_2 process the high roughnesses at the lowest deposition temperatures may arise from low nucleation densities as the nuclei can grow larger before coming into contact with each other. This results in films with large grains and rough surfaces. Such substantial increases in grain sizes and surface roughnesses specifically at lower deposition temperatures (225–250 °C) has not been reported before for oxygen-based ALD Ir processes with Ir(acac)$_3$ and (EtCp)Ir(COD) precursors. It would be though expected that nucleation could be delayed and lead to rougher films near the onset deposition temperatures of oxygen-based processes also with other precursors than only (MeCp)Ir(CHD).

5.1.4 Resistivities

Resistivities of Ir metal films grown with the (MeCp)Ir(CHD)–O_2, (MeCp)Ir(CHD)–O_3–H_2 and Ir(acac)$_3$–O_3–H_2 processes are summarized in Table 27. The resistivities of about 40–60 nm thick films deposited with the (MeCp)Ir(CHD)–O_2 process are similar to the

resistivities obtained with the other oxygen-based Ir ALD processes. In contrast, the films grown to similar thicknesses with the ozone-based $Ir(acac)_3$–O_3–H_2 and (MeCp)Ir(CHD)–O_3–H_2 processes are more resistive than the films deposited with the oxygen-based processes (Table 27). The resistivity is dependent on the film thickness but also on the deposition temperature. The metal films grown with the (MeCp)Ir(CHD)–O_3–H_2 and $Ir(acac)_3$–O_3–H_2 processes at lower temperatures do not have as large grains and are not so oriented as the films deposited at considerably higher temperatures with the oxygen-based processes. This results in higher resistivities but also in smoother films as was discussed previously.

Table 27. Summary of resistivities of Ir metal films.

Process	Thickness (nm)	Resistivity (μΩ cm)	$T_{dep.}$ (°C)	Ref.
$Ir(acac)_3$–O_2	70	<12	225–400	41
(MeCp)Ir(CHD)–O_2	40–60	8–10	225–350	V
(EtCp)Ir(COD)–O_2	NA	9	290	186
$Ir(acac)_3$–ozone–H_2	60	11–12	165–200	IV
(MeCp)Ir(CHD)–ozone–H_2	50	12–13	160	VI
(MeCp)Ir(CHD)–ozone–H_2	40	14–16	120	VI
(MeCp)Ir(CHD)–O_2	30	12	300	V
$Ir(acac)_3$–ozone–H_2	20	16–17	185	IV
(MeCp)Ir(CHD)–ozone–H_2	20–25	16–21	120–180	VI
(MeCp)Ir(CHD)–O_2	20	14	300	V
(MeCp)Ir(CHD)–O_2	10	17–18	300	V

The resistivities of the iridium oxide films are shown in Table 28. The iridium oxide films are considerably more resistive than the Ir metal films (Table 27). About 40 nm thick IrO_2 films deposited from $Ir(acac)_3$ and O_3 at 185 °C had resistivities of about 170–200 μΩcm. The slightly thicker film (50 nm) grown with the (MeCp)Ir(CHD)–O_3 process at lower temperature (160 °C) had a similar resistivity. The oxygen-based IrO_2 process using (EtCp)Ir(COD) and O_2 has been reported to deposit films that were more conductive (120

μΩcm).[186] These films were grown at higher temperature (290 °C) than the present films with ozone (Table 28). The bulk resistivity of IrO_2 is around 35–60 μΩcm (Table 2; Chapter 2.2).

Table 28. Summary of resistivities of the iridium oxide films.

Process	Thickness (nm)	Resistivity (μΩ cm)	$T_{dep.}$ (°C)	Ref.
$Ir(acac)_3$–ozone	40	170–200	185	I
(MeCp)Ir(CHD)–ozone	50	~200	160	VI
(EtCp)Ir(COD)–O_2	NA	120	290	186

5.1.5 Impurity contents

The impurity contents of the developed iridium oxide and iridium metal processes are summarized in Table 29. In the iridium oxide films grown with the $Ir(acac)_3$–O_3 and (MeCp)Ir(CHD)–O_3 processes the carbon and hydrogen impurities decreased with increasing deposition temperature; however the impurity contents were quite low in all the films grown at 160 °C and above. The iridium oxide film grown at 120 °C had a substantial excess carbon, hydrogen and oxygen contents. The large hydrogen content and the high O/Ir ratio (2.3) suggest that the film contained a quite high amount of hydroxyl groups. This is reasonable because of the combined effect of the low deposition temperature, the formation of H_2O reaction by-product, and the relatively short purge times separating the precursors. The use of substantially longer purges could likely result in films with less hydroxyl groups, and hence lower residual hydrogen and oxygen contents.

Table 29. Elemental compositions of the iridium oxide and metal thin films as measured with ERDA and TOF-ERDA.

dep. temp. (°C)	Ir (at.%)	O (at.%)	C (at.%)	H (at.%)	Other (at.%)	O : Ir ratio
Ir(acac)$_3$–O$_3$						
165	30.3 ± 0.4	64.5 ± 0.5	0.74 ± 0.11	4.50 ± 0.08		2.1 (2.08–2.17)
175	30.9 ± 0.4	64.2 ± 0.5	0.99 ± 0.15	3.98 ± 0.09		2.1 (2.03–2.12)
185	31.7 ± 0.4	64.8 ± 0.5	< 0.5	3.50 ± 0.07		2.0 (2.00–2.09)
200	37.1 ± 0.4	59.7 ± 0.5	< 0.5	3.21 ± 0.06		1.6 (1.57–1.64)
(MeCp)Ir(CHD)–O$_3$						
120	20 ± 3	46 ± 5	8 ± 3	18 ± 4	(Al 7)	2.3 (1.8–3.0)
160	31 ± 3	62 ± 5	2 ± 1	5 ± 1		2.0 (1.7–2.4)
Ir(acac)$_3$–O$_3$–H$_2$						
165	94 ± 1	3.6 ± 0.3	0.6 ± 0.1	1.8 ± 0.3		0.04
175	91 ± 1	7.0 ± 0.3	0.4 ± 0.1	1.6 ± 0.3		0.08
185	94 ± 1	3.7 ± 0.2	0.3 ± 0.1	1.9 ± 0.3		0.04
200	92 ± 1	6.3 ± 0.3	0.5 ± 0.1	1.2 ± 0.2		0.07
(MeCp)Ir(CHD)–O$_3$–H$_2$						
120	81 ± 5	12 ± 4	1.2 ± 0.6	6 ± 3		0.15 (0.09–0.21)
160	90 ± 5	6 ± 3	0.2 ± 0.1	3 ± 1		0.07 (0.05–0.08)
(MeCp)Ir(CHD)–O$_2$						
225	90.6 ± 1.1	5.8 ± 0.3	0.8 ± 0.1	2.8 ± 0.4		0.06
250	90.3 ± 1.0	6.9 ± 0.3	0.3 ± 0.1	2.4 ± 0.4		0.08
275	94.8 ± 1.0	3.0 ± 0.2	0.6 ± 0.1	1.6 ± 0.3		0.03
300	95.4 ± 0.9	2.6 ± 0.2	0.6 ± 0.1	1.4 ± 0.2		0.03
350	95.8 ± 0.8	3.3 ± 0.2	0.3 ± 0.1	0.7 ± 0.2		0.03

The impurity contents of the Ir metal films deposited with the O_3–H_2 based ALD processes were reasonable regardless of the applied process or the deposition temperature (Table 29). The Ir film grown at 120 °C contained substantially high contents of oxygen (12 at.%) and carbon (6 at.%) impurities. In general, lower deposition temperatures led into somewhat higher impurity contents in the films. The (MeCp)Ir(CHD)–O_2 ALD Ir process at 225–250 °C resulted in similar impurity contents as found from the films grown with the (MeCp)Ir(CHD)–O_3–H_2 ALD Ir process at 65–90 °C lower temperature (160 °C). However, the impurity contents in the oxygen-based (MeCp)Ir(CHD)–O_2 Ir process also decreased with increasing growth temperature (Table 29).

Overall, impurity contents reported in the literature for the ALD Ir metal and oxide processes are quite limited (Tables 12 and 15, Chapters 3.7 and 3.8). The $Ir(acac)_3$–O_2 ALD Ir process produces pure thin films with <0.5 at.% oxygen, <0.3 at.% carbon, and 1.0 at.% hydrogen at wide deposition temperature range between 225 and 350 °C.[41] This indicates that in terms of film purity the (MeCp)Ir(CHD) is not comparable to the $Ir(acac)_3$ in the oxygen-based processes. It has been however reported[186] that depending on the oxygen partial pressure in the similar (EtCp)Ir(COD)–O_2 process either Ir or IrO_2 is formed. Thus, the high content of oxygen in the Ir films deposited with the (MeCp)Ir(CHD–O_2 process can originate from the relatively high flow rate of oxygen (20 sccm) introduced into the reactor.[V] It is interesting to point out that the reported $Ir(acac)_3$–O_2 ALD Ir process used air with flow rates varied from 5 to 40 sccm.[41] The applied air flow rate was not specified for the Ir films measured with TOF-ERDA;[41] however a low flow rate (5 sccm) was used to study saturation of the growth rate. It can thus be speculated that the oxygen dose may affect the oxygen content in some degree although the correlation has not been examined.

5.2 Rhodium oxide and metal

Rh_2O_3 and Rh films were deposited using the $Rh(acac)_3$–O_3 and $Rh(acac)_3$–O_3–H_2 pulsing sequences between 160 and 180 °C (Figure 20).[III,VII] The relatively high source temperature needed to sublime $Rh(acac)_3$ (150 °C) limited exploring the lowest growth temperature possible with ozone. In the $Rh(acac)_3$–O_3 process a partial reduction of Rh_2O_3

to Rh was observed already at 190 °C and thus 180 °C was considered as the high temperature limit of the ozone-based Rh_2O_3 process. The reported onset deposition temperature in the $Rh(acac)_3$–O_2 ALD Rh process was 200 °C although the growth rates were given for films grown at 250 °C only.[167] This is quite surprising considering that the $Rh(acac)_3$–O_2 process has a high growth rate (about 0.8 Å/cycle) at 250 °C. In MOCVD the reported[238] onset temperature for $Rh(acac)_3$ to react in the presence of O_2 is 200 °C while the onset decomposition temperature of $Rh(acac)_3$ in vacuum is 395 °C. In ALD thermal self-decomposition of $Rh(acac)_3$ has been observed at 300 °C.[167]

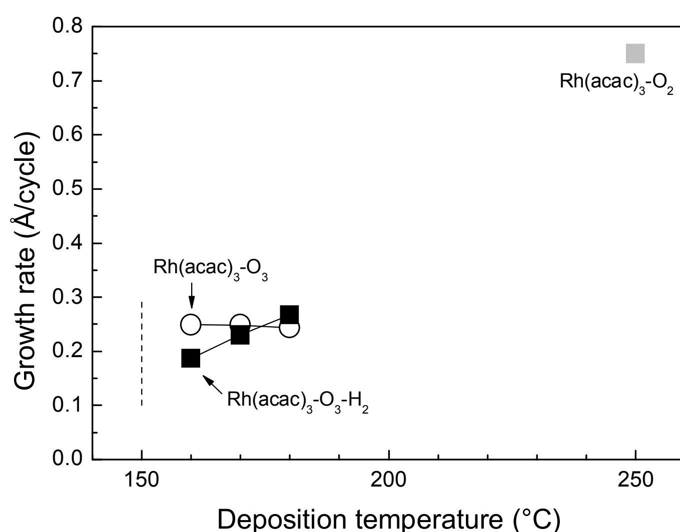

Figure 20. Growh rates of ALD processes using $Rh(acac)_3$ as a function of deposition temperature.[III,VII,167] Solid symbols denote Rh metal films while open symbols correspond to rhodium oxide films. The growth rate for $Rh(acac)_3$–O_2 process was adapted from Ref. 167. The dashed line marks the source temperature applied for $Rh(acac)_3$.

The $Rh(acac)_3$–O_3 process resulted in x-ray amorphous Rh_2O_3 between 160 and 180 °C (Figure 21a and c). The growth rate was about 0.2–0.3 Å/cycle but substantial thickness non-uniformity was found across the substrate. The trailing edges of the substrates with respect of gas flow direction received most likely substantially lower ozone doses than the leading edges because of the combination of the effective ozone decomposition by the catalytically active rhodium oxide and the flow-type ALD reactor setup, thus leading to

thickness non-uniformity across the substrates.[III] This was compensated by performing the deposition in two stages separated by 180 ° substrate rotation. [III]

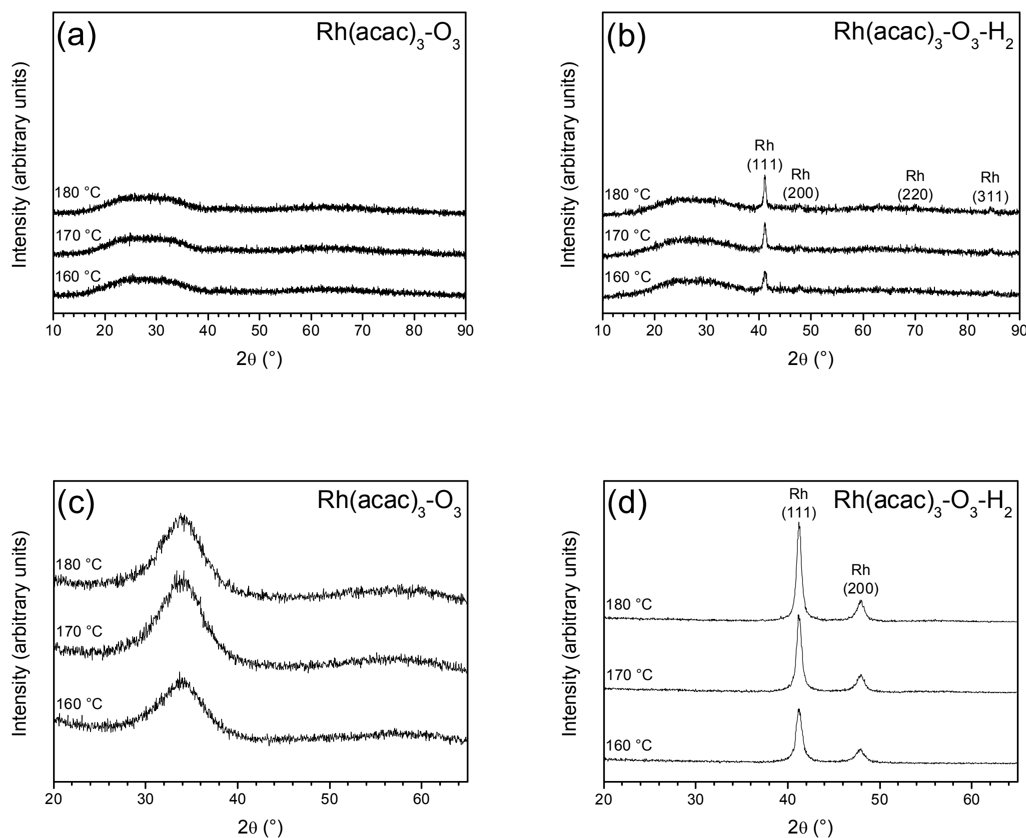

Figure 21. θ–2θ XRD patterns of the (a) rhodium oxide [$Rh(acac)_3$–O_3] and (b) rhodium [$Rh(acac)_3$–O_3–H_2] thin films deposited between 160 and 180 °C on Al_2O_3 coated soda lime glass. (c) and (d) show the corresponding GIXRD patterns of the films grown on Al_2O_3 coated Si.

The Rh thin films were deposited at 160–180 °C using $Rh(acac)_3$, ozone, and molecular H_2 on in-situ grown Al_2O_3 (Figure 21b and d).[VII] The film growth rate increased from roughly 0.2 to 0.3 Å/cycle with increasing deposition temperature (Figure 20). The growth rate at 180 °C was substantially lower (0.3 Å/cycle) than at 250 °C with the oxygen-based chemistry (~0.8 Å/cycle).[167]

The surface roughnesses of the films grown with the $Rh(acac)_3$–O_3–H_2 and $Rh(acac)_3$–O_3 processes are shown in Table 30. The x-ray amorphous Rh_2O_3 films were very smooth as the surface roughnesses of about 80 nm thick films were between 0.5 and 1.4 nm (unpublished results). The surface roughnesses of about 20–30 nm thick Rh films deposited with the $Rh(acac)_3$–O_3–H_2 process were low. The Rh film grown at 160 °C was somewhat rougher (1.7 nm) than the films grown at higher temperatures (1.1–1.3 nm). The resistivities of the 20–30 nm thick Rh films are comparable to the films grown by the oxygen-based process at 250 °C (Table 30). The Rh_2O_3 films are roughly thousandfold more resistive than the Rh metal films. The bulk resistivity of Rh_2O_3 is about 5×10^6 μΩcm (Table 2; Chapter 2.2) while the resistivities of the films grown by the $Rh(acac)_3$–O_3 process were in the order of $5–11\times10^3$ μΩcm.

Table 30. Surface roughnesses and resistivities of the films deposited with the $Rh(acac)_3$–O_3 and $Rh(acac)_3$–O_3–H_2 processes. The $Rh(acac)_3$–O_2 process[167] was included as a reference.

Process	Thickness (nm)	Roughness (nm)	Resistivity (μΩ cm)	$T_{dep.}$ (°C)	Ref.
$Rh(acac)_3$–ozone	~80	$0.7^{160°C}$, $1.4^{170°C}$	6000–8000	160, 170	III, *a*
(Rh_2O_3 amorph.)	~80	0.5	5000–6000	180	III, *a*
	~40,60		11000	170	III
$Rh(acac)_3$–ozone–H_2	19	1.7	11	160	VII
(Rh)	23	1.1	11	170	VII
	27	1.3	10	180	VII
$Rh(acac)_3$–O_2	15		24	250	167
(Rh)	25		10		
	40		10		

a unpublished surface roughness data

The elemental compositions of the films deposited with the $Rh(acac)_3$–O_3 and $Rh(acac)_3$–O_3–H_2 processes are collected to Table 31. The Rh_2O_3 films contained a relatively low amount of carbon (about 1 at.%) while hydrogen contents were considerably higher (6 at.%). The Rh metal films grown with the $Rh(acac)_3$–O_3–H_2 process had lower hydrogen content (1.5–3 at.%) than the Rh_2O_3 films despite using the H_2 reductant. The Rh metal

films contained 1–3 at.% oxygen depending on the deposition temperature (Table 31). The Rh film grown using the $Rh(acac)_3$–O_2 process at 250 °C was reported to have 2.3 at.% oxygen, 1.6 at.% carbon, and less than 0.1 at.% hydrogen impurities.[167] In comparison, the Rh film deposited at 70 °C lower temperature with the $Rh(acac)_3$–O_3–H_2 process has lower oxygen (0.7 at.%) and carbon (0.3 at.%) contents with an expense of increased hydrogen content (1.5 at.%).

Table 31. Elemental compositions of the rhodium oxide and rhodium metal thin films as measured with ERDA and TOF-ERDA.

dep. temp. (°C)	Rh (at.%)	O (at.%)	C (at.%)	H (at.%)	O : Rh ratio
$Rh(acac)_3$–O_3					
160	35.7 ± 0.1	56.8 ± 1.1	1.2 ± 0.2	6.4 ± 0.1	1.59 (1.56–1.63)
170	36.2 ± 0.1	56.6 ± 1.1	1.4 ± 0.1	5.9 ± 0.1	1.56 (1.53–1.60)
180	36.6 ± 0.1	57.4 ± 1.1	0.5 ± 0.2	5.5 ± 0.1	1.57 (1.53–1.60)
$Rh(acac)_3$–O_3–H_2					
160	~94	3 ± 1	0.6 ± 0.2	3 ± 1	0.03
180	~98	0.7 ± 0.3	0.3 ± 0.1	1.5 ± 0.5	0.01

5.3 Palladium oxide and metal

Palladium oxide (PdO) and palladium metal films were deposited between 130 and 160 °C on in-situ grown Al_2O_3 using the $Pd(thd)_2$–O_3 and $Pd(thd)_2$–O_3–H_2 precursor sequences (Figure 22).[VII] The lowest possible growth temperature was set by the source temperature required to sublime $Pd(thd)_2$ (120 °C). The $Pd(thd)_2$–O_3 process resulted in partly metallic films at 170 °C instead of phase pure PdO, and thus 160 °C was considered the upper limit for the ALD of PdO.

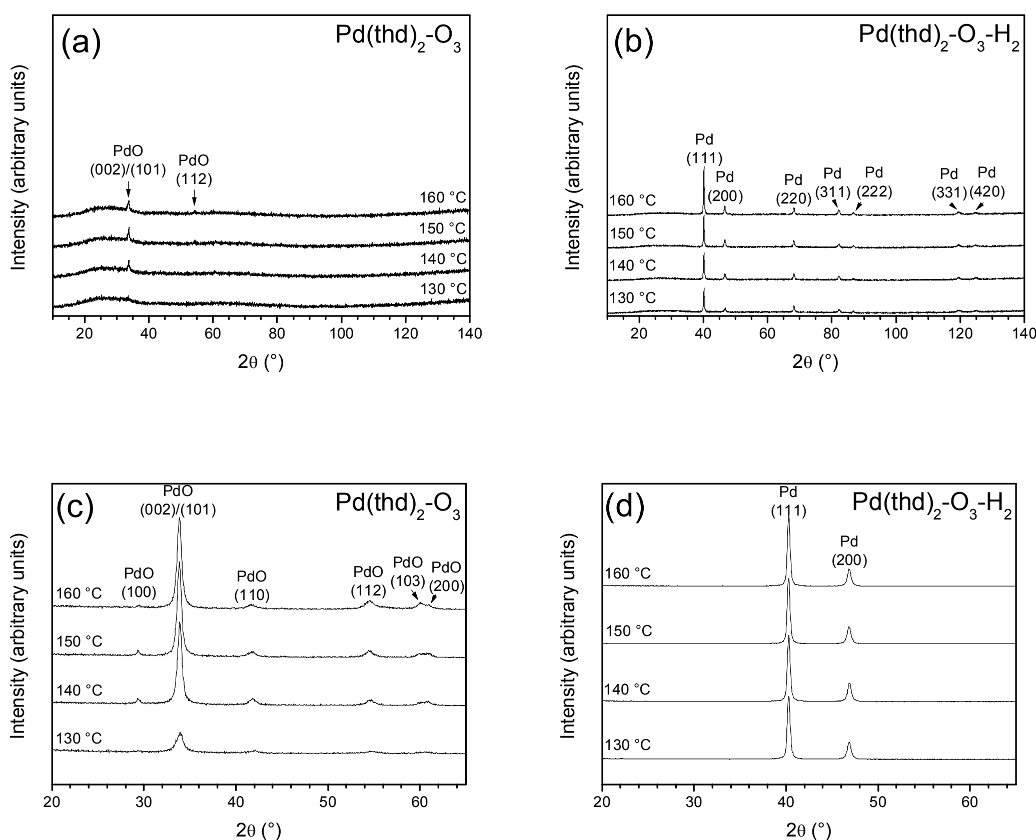

Figure 22. θ–2θ XRD patterns of the (a) palladium oxide [$Pd(thd)_2$–O_3] and (b) palladium [$Pd(thd)_2$–O_3–H_2] thin films deposited between 130 and 160 °C. The substrate was soda lime glass with an Al_2O_3 nucleation layer. (c) and (d) show the corresponding GIXRD patterns of the films on Al_2O_3 coated Si.

The growth rates of the PdO and Pd metal ALD processes were examined between 130 and 160 °C (Figure 23). Uniform PdO films were grown with the $Pd(thd)_2$–O_3 ALD process and the growth rate was about 0.1 Å/cycle at the lowest temperature while at 140 °C and above the growth rate leveled to 0.2 Å/cycle. The $Pd(thd)_2$–O_3–H_2 pulsing sequence on the other hand resulted in non-uniform Pd films with substantially higher growth rates (0.5–0.7 Å/cycle as measured from the middle of the substrate) between 130 and 160 °C (Figure 23). As an example, the growth rate of the Pd film grown at 140 °C decreased from 0.9 to 0.4 Å/cycle while moving along the gas flow direction from the leading edge (closest to the precursor inlet) to the trailing edge of the substrate.

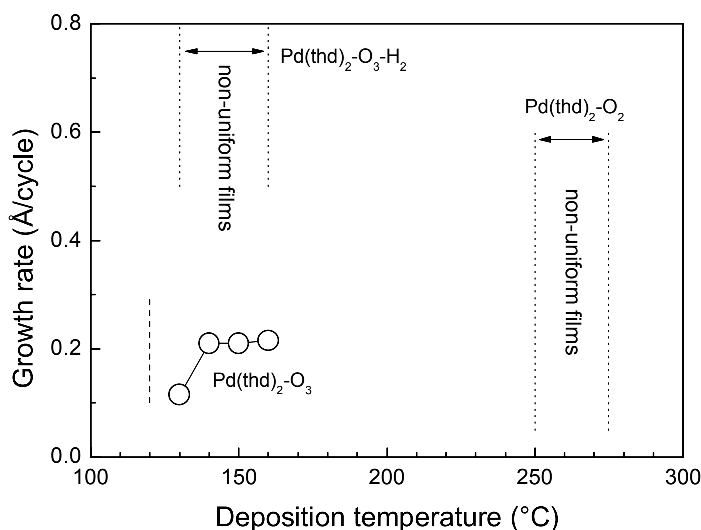

Figure 23. Growth rates of the ALD processes using $Pd(thd)_2$ as a function of deposition temperature.[VII] Open symbols denote palladium oxide films while the non-uniform films are Pd metal. The results of the $Pd(thd)_2$–O_2 pulsing sequence between 250 and 275 °C were adapted from the ref. 56. The dashed line marks the source temperature applied for $Pt(thd)_2$.

The Pd films deposited with molecular O_2 from the same $Pd(thd)_2$ precursor at considerably higher temperatures (250–275 °C) than with O_3–H_2 have been reported to be non-uniform too (Figure 23).[56] The non-uniformity was suggested to result from possible etching of the as-deposited Pd film by $Pd(thd)_2$ at those higher temperatures.[56] Etching could be expected to be limited when substantially lower temperatures (130−160 °C) are used. Indeed, the $Pd(thd)_2$–O_3 process for PdO did not exhibit notable etching behavior. The non-uniformity issues found in the low temperature ALD growth of Pd from the $Pd(thd)_2$–O_3–H_2 process can not thus be explained by etching. Some guidance can be got from a comparison between the ozone-based PdO and Pd film growths. First, the Pd film growth rates (0.5–0.7 Å/cycle) were much higher than the corresponding PdO growth rates (0.1–0.2 Å/cycle). This order is the opposite to the other corresponding noble metal/noble metal oxide process pairs, i.e. Ir/IrO_2, Rh/Rh_2O_3, and Pt/PtO_x, where the oxide growth rates were higher than the metal growth rates.

The fast but non-uniform growth of the Pd films in the direction of the precursor gas flow could originate from the catalytic properties of Pd. Pd is a well known catalyst material and is able to dissociate, adsorb, and also absorb hydrogen efficiently. Importantly, the earlier thermal ALD Pd processes use solely either molecular H_2 or formalin instead of molecular O_2, which contrasts greatly with other thermal ALD noble metal processes (Chapter 3). The QCM results from the reductive ALD Pd growth suggest that $Pd(hfac)_2$ reacts with hydrogen atoms left on the Pd surface after the H_2 or formalin pulses.[42] This is probably the case in the $Pd(thd)_2$–O_3–H_2 process as well, i.e. during the H_2 pulse Pd may adsorb or even absorb some hydrogen, which is then available to react with the $Pd(thd)_2$. The hydrogen on the surface would remove one or both of the ligands from $Pd(thd)_2$ and form Hthd. Even a single surface hydrogen atom can protonate a very large thd ligand and be removed as a whole Hthd. The less steric hindrance is caused by the ligands and palladium is adsorbed more densely to the surface. $Pd(thd)_2$ can most likely adsorb also stoichiometrically at low temperatures similar to $Ir(acac)_3$ in the corresponding Ir and IrO_2 ALD processes using $Ir(acac)_3$–O_3–H_2 and $Ir(acac)_3$–O_3 pulsing sequences.[30] Thus the observed high growth rates of the Pd films can be explained by the reaction of $Pd(thd)_2$ with surface hydrogen, which, after the depletion of surface hydrogen, is followed by stoichiometric adsorption of $Pd(thd)_2$ on the surface until the surface becomes saturated.

In the cross-flow reactor used here the reaction byproducts are travelling in front of the precursor pulse producing them, and can thereby readsorb without competition. Therefore the thickness non-uniformity can result from the readsorption of Hthd ligands released in the reactions of $Pd(thd)_2$ and surface hydrogen. The Hthd ligand may form $Pd(thd)_x$ species on the surface upon readsorption and block adsorption and reaction sites from $Pd(thd)_2$. As the precursor pulse front travels along the substrate surface, an increasing amount of Hthd is being formed towards the trailing edge of the substrate, thereby blocking an increasing amount of adsorption and reaction sites from $Pd(thd)_2$, and thus creating the thickness gradient. It should be emphasized that in the showerhead ALD reactors such non-uniformity should not develop because all sites on the substrate surface receive the precursor at about the same time. One can thus expect that the $Pd(thd)_2$–O_3–H_2 process could still produce uniform Pd films in the showerhead ALD reactors.

It should be noted that several oxidation agents, such as H_2O_2, H_2O, O_2 and ozone, have been previously screened for PdO deposition using $Pd(hfac)_2$ as the palladium precursor.[42] However, no growth of Pd on Al_2O_3 was achieved with these reactants,[42] surprisingly not even with the highly reactive ozone. In this respect, the $Pd(thd)_2$ shows clearly different behavior compared to the fluorinated $Pd(hfac)_2$.

The surface roughnesses and resistivities of the crystalline PdO films grown by the $Pd(thd)_2$–O_3 process between 130 and 160 °C are presented in Table 32. The surface roughnesses of about 40 nm thick PdO films were 1.3–2.8 nm. The thinner film (23 nm) grown at 130 °C was smoother (0.9 nm) and more resistive (3×10^5 µΩcm) than the twice thicker films grown at higher temperatures. The resistivities of about 40 nm thick PdO films were 2–3×10^4 µΩcm.

Table 32. Surface roughnesses and resistivities of the grown PdO films.

$T_{dep.}$	130 °C	140 °C	150 °C	160 °C
Thickness (nm)	23	42	42	43
Roughness (nm)	0.9	1.8	1.3	2.8
Resistivity (µΩ cm)	~3×10^5	2.1×10^4	2.1×10^4	2.7×10^4

The elemental contents of PdO and Pd films grown at 130 and 150 °C are shown in Table 33. The palladium oxide film grown at 130 °C is overstoichiometric ($PdO_{1.3}$) and contains about 7 at.% hydrogen and 0.4 at.% carbon impurities while the Pd film grown at the same temperature is pure having ≤ 0.3 at.% oxygen, hydrogen, and carbon each. The PdO film grown at higher temperature (150 °C) is stoichiometric PdO and contains 3 at.% hydrogen and less than 0.2 at.% carbon. The Pd film deposited at 150 °C has substantially higher impurity contents (~3.5 at.% oxygen, ~1.6 at.% hydrogen) than the Pd film grown at 130 °C (0.3 at.% oxygen, <0.2 at.% hydrogen). The impurities given here are upper limit estimations as the sample was hard to analyze because of the thickness non-uniformity. The overall low amounts of hydrogen in the Pd films suggest that the Pd films do not absorb permanently hydrogen in larger amounts despite that H_2 was used as the reductant.

Table 33. Elemental compositions of the palladium oxide and palladium metal thin films as measured with TOF-ERDA.

dep. temp. (°C)	Pd (at.%)	O (at.%)	C (at.%)	H (at.%)	O : Pd ratio
$Pd(thd)_2$–O_3					
130	39 ± 3	49 ± 4	0.4 ± 0.1	7 ± 2	1.26 (1.07–1.47)
150	47 ± 4	48 ± 4	< 0.2	3 ± 1	1.02 (0.86–1.16)
$Pd(thd)_2$–O_3–H_2					
130	99.5 ± 0.5	0.3 ± 0.1	0.2 ± 0.1	< 0.2	<0.01
150	95 ± 5	~3.5	~0.4	~1.6	~0.04

5.4 Platinum oxide and metal

Platinum oxide and platinum metal ALD processes using $Pt(acac)_2$–O_3 and $Pt(acac)_2$–O_3–H_2 precursor sequences were developed.[II,VII] The source temperature of $Pt(acac)_2$ (110 °C) restricted examining the low temperature limits of the processes as films were grown already at 120 °C. The temperature window for the platinum oxide film growth was narrow (120–130 °C) as the films deposited at 140 °C were already metallic platinum (Figure 24a and c). The $Pt(acac)_2$–O_3–H_2 pulsing sequence at 120 and 130 °C resulted in the growth of Pt metal films (Figure 24b and d).

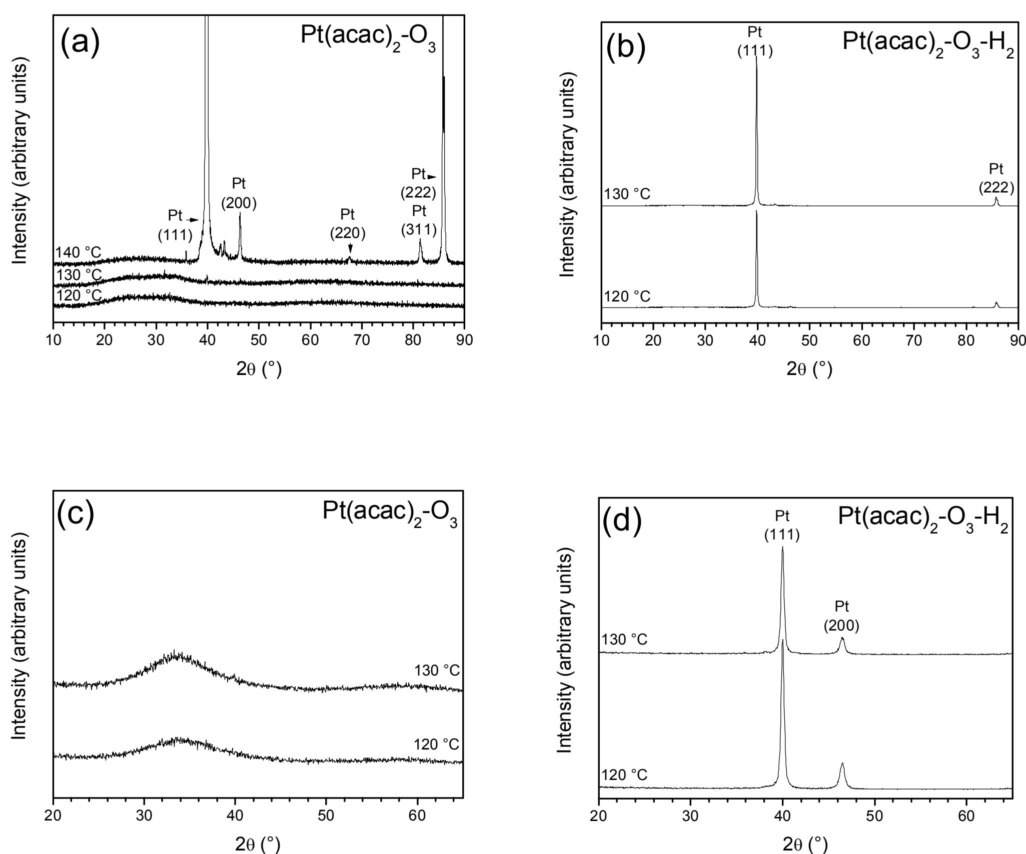

Figure 24. θ–2θ XRD patterns of the (a) platinum oxide [$Pt(acac)_2$–O_3] and (b) platinum metal [$Pt(acac)_2$–O_3–H_2] thin films grown at 120 and 130 °C on Al_2O_3 coated soda lime glass. (c) and (d) are showing the corresponding GIXRD patterns of the films deposited on Al_2O_3 coated Si.

The platinum oxide growth rates were 0.3 and close to 0.5 Å/cycle at 120 and 130 °C, respectively (Figure 25). At higher temperatures the films became metallic Pt. The Pt growth rate was over 0.5 Å/cycle at 140 °C and rose close to 0.6 Å/cycle between 150 and 170 °C. The Pt film grown at 200 °C had an even higher growth rate (0.7 Å/cycle); however notable thickness non-uniformity across the substrate was observed already at 150 °C, and the non-uniformity increased considerably at 200 °C. The $Pt(acac)_2$–O_2 process has been reported to result in non-uniform Pt films at 210–220 °C,[56] which is consistent with the observation on the $Pt(acac)_2$–O_3 process at 200 °C. $Pt(acac)_2$ has shown partial thermal decomposition previously already at 180–200 °C in the F-120 reactor conditions,[84,239] which explains the non-uniformity issues at 200 °C and above.

The metallic film grown from $Pt(acac)_2$ and ozone at 140 °C was very uniform in thickness across the substrate (Figure 25). The Pt films grown with the $Pt(acac)_2$–O_3–H_2 process had growth rates less than 0.3 Å/cycle at 120 and 130 °C (Figure 25), which are only about half the growth rate obtained at 140 °C without using molecular H_2.

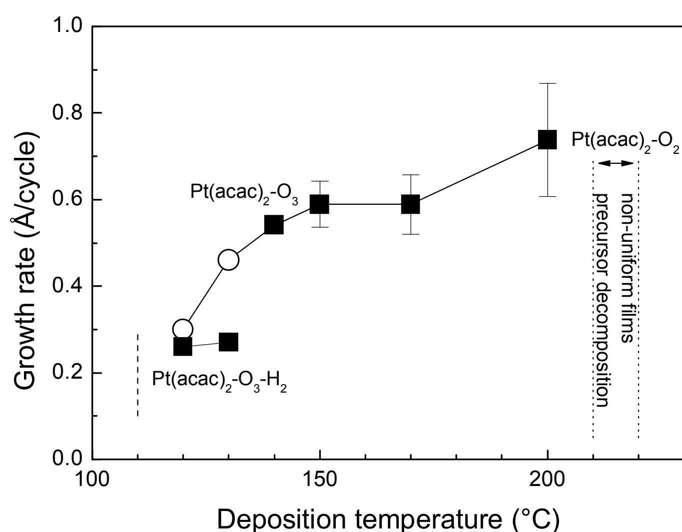

Figure 25. Growth rates of ALD processes using $Pt(acac)_2$ as a function of deposition temperature.[II,VII] Solid symbols denote Pt metal films while open symbols correspond to platinum oxide films. The dashed line at 110 °C indicates the source temperature used for $Pt(acac)_2$. The $Pt(acac)_2$–O_2 sequence between 210 and 220 °C was adapted from Ref. 56.

The surface roughnesses of about 50 nm thick platinum films grown with the $Pt(acac)_2$–O_3–H_2 process at 120 and 130 °C were 2.3 and 2.0 nm, respectively. The amorphous platinum oxide film deposited using the $Pt(acac)_2$–O_3 process at 130 °C to a similar thickness had a roughness of about 0.5 nm. The 50 nm thick Pt film grown with the MeCpPtMe–air(O_2) process at 300 °C had a surface roughness of about 4 nm,[213] while using pure O_2 instead of air resulted in a smoother surface (1.2 nm).[47]

The resistivities of the 50 nm thick Pt films grown with the $Pt(acac)_2$–O_3–H_2 process were about 12–14 μΩcm while the resistivity of the platinum oxide films deposited with the $Pt(acac)_2$–O_3 were five decades higher (~2 Ωcm). The 50 nm thick Pt film grown using the

$MeCpPtMe_3$–O_2 process was reported[47] to have a resistivity of about 13 μΩcm whereas the 110 nm thick film deposited with the $MeCpPtMe_3$–air process had a resistivity of 12 μΩcm.[213] Similarly, the resistivity of 110 nm thick metallic Pt film grown using $Pt(acac)_2$ and ozone at 140 °C was about 11 μΩcm. These results show that Pt metal films grown with the ozone-based processes at low temperatures (120–140 °C) have similar resistivities as the films deposited with oxygen-based processes.

The compositions of the films were analyzed by ERDA and TOF-ERDA (Table 34). The ERDA measurements on the platinum oxide films proved to be problematic as the energetic ion beam reduced platinum oxide during the analysis. Therefore the results on the PtO_x films deposited at 120 and 130 °C were compensated for the elemental losses. The corrected analyses give more accurate results on the actual composition of the PtO_x films but can still contain errors because of the applied correction procedure and quite low oxygen to platinum ratios. More details on the analysis results with and without the elemental loss corrections can be found from the reference [II].

Table 34. Elemental compositions of the platinum oxide and platinum metal thin films as measured with ERDA and TOF-ERDA.

dep. temp. (°C)	Pt (at.%)	O (at.%)	C (at.%)	H (at.%)	O : Pt ratio
$Pt(acac)_2$–O_3					
120[a]	37.4 ± 0.6	49.1 ± 4.7	<0.5	13.5 ± 0.5	1.31 (1.17–1.46)
130[a]	34.9 ± 0.6	54.8 ± 3.0	<0.5	10.3 ± 0.4	1.57 (1.51–1.69)
140	93.6 ± 0.1	5.8 ± 0.4	<0.5	0.65 ± 0.01	0.06
150	93.8 ± 0.1	5.7 ± 0.3	<0.5	0.46 ± 0.01	0.06
200	91.3 ± 0.1	8.3 ± 0.5	<0.5	0.38 ± 0.01	0.09
$Pt(acac)_2$–O_3–H_2					
120	>98	<1	<0.5	<0.5	<0.01
130	>98	<1	<0.3	<0.5	<0.01

a results corrected by elemental loss compensation

The platinum oxide films were highly oxygen deficient from the stable crystalline PtO_2 at both 120 °C ($PtO_{1.3}$) and 130 °C ($PtO_{1.6}$). The PtO_x films contained less than 0.5 at.% carbon but a high amount of hydrogen (10–14 at.%). The metallic Pt film grown with the $Pt(acac)_2$–O_3 process at 140 °C was more pure and had similar carbon (<0.5 at.%) and considerably lower hydrogen content (0.7 at.%) compared to the PtO_x films grown at 130 °C. The Pt film deposited at 140 °C contained about 6 at.% oxygen.

The Pt metal films grown using the $Pt(acac)_2$–O_3–H_2 pulsing sequence were pure having less than 1 at.% oxygen, carbon, and hydrogen impurities each. These values are very low taken into account that the films were grown at low temperatures of 120–130 °C. At those temperatures the H_2O byproduct can be difficult to efficiently evacuate from the deposition chamber; however relatively short 2 s precursor pulses and purges were used in these depositions while maintaining excellent film purity.

Also $MeCpPtMe_3$ was examined with ozone for thermal ALD of platinum oxide (unpublished results). The platinum oxide films were grown between 110 and 130 °C while metallic Pt was obtained at 140 °C and above (Figure 26). The growth rate of PtO_x using $MeCpPtMe_3$–O_3 was about 0.1 Å/cycle at 110 °C and rose to about 0.3 and 0.4 Å/cycle at 120 and 130 °C, respectively. The oxide–metal transition temperature and PtO_x growth rates are similar to the $Pt(acac)_2$–O_3 process (Figures 24 and 25).

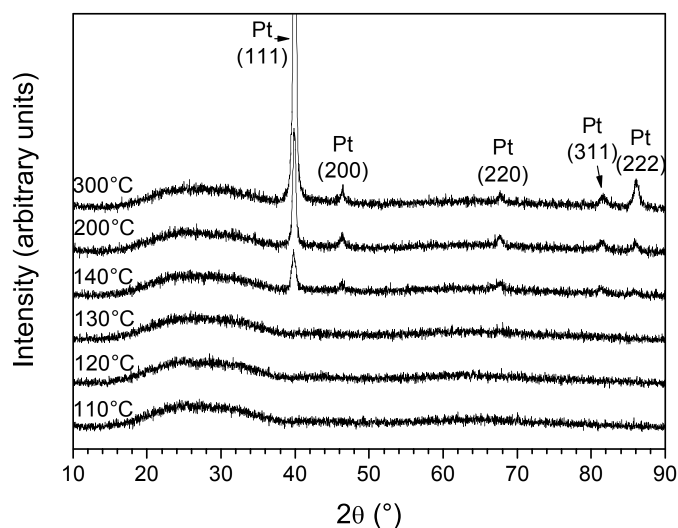

Figure 26. θ–2θ XRD patterns of the films grown using $MeCpPtMe_3$ and ozone on soda lime glass at various temperatures (unpublished results). The pulse lengths for $MeCpPtMe_3$ and ozone were 2 and 1 s, respectively, while purges were 1 s each. A total of 500 cycles was applied in each deposition.

The $MeCpPtMe_3$–O_3 PtO_x process had however drawbacks. Longer $MeCpPtMe_3$ pulses led to a reduction of the oxide to more metallic in appearance. This was noted as a drastic decrease in resistivity as well (Figure 27; 4 s pulse length). The repetition of the process was difficult as the $MeCpPtMe_3$ pulse length (dose) determined the film composition. Because the total time of one ALD cycle determines how much time $MeCpPtMe_3$ has to sublime in the internal source vessel between the pulses, hence affecting the $MeCpPtMe_3$ dose, even changes in the lengths of the purge periods affected whether oxide or metal was formed (Figure 28). Also large variations in sheet resistances and areas of different transparency were observed across the films in some depositions; however films with uniform sheet resistances across the substrates were mostly obtained.

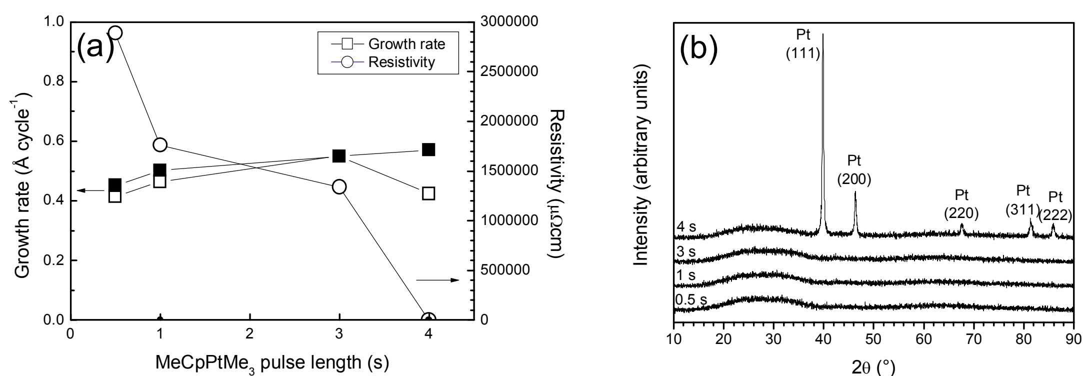

Figure 27. (a) Growth rates and resistivities, and (b) θ–2θ XRD patterns of the films deposited at 130 °C using $MeCpPtMe_3$ with different pulse lengths and ozone (unpublished results). The films were grown on soda lime glasses (open symbols) and Si substrates (solid). The XRD patterns were measured from films grown on soda lime glass. The pulse length for ozone was 2 s while the purges were 1 s.

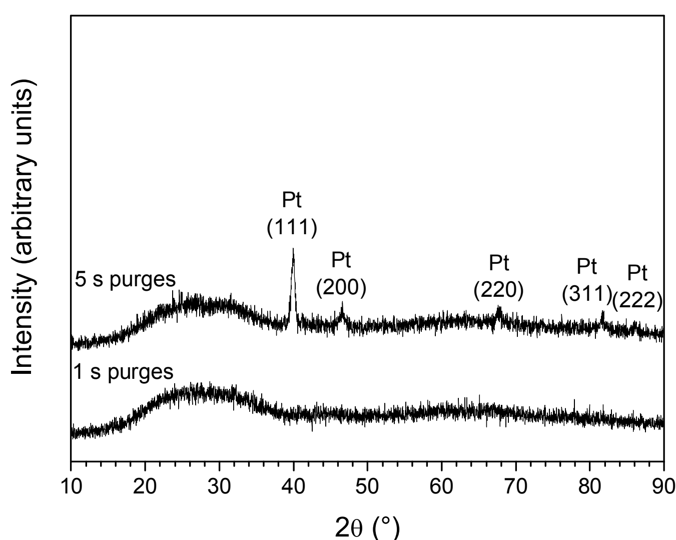

Figure 28. θ–2θ XRD patterns of the films grown using $MeCpPtMe_3$ and ozone on Al_2O_3 coated soda lime glass at 130 °C (unpublished results). The pulse lengths for $MeCpPtMe_3$ and ozone were 2 and 1 s. The purge times after both precursors were either 1 or 5 s as noted in the figure. A total of 500 cycles was applied in both depositions.

5.5 General aspects of the low-temperature ozone-based ALD processes

The ozone-based noble metal oxide and noble metal ALD processes are new and have not yet been thoroughly examined and compared with other ALD and PEALD processes. Therefore this chapter highlights and discusses some issues related to the ozone-based ALD of noble metals and their oxides. This includes some potential benefits and drawbacks of the low-temperature ozone-based ALD processes.

The most distinct difference between the ozone-based and oxygen-based thermal ALD processes is the deposition temperature. The oxygen-based processes require mostly temperatures of 200 °C and above to be successful in growing noble metals while the ozone-based processes facilitate noble metal oxide deposition at lower temperatures, and with H_2 these low-temperature oxide processes can be converted to metal processes. Based on the IrO_2 and PtO_x results, the lowest temperature where the ozone-based chemistry is still effective is about 100–120 °C.

Development of ozone-based Ru and Os processes may prove to be challenging because volatile higher oxidation-state tetroxides of Ru and Os can form easily. Even so, ozone has been used successfully to deposit Ru films by ALD at higher temperatures (225–275 °C).[113] Therefore, by controlling the ozone dose carefully also at lower temperatures the growth of ruthenium and osmium oxides could be feasible. Consequently the ALD of Ru and Os could be possible by the oxidation–reduction pathway at as low temperatures as shown with the other platinum group metals.

Reaction mechanisms in thermal ALD of noble metals depend on the reactants and deposition temperatures used. In the oxygen-based processes catalytically active noble metal surface is needed to dissociate O_2 to atomic O so that the ligands of the noble metal precursor are combusted and the film is grown. The requirement of O_2 dissociation can be linked to the need of high deposition temperatures of above 200 °C and to the difficulties in nucleation on various surfaces that are not catalytically active in dissociating O_2. The reductive ALD Pd processes deposit films at as low temperatures as 80 °C but the surface must in this case activate H_2 by dissociating it to atomic H. $Pd(hfac)_2$ releases a Hhfac

ligand during adsorption and rest of the ligands are discharged from the surface during the H_2 pulse. The ALD of Pd suffers from prolonged nucleation periods and the possibility of the surface poisoning by the Hhfac byproduct. The reaction mechanism in the ALD of Pd bears thus similarity with the oxygen-based ALD noble metal processes where atomic oxygen is responsible for the partial combustion of the precursor upon adsorption to the surface. By contrast, in the ozone-based process below 200 °C the noble metal precursor [Ir(acac)$_3$] adsorbs on the surface stoichiometrically regardless the availability (IrO_2) or absence (Ir) of oxygen on the surface.[30]

The stoichiometric adsorption of the noble metal precursor and the use of reactive ozone allow the ozone-based processes to nucleate easily on various surfaces. This has been exploited in the ozone-based ALD of Ir and IrO_2 directly on PVP,[199] which is a polymer that can effectively block the growth of noble metals by the oxygen-based ALD processes.[71,199] The nucleation of the ozone-based processes on various substrates has not yet been examined in detail and thus the possibility of using the low temperature ozone-based noble metals and oxides for non-selective ALD as their own or as nucleation layers for the oxygen-based processes can only be suggested.

A potential drawback of the stoichiometric adsorption pathway at low temperatures is the possibility of desorption of the precursor from the surface. Another concern could be the formation of H_2O byproduct which can be hard to evacuate effectively from the reactor at low temperatures. These disadvantages could be however alleviated by optimizing process parameters, purges and reactor designs. Alternatively, in the ozone-based noble metal processes the formation of H_2O might be minimized by using other reducing agents than H_2. These could include for example carbon monoxide, methane, and other compounds which could steal oxygen from the noble metal oxide surface. Both the noble metal oxides and noble metals are catalytically very active materials, and thus the reduction of the noble metal oxide surface to the more stable noble metal should be relatively straightforward with other reducing agents too.

Lower growth temperatures have been achieved by using also oxygen plasma as more reactive oxidation agent than molecular oxygen. For example, PtO_2 and Pt have been grown by PEALD using oxygen plasma at even lower temperatures (100 °C)[225,226] than

with ozone. The oxygen plasma results in overstoichiometric platinum dioxide films ($PtO_{2.2}$)[225,226] while ozone produces films which are understoichiometric ($PtO_{1.6}$)[II] showing that ozone in thermal ALD is not comparable to oxygen plasma in PEALD in terms of reactivity. Noble metals can be grown by PEALD also reductively using H_2 and NH_3 plasmas, thus the reactive plasmas give the PEALD an advantage in the development of low temperature processes.

The ozone-based processes can potentially oxidize a substrate and form an intermediate oxide layer between the film and the substrate, and this is even more probable in the oxygen plasma based PEALD. The oxidation is eliminated in PEALD by using reductive plasmas, but highly energetic radical species from the plasma can still cause substrate damage. The recombination of plasma species in PEALD may limit conformal growth especially in high aspect ratios; however ozone can also decompose to non-reactive species causing conformality issues. This is especially true when catalytically active materials are grown as seen in the case of Rh_2O_3 deposition.[III]

The above issues related to the advantages and disadvantages of the ozone-based noble metal oxide and noble metal ALD growth show that ozone bridges the gap between the thermal oxygen-based ALD and PEALD processes. The ozone-based noble metal and oxide processes combine some of the good properties of the other two approaches, but also fall short of these because of a lack of higher thermal budget used in the oxygen-based ALD processes and a lack of more reactive reactants used in the PEALD.

5.6 Osmium

Os films were grown by ALD between 325 and 375 °C from $OsCp_2$ and molecular O_2.[VIII] All the films consisted of only metallic Os according to XRD. The films grown at 300 °C were very thin and non-uniform after 1000 cycles; therefore the low temperature limit of the Os ALD process on Al_2O_3 was considered to be 325 °C (Figure 29). The film growth was studied also at 400 °C but most of the metallic film was etched away. The growth rates including nucleation delays were roughly 0.2 Å/cycle at 325 °C and 0.3 Å/cycle between 350 and 375 °C (Figure 29).

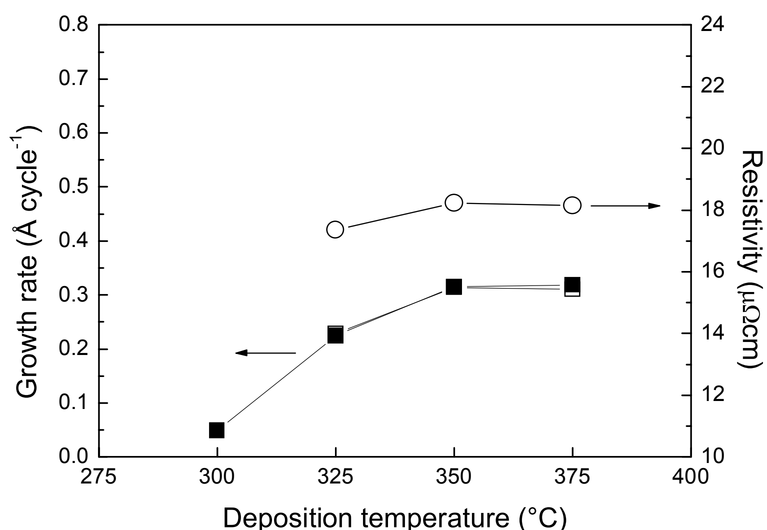

Figure 29. Growth rates and resistivities of the Os films on Al_2O_3 surface as a function of deposition temperature. $OsCp_2$ and O_2 pulses were 3 s and 2 s, respectively, with 1 s purges. 1000 cycles were applied in each deposition. Open and solid symbols denote Os films on Al_2O_3 coated soda lime glasses and Si substrates, respectively.

About 30 nm thick Os films had resistivities of about 18–19 μΩcm. The films were very pure containing less than 1 at.% oxygen, carbon, and hydrogen impurities each (Table 35). The ALD Os process was noted to have a substantial nucleation delay of about 350 cycles at 350 °C on Al_2O_3 surface, which means that either Os nanoparticles or Os thin films can be deposited by adjusting the number of deposition cycles. The surface roughnesses of about 30 nm thick films decreased with increasing deposition temperature from 2.8 nm (26 nm, 325 °C) to 1.5 nm (34 nm, 375 °C). This is related to more efficient and faster nucleation of Os at higher deposition temperatures.

Table 35. Elemental composition of the Os films as measured with TOF-ERDA.

dep. temp. (°C)	Os (at.%)	O (at.%)	C (at.%)	H (at.%)
325	98.5 ± 1.0	<1	0.5 ± 0.3	0.5 ± 0.4
350	99.0 ± 1.0	<0.5	<0.2	<0.3
375	98.5 ± 1.0	<0.5	0.5 ± 0.3	0.5 ± 0.4

6 Conclusions

This thesis examined noble metal oxide and noble metal thin film growth by ozone-based ALD processes. Oxide films of Ir, Rh, Pt, and Pd were deposited using reactive ozone at temperatures below 200 °C. The corresponding metal films were grown by adding a reductive H_2 step after every noble metal oxide growth cycle. The oxidation–reduction reaction pathway led to ALD of noble metals at lower temperatures than possible with the corresponding oxygen-based ALD noble metal processes. In addition, an ALD Os process was developed using conventional molecular oxygen to complement the selection of ALD noble metal materials.

The noble metal oxide film growth was facilitated with ozone at lower temperatures and in a simpler way compared to the earlier oxygen-based noble metal oxide processes that rely on the sensitive control of growth parameters. The ozone-based noble metal oxide processes were limited to narrow deposition temperature ranges between the precursor sublimation temperatures and the reduction to metal close to about 200 °C. The Rh_2O_3 ALD process needed atypical deposition procedure to achieve good thickness uniformity which should be addressed in the future.

The developed ozone-based noble metal oxide and noble metal ALD processes proved to be promising. The growth rates, purities, resistivities and surface roughnesses of the films were reasonable despite the low deposition temperatures and the lack of more aggressive plasma species. In some cases the properties of the noble metal films were comparable to the films grown at higher temperatures by the oxygen-based processes. The non-uniform and fast growth of the Pd films indicates that the O_3–H_2 reaction pathway may involve unique complications.

Open questions related to possible benefits and drawbacks of the ozone-based processes still remain. More thorough investigation of the processes studied in this thesis and additional ozone-based processes are needed. The understanding of the oxidation–reduction reaction pathway and the chemistry of the intermediate surfaces with catalytic properties will eventually determine the true potential of the low-temperature ozone-based processes. The need for more volatile noble metal precursors is immediate; however

controlling surface reactions by ligands of noble metal precursors and by reducing agents other than H_2 could also prove to be useful for ozone-based noble metal ALD processes.

Acknowledgements

The research and experimental work for this dissertation was carried out in the Laboratory of Inorganic Chemistry at the Department of Chemistry of the University of Helsinki.

I am most grateful to Prof. Mikko Ritala and Prof. Markku Leskelä for their guidance, advice, and support. It has been a privilege to have you as my supervisors and to have the opportunity to work in the ALD group.

I would like to express my gratitude to all the co-authors as without your valuable contributions this work would have been lacking depth. Dr. Frans Munnik, Dr. Ulrich Kreissig, Dr. Leila Costelle, and Doc. Timo Sajavaara are thanked for film composition analyses. I am grateful for Doc. Marianna Kemell for scanning electron microscopy and Doc. Esa Puukilainen for atomic force microscopy. In addition, I am indebted to Timo Hatanpää and Dr. Tero Pilvi for development and synthesis of an ALD precursor.

I would like to acknowledge two individuals who have influenced me greatly and to whom I owe my gratitude. I thank Dr. Jarkko Ihanus for tutoring me during the experimental part of my M.Sc. studies and teaching me good ALD reactor and laboratory practice. I thank Dr. Titta Aaltonen for introducing me to the ALD of noble metals and to the tools required to analyze metallic films. I would like to thank all the present and former colleagues in the ALD group and at the Laboratory of Inorganic Chemistry for creating most pleasant working atmosphere. Furthermore, I thank Dr. Jarkko Ihanus, Prof. Seán Barry, and Emma Härkönen for sharing the office with me during my dissertation research.

The long term financial support from ASM Microchemistry and the Finnish Funding Agency for Technology and Innovation (Tekes) is gratefully acknowledged. I thank Dr. Suvi Haukka, Dr. Marko Tuominen, and the staff of ASM Microchemistry for their advice, help, and fruitful co-operation. In addition, I would like to express my gratitude to ASM Microchemistry and the Finnish Centre of Excellence in Atomic Layer Deposition for their support in preparation of this dissertation. Furthermore, I am most grateful for the Häme Student Foundation for awarding a personal grant during my doctoral studies.

I owe my sincere appreciation to my parents, Tuire and Kari, and to my brother, Tero, for all the support and encouragement they have given me over the years. I also thank all my friends for their support, and especially for all the good and enjoyable moments which helped me to carry through this journey. Pauleena, mere words just cannot describe how thankful I am for all your love and understanding.

This dissertation is dedicated to the memory of my father.

Espoo, April 2013

Jani Hämäläinen

References

(1) T. Aaltonen, Ph.D. thesis, University of Helsinki, Finland, 2005. Available from http://ethesis.helsinki.fi/en/.

(2) Encyclopaedia Britannica Online, 2012.

(3) Oxford Dictionaries Online, 2012.

(4) CRC Handbook of Chemistry and Physics, 92nd Edition (Internet version 2012), online.

(5) ICCD Powder Diffraction File, PDF-2 Database Sets 1–47, 1997.

(6) A. Ferretti, D. B. Rogers and J. B. Goodenough, *J. Phys. Chem. Solids* **26** (1965) 2007.

(7) W. D. Ryden, A. W. Lawson and C. C. Sartain, *Phys. Rev. B* **1** (1970) 1494.

(8) P. C. Yen, R. S. Chen, C. C. Chen, Y. S. Huang and K. K. Tiong, *J. Cryst. Growth* **262** (2004) 271.

(9) A. Roy and J. Ghose, *Mater. Res. Bull.* **33** (1998) 547.

(10) R. D. Shannon, *Solid State Commun.* **6** (1968) 139.

(11) R. D. Shannon, *Solid State Commun.* **7** (1969) 257.

(12) T. P. Pearsall and C. A. Lee, *Phys. Rev. B* **10** (1974) 2190.

(13) D. B. Rogers, R. D. Shannon, A. W. Sleight and J. L. Gillson, *Inorg. Chem.* **8** (1969) 841.

(14) M. Ritala and M. Leskelä, in *Handbook of Thin Film Materials*, ed. H. S. Nalwa, Academic Press, San Diego, CA, 2001, vol. 1, pp. 103-159.

(15) M. Ritala and J. Niinistö, in *Chemical Vapor Deposition: Precursors, Processes and Applications*, ed. A. C. Jones and M. L. Hitchman, The Royal Society of Chemistry, Cambridge, UK, 2009, pp. 158–206.

(16) S. M. George, *Chem. Rev.* **110** (2010) 111.

(17) V. Miikkulainen, M. Leskelä, M. Ritala and R. L. Puurunen, *J. Appl. Phys.* **113** (2013) 021301.

(18) R. L. Puurunen, *J. Appl. Phys.* **97** (2005) 121301.

(19) M. Leskelä, M. Ritala and O. Nilsen, *MRS Bull.* **36** (2011) 877.

(20) M. Ritala and J. Niinistö, *ECS Trans.* **25** (2009) 641.

(21) S. Haukka, *ECS Trans.* **3** (2007) 15.

(22) C. Marichy, M. Bechelany and N. Pinna, *Adv. Mater.* **24** (2012) 1017.

(23) J. W. Elam, N. P. Dasgupta and F. B. Prinz, *MRS Bull.* **36** (2011) 899.

(24) R. Seymour *Platinum Metals Rev.* **52** (2008) 231.

(25) M. Ritala, K. Kukli, A. Rahtu, P. I. Räisänen, M. Leskelä, T. Sajavaara and J. Keinonen, *Science* **288** (2000) 319.

(26) H. C. M. Knoops, E. Langereis, M. C. M. van de Sanden and W. M. M. Kessels, *J. Electrochem. Soc.* **157** (2010) G241.

(27) H. B. Profijt, S. E. Potts, M. C. M. van de Sanden and W. M. M. Kessels, *J. Vac. Sci. Technol. A* **29** (2011) 050801.

(28) W. M. M. Kessels and M. Putkonen, *MRS Bull.* **36** (2011) 907.

(29) T. Aaltonen, A. Rahtu, M. Ritala and M. Leskelä, *Electrochem. Solid-State Lett.* **6** (2003) C130.

(30) K. Knapas and M. Ritala, *Chem. Mater.* **23** (2011) 2766.

(31) W. M. M. Kessels, H. C. M. Knoops, S. A. F. Dielissen, A. J. M. Mackus and M. C. M. van de Sanden, *Appl. Phys. Lett.* **95** (2009) 013114.

(32) T. Aaltonen, M. Ritala, K. Arstila, J. Keinonen and M. Leskelä, *Chem. Vap. Deposition* **10** (2004) 215.

(33) N. Leick, S. Agarwal, A. J. M. Mackus and W. M. M. Kessels, *Chem. Mater.* **24** (2012) 3696.

(34) S. T. Christensen and J. W. Elam, *Chem. Mater.* **22** (2010) 2517.

(35) J. S. King, A. Wittstock, J. Biener, S. O. Kucheyev, Y. M. Wang, T. F. Baumann, S. K. Giri, A. V. Hamza, M. Baeumer and S. F. Bent, *Nano Lett.* **8** (2008) 2405.

(36) A. J. M. Mackus, N. Leick, L. Baker and W. M. M. Kessels, *Chem. Mater.* **24** (2012) 1752.

(37) I. J. M. Erkens, A. J. M. Mackus, H. C. M. Knoops, P. Smits, T. H. M. van de Ven, F. Roozeboom and W. M. M. Kessels, *ECS J. Solid State Sci. Technol.* **1** (2012) P255.

(38) S. K. Kim, S. Hoffmann-Eifert and R. Waser, *J. Phys. Chem. C* **113** (2009) 11329.

(39) S. K. Kim, S. Hoffmann-Eifert and R. Waser, *ECS Trans.* **25** (2009) 289.

(40) W.-H. Kim, S.-J. Park, D. Y. Kim and H. Kim, *J. Korean Phys. Soc.* **55** (2009) 32.

(41) T. Aaltonen, M. Ritala, V. Sammelselg and M. Leskelä, *J. Electrochem. Soc.* **151** (2004) G489.

(42) J. W. Elam, A. Zinovev, C. Y. Han, H. H. Wang, U. Welp, J. N. Hryn and M. J. Pellin, *Thin Solid Films* **515** (2006) 1664.

(43) D. Longrie, K. Devloo-Casier, D. Deduytsche, S. Van den Berghe, K. Driesen and C. Detavernier, *ECS J. Solid State Sci. Technol.* **1** (2012) Q123.

(44) S. K. Kim, J. H. Han, G. H. Kim and C. S. Hwang, *Chem. Mater.* **22** (2010) 2850.

(45) B. H. Choi, Y. H. Lim, J. H. Lee, Y. B. Kim, H.-N. Lee and H. K. Lee, *Microelectron. Eng.* **87** (2010) 1391.

(46) K. Kukli, M. Ritala, M. Kemell and M. Leskelä, *J. Electrochem. Soc.* **157** (2010) D35.

(47) T. Aaltonen, M. Ritala, Y.-L. Tung, Y. Chi, K. Arstila, K. Meinander and M. Leskelä, *J. Mater. Res.* **19** (2004) 3353.

(48) A. J. M. Mackus, J. J. L. Mulders, M. C. M. van de Sanden and W. M. M. Kessels, *J. Appl. Phys.* **107** (2010) 116102.

(49) Y. Zhu, K. A. Dunn and A. E. Kaloyeros, *J. Mater. Res.* **22** (2007) 1292.

(50) X. Liang, Y. Zhou, J. Li and A. W. Weimer, *J. Nanopart. Res.* **13** (2011) 3781.

(51) T. Aaltonen, P. Alén, M. Ritala and M. Leskelä, *Chem. Vap. Deposition* **9** (2003) 45.

(52) S. T. Christensen, J. W. Elam, B. Lee, Z. Feng, M. J. Bedzyk and M. C. Hersam, *Chem. Mater.* **21** (2009) 516.

(53) K. Kukli, J. Aarik, A. Aidla, T. Uustare, I. Jõgi, J. Lu, M. Tallarida, M. Kemell, A.-A. Kiisler, M. Ritala and M. Leskelä, *J. Cryst. Growth* **312** (2010) 2025.

(54) S. K. Kim, S. Han, J. H. Han and C. S. Hwang, *Appl. Surf. Sci.* **257** (2011) 4302.

(55) B. H. Choi, J. H. Lee, H. K. Lee and J. H. Kim, *Appl. Surf. Sci.* **257** (2011) 9654.

(56) T. Aaltonen, M. Ritala and M. Leskelä, in Advanced Metallization Conference 2004 (AMC 2004), eds. D. Erb, P. Ramm, K. Masu, and A. Osaki, Materials Research Society, 2005, 663–667.

(57) J. W. Elam, A. V. Zinovev, M. J. Pellin, D. J. Comstock and M. C. Hersam, *ECS Trans.* **3** (2007) 271.

(58) K. J. Park, D. B. Terry, S. M. Stewart and G. N. Parsons, *Langmuir* **23** (2007) 6106.

(59) S.-S. Yim, D.-J. Lee, K.-S. Kim, S.-H. Kim, T.-S. Yoon and K.-B. Kim, *J. Appl. Phys.* **103** (2008) 113509.

(60) P. Shrestha, D. Gu, N. H. Tran, K. Tapily, H. Baumgart and G. Namkoong, *ECS Trans.* **33** (2010) 127.

(61) S. K. Kim, S. Y. Lee, S. W. Lee, G. W. Hwang, C. S. Hwang, J. W. Lee and J. Jeong, *J. Electrochem. Soc.* **154** (2007) D95.

(62) J. Heo, S. Y. Lee, D. Eom, C. S. Hwang and H. J. Kim, *Electrochem. Solid-State Lett.* **11** (2008) G5.

(63) Y.-C. Hsueh, C.-T. Hu, C.-C. Wang, C. Liu and T.-P. Perng, *ECS Trans.* **16** (2008) 855.

(64) C. Liu, C.-C. Wang, C.-C. Kei, Y.-C. Hsueh and T.-P. Perng, *Small* **5** (2009) 1535.

(65) S. Coombs, A. Dameron, C. Engtrakul, S. Pylypenko, J. Lee, T. S. Olson, C. Bochert, T. Gennett, L. Simpson, B. Pivovar and H. N. Dinh, *ECS Trans.* **33** (2010) 221.

(66) J. Heo, S.-J. Won, D. Eom, S. Y. Lee, Y. B. Ahn, C.-S. Hwang and H. J. Kim, *Electrochem. Solid-State Lett.* **11** (2008) H210.

(67) Y.-C. Hsueh, C.-C. Wang, C. Liu, C.-C. Kei and T.-P. Perng, *Nanotechnology* **23** (2012) 405603.

(68) J. Bult, A. Dameron, S. Pylypenko, C. Engtrakul, C. Bochert, L. Chen, G. Leong, S. Frisco, L. Simpson, H. N. Dinh and B. Pivovar, *ECS Trans.* **33** (2010) 89.

(69) G.-J. Choi, S. K. Kim, S. Y. Lee, W. Y. Park, M. Seo, B. J. Choi and C. S. Hwang, *J. Electrochem. Soc.* **156** (2009) G71.

(70) E. Färm, M. Kemell, M. Ritala and M. Leskelä, *J. Phys. Chem. C* **112** (2008) 15791.

(71) E. Färm, M. Kemell, E. Santala, M. Ritala and M. Leskelä, *J. Electrochem. Soc.* **157** (2010) K10.

(72) E. Färm, M. Kemell, M. Ritala and M. Leskelä, *Chem. Vap. Deposition* **12** (2006) 415.

(73) E. Färm, M. Kemell, M. Ritala and M. Leskelä, *Thin Solid Films* **517** (2008) 972.

(74) K. J. Park, J. M. Doub, T. Gougousi and G. N. Parsons, *Appl. Phys. Lett.* **86** (2005) 051903.

(75) X. Jiang and S. F. Bent, *ECS Trans.* **3** (2007) 249.

(76) E. Färm, Ph.D. thesis, University of Helsinki, Finland, 2011. Available from http://ethesis.helsinki.fi/en/.

(77) E. Färm, S. Lindroos, M. Ritala and M. Leskelä, *Chem. Mater.* **24** (2012) 275.

(78) M. Lashdaf, T. Hatanpää, A. O. I. Krause, J. Lahtinen, M. Lindblad and M. Tiitta, *Appl. Catal. A* **241** (2003) 51.

(79) M. Lashdaf, A. O. I. Krause, M. Lindblad, M. Tiitta and T. Venäläinen, *Appl. Catal. A* **241** (2003) 65.

(80) H. Vuori, A. Pasanen, M. Lindblad, M. Valden, M. Veringa Niemelä and A. O. I. Krause, *Appl. Surf. Sci.* **257** (2011) 4204.

(81) D. C. Cronauer, G. Jacobs, L. Linganiso, A. J. Kropf, J. W. Elam, S. T. Christensen, C. L. Marshall and B. H. Davis, *Catal. Lett.* **141** (2011) 968.

(82) E. Rikkinen, A. Santasalo-Aarnio, S. Airaksinen, M. Borghei, V. Viitanen, J. Sainio, E. I. Kauppinen, T. Kallio and A. O. I. Krause, *J. Phys. Chem. C* **115** (2011) 23067.

(83) W. Setthapun, W. D. Williams, S. M. Kim, H. Feng, J. W. Elam, F. A. Rabuffetti, K. R. Poeppelmeier, P. C. Stair, E. A. Stach, F. H. Ribeiro, J. T. Miller and C. L. Marshall, *J. Phys. Chem. C* **114** (2010) 9758.

(84) H. Vuori, M. Lindblad and A. O. I. Krause, *Stud. Surf. Sci. Catal.* **162** (2006) 505.

(85) H. Vuori, R. J. Silvennoinen, M. Lindblad, H. Österholm and A. O. I. Krause, *Catal. Lett.* **131** (2009) 7.

(86) R. J. Silvennoinen, O. J. T. Jylhä, M. Lindblad, J. P. Sainio, R. L. Puurunen and A. O. I. Krause, *Appl. Surf. Sci.* **253** (2007) 4103.

(87) J. Lu, Y. Lei and J. W. Elam, in *Noble Metals*, ed. Y.-H. Su, InTech, 2012, pp. 159-178. Available from http://www.intechopen.com/books/noble-metals/atomic-layer-deposition-of-noble-metals-new-developments-in-nanostructured-catalysts.

(88) H. Feng, J. W. Elam, J. A. Libera, W. Setthapun and P. C. Stair, *Chem. Mater.* **22** (2010) 3133.

(89) D. N. Goldstein and S. M. George, *Appl. Phys. Lett.* **95** (2009) 143106.

(90) D. N. Goldstein and S. M. George, *Thin Solid Films* **519** (2011) 5339.

(91) X. Liang, L. B. Lyon, Y.-B. Jiang and A. W. Weimer, *J. Nanopart. Res.* **14** (2012) 943.

(92) S.-H. Kwon, O.-K. Kwon, J.-H. Kim, H.-R. Oh, K.-H. Kim and S.-W. Kang, *J. Electrochem. Soc.* **155** (2008) H296.

(93) S.-J. Park, W.-H. Kim, H.-B.-R. Lee, W. J. Maeng and H. Kim, *Microelectron. Eng.* **85** (2008) 39.

(94) J. Swerts, M. M. Salimullah, M. Popovici, M.-S. Kim, M. A. Pawlak, A. Delabie, M. Schaekers, K. Tomida, B. Kaczer, K. Opsomer, C. Vrancken, I. Debusschere, L. Altimime, J. A. Kittl and S. Van Elshocht, *ECS. Trans.* **41** (2011) 41.

(95) J. Swerts, A. Delabie, M. M. Salimullah, M. Popovici, M.-S. Kim, M. Schaekers and S. Van Elshocht, *ECS Solid State Lett.* **1** (2012) P19.

(96) L. Baker, A. S. Cavanagh, D. Seghete, S. M. George, A. J. M. Mackus, W. M. M. Kessels, Z. Y. Liu and F. T. Wagner, *J. Appl. Phys.* **109** (2011) 084333.

(97) J. J. Kelly, T. Vo, O. van der Straten, Q. Huang, B. Baker, X. Shao, S. Chiang and J. O. Dukovic, *ECS Trans.* **16** (2008) 201.

(98) J. Kelly, O. van der Straten, T. Vo, R. Janek and Y. Dordi, *ECS Trans.* **33** (2010) 145.

(99) O. van der Straten, J. Wynne, T. Vo, J. Maniscalco, T. Nogami, I. Ali, S. Chiang, J. Ren and P. Ma, *ECS Trans.* **16** (2008) 193.

(100) S.-H. Kim, H. T. Kim, S.-S. Yim, D.-J. Lee, K.-S. Kim, H.-M. Kim, K.-B. Kim and H. Sohn, *J. Electrochem. Soc.* **155** (2008) H589.

(101) H. Kim, *Surf. Coat. Technol.* **200** (2006) 3104.

(102) S. Armini, S. Demuynck, Z. El-mekki, J. Swerts, M. Nagar, A. Radisic, N. Heylen, G. Beyer, L. Leunissen and P. Vereecken, *ECS Trans.* **35** (2011) 117.

(103) M. Schaekers, J. Swerts, L. Altimime and Z. Tőkei, *ECS Trans.* **34** (2011) 509.

(104) S.-H. Kwon, O.-K. Kwon, J.-S. Min and S.-W. Kang, *J. Electrochem. Soc.* **153** (2006) G578.

(105) T. Cheon, S.-H. Choi, S.-H. Kim and D.-H. Kang, *Electrochem. Solid-State Lett.* **14** (2011) D57.

(106) M. Tungare, S. Kumar, M. Li and E. T. Eisenbraun, *ECS Trans.* **3** (2006) 303.

(107) A. Salzer, *Pure Appl. Chem.* **71** (1999) 1557.

(108) X. Jiang, T. M. Gür, F. B. Prinz and S. F. Bent, *Chem. Mater.* **22** (2010) 3024.

(109) O.-K. Kwon, J.-H. Kim, H.-S. Park and S.-W. Kang, *J. Electrochem. Soc.* **151** (2004) G109.

(110) D.-J. Lee, S.-S. Yim, K.-S. Kim, S.-H. Kim and K.-B. Kim, *Electrochem. Solid-State Lett.* **11** (2008) K61.

(111) S.-H. Kwon, O.-K. Kwon, J.-H. Kim, S.-J. Jeong, S.-W. Kim and S.-W. Kang, *J. Electrochem. Soc.* **154** (2007) H773.

(112) S.-J. Park, W.-H. Kim, W. J. Maeng, Y. S. Yang, C. G. Park, H. Kim, K.-N. Lee, S.-W. Jung and W. K. Seong, *Thin Solid Films* **516** (2008) 7345.

(113) J.-Y. Kim, D.-S. Kil, J.-H. Kim, S.-H. Kwon, J.-H. Ahn, J.-S. Roh and S.-K. Park, *J. Electrochem. Soc.* **159** (2012) H560.

(114) M. Nakahara, S. Tsunekawa, K. Watanabe, T. Arai, T. Yunogami and K. Kuroki, *J. Vac. Sci. Technol. B* **19** (2001) 2133.

(115) O.-K. Kwon, S.-H. Kwon, H.-S. Park and S.-W. Kang, *Electrochem. Solid-State Lett.* **7** (2004) C46.

(116) O.-K. Kwon, S.-H. Kwon, H.-S. Park and S.-W. Kang, *J. Electrochem. Soc.* **151** (2004) C753.

(117) J. Musschoot, Q. Xie, D. Deduytsche, K. De Keyser, D. Longrie, J. Haemers, S. Van den Berghe, R. L. Van Meirhaeghe, J. D´Haen and C. Detavernier, *Microelectron. Eng.* **87** (2010) 1879.

(118) Q. Xie, Y.-L. Jiang, J. Musschoot, D. Deduytsche, C. Detavernier, R. L. Van Meirhaeghe, S. Van den Berghe, G.-P. Ru, B.-Z. Li and X.-P. Qu, *Thin Solid Films* **517** (2009) 4689.

(119) M.-G. Ko, W.-S. Kim, S.-K. Park, H.-D. Kim and J.-W. Park, *J. Korean Phys. Soc.* **53** (2008) 2123.

(120) C.-C. Chang and F.-M. Pan, *J. Electrochem. Soc.* **158** (2011) G97.

(121) W.-H. Kim, S.-J. Park, J.-Y. Son and H. Kim, *Nanotechnology* **19** (2008) 045302.

(122) S. K. Kim, S. Han, G. H. Kim, J. H. Jang, J. H. Han and C. S. Hwang, *J. Electrochem. Soc.* **158** (2011) D477.

(123) K. Kawano, H. Kosuge, N. Oshima and H. Funakubo, *Electrochem. Solid-State Lett.* **10** (2007) D60.

(124) O. van der Straten, S. M. Rossnagel, J. P. Doyle and K. P. Rodbell, *ECS Trans.* **1** (2006) 51.

(125) K. Kukli, M. Kemell, E. Puukilainen, J. Aarik, A. Aidla, T. Sajavaara, M. Laitinen, M. Tallarida, J. Sundqvist, M. Ritala and M. Leskelä, *J. Electrochem. Soc.* **158** (2011) D158.

(126) C. Zhao, M. A. Pawlak, M. Popovici, M. Schaekers, E. Sleeckx, E. Vancoille, D. J. Wouters, Zs. Tokei and J. A. Kittl, *ECS Trans.* **25** (2009) 377.

(127) K. Kukli, J. Aarik, A. Aidla, I. Jõgi, T. Arroval, J. Lu, T. Sajavaara, M. Laitinen, A.-A. Kiisler, M. Ritala, M. Leskelä, J. Peck, J. Natwora, J. Geary, R. Spohn, S. Meiere and D. M. Thompson, *Thin Solid Films* **520** (2012) 2756.

(128) S. K. Park, R. Kanjolia, J. Anthis, R. Odedra, N. Boag, L. Wielunski and Y. J. Chabal, *Chem. Mater.* **22** (2010) 4867.

(129) S. K. Park, K. Roodenko, Y. J. Chabal, L. Wielunski, R. Kanjolia, J. Anthis, R. Odedra and N. Boag, *Mater. Res. Soc. Symp. Proc.* **1156** (2009) 1156-D04-02.

(130) N. Leick, R. O. F. Verkuijlen, L. Lamagna, E. Langereis, S. Rushworth, F. Roozeboom, M. C. M. van de Sanden and W. M. M. Kessels, *J. Vac. Sci. Technol. A* **29** (2011) 021016.

(131) S.-S. Yim, D.-J. Lee, K.-S. Kim, M.-S. Lee, S.-H. Kim and K.-B. Kim, *Electrochem. Solid-State Lett.* **11** (2008) K89.

(132) J. Heo, D. Eom, S. Y. Lee, S.-J. Won, S. Park, C. S. Hwang and H. J. Kim, *Chem. Mater.* **21** (2009) 4006.

(133) M. Zhang, W. Chen, S.-J. Ding, Z.-Y. Liu, Y. Huang, Z.-W. Liao and D. W. Zhang, *J. Phys. D: Appl. Phys.* **41** (2008) 032007.

(134) D.-J. Lee, S.-S. Yim, K.-S. Kim, S.-H. Kim and K.-B. Kim, *Nanotechnology* **22** (2011) 095305.

(135) J. Biener, T. F. Baumann, Y. Wang, E. J. Nelson, S. O. Kucheyev, A. V. Hamza, M. Kemell, M. Ritala and M. Leskelä, *Nanotechnology* **18** (2007) 055303.

(136) S.-S. Yim, M.-S. Lee, K.-S. Kim and K.-B. Kim, *Appl. Phys. Lett.* **89** (2006) 093115.

(137) S. T. Christensen, H. Feng, J. L. Libera, N. Guo, J. T. Miller, P. C. Stair and J. W. Elam, *Nano Lett.* **10** (2010) 3047.

(138) Y.-S. Min, E. J. Bae, K. S. Jeong, Y. J. Cho, J.-H. Lee, W. B. Choi and G.-S. Park, *Adv. Mater.* **15** (2003) 1019.

(139) T.-K. Eom, W. Sari, K.-J. Choi, W.-C. Shin, J. H. Kim, D.-J. Lee, K.-B. Kim, H. Sohn and S.-H. Kim, *Electrochem. Solid-State Lett.* **12** (2009) D85.

(140) S.-H. Choi, T. Cheon, S.-H. Kim, D.-H. Kang, G.-S. Park and S. Kim, *J. Electrochem. Soc.* **158** (2011) D351.

(141) S.-H. Kim, *ECS Trans.* **41** (2011) 19.

(142) W. Sari, T.-K. Eom, S.-H. Kim and H. Kim, *J. Electrochem. Soc.* **158** (2011) D42.

(143) T. E. Hong, K.-Y. Mun, S.-K. Choi, J.-Y. Park, S.-H. Kim, T. Cheon, W. K. Kim, B.-Y. Lim and S. Kim, *Thin Solid Films* **520** (2012) 6100.

(144) T.-K. Eom, S.-H. Kim, D.-H. Kang and H. Kim, *J. Electrochem. Soc.* **158** (2011) D657.

(145) K. Gregorczyk, L. Henn-Lecordier, J. Gatineau, C. Dussarrat and G. Rubloff, *Chem. Mater.* **23** (2011) 2650.

(146) K. Gregorczyk, P. Banerjee and G. W. Rubloff, *Mater. Lett.* **73** (2012) 43.

(147) Y. W. Song, J. Lee, K. Lee, Y. Lee and H. K. Jang, *ECS Trans.* **2** (2006) 1.

(148) H. Li, T. Aaltonen, Z. Li, B. S. Lim and R. G. Gordon, *Open Inorg. Chem. J.* **2** (2008) 11.

(149) H. Wang, R. G. Gordon, R. Alvis and R. M. Ulfig, *Chem. Vap. Deposition* **15** (2009) 312.

(150) H. Li, D. B. Farmer, R. G. Gordon, Y. Lin and J. Vlassak, *J. Electrochem. Soc.* **154** (2007) D642.

(151) J. Gatineau, K. Yanagita and C. Dussarrat, *Microelectron. Eng.* **83** (2006) 2248.

(152) J. H. Han, S. W. Lee, S. K. Kim, S. Han, C. S. Hwang, C. Dussarrat and J. Gatineau, *Chem. Mater.* **22** (2010) 5700.

(153) M Schaekers, B. Capon, C. Detavernier and N. Blasco, *ECS Trans.* **33** (2010) 135.

(154) J.-H. Ahn, J.-Y. Kim, J.-H. Kim, J.-S. Roh and S.-W. Kang, *Electrochem. Solid-State Lett.* **12** (2009) G5.

(155) J.-H. Ahn, J.-Y. Kim, J.-H. Kim, J.-S. Roh and S.-W. Kang, *ECS Trans.* **16** (2008) 335.

(156) S.-H. Kwon and K.-H. Kim, *J. Solid State Electrochem.* **14** (2010) 225.

(157) S. Maikap, T. Y. Wang, P. J. Tzeng, C. H. Lin, L. S. Lee, J. R. Yang and M. J. Tsai, *Appl. Phys. Lett.* **90** (2007) 253108.

(158) W. Banerjee and S. Maikap, in 9th International Conference on Solid-State and Integrated-Circuit Technology (ICSICT 2008), 2008, pp. 951–954.

(159) S. Maikap, W. Banerjee, T. C. Tien, T. Y. Wang and J. R. Yang, *J. Nanomater.* **2011** (2011) 810879.

(160) A. Das, S. Maikap, C.-H. Lin, P.-J. Tzeng, T.-C. Tien, T.-Y. Wang, L. B. Chang, J.-R. Yang and M.-J. Tsai, *Microelectron. Eng.* **87** (2010) 1821.

(161) S. Bang, S. Lee, T. Park, Y. Ko, S. Shin, S.-Y. Yim, H. Seo and H. Jeon, *J. Mater. Chem.* **22** (2012) 14141.

(162) K. Hušeková, E. Dobročka, A. Rosová, J. Šoltýs, A. Šatka, F. Fillot and K. Fröhlich, *Thin Solid Films* **518** (2010) 4701.

(163) A. Salaün, S. B. Newcomb, I. M. Povey, M. Salaün, L. Keeney, A. O´Mahony and M. E. Pemble, *Chem. Vap. Deposition* **17** (2011) 114.

(164) J.-H. Kim, D.-S. Kil, S.-J. Yeom, J.-S. Roh, N.-J. Kwak and J.-W. Kim, *Appl. Phys. Lett.* **91** (2007) 052908.

(165) S. W. Lee, J. H. Han, S. K. Kim, S. Han, W. Lee and C. S. Hwang, *Chem. Mater.* **23** (2011) 976.

(166) C. J. Smart, A. Gulhati and S. K. Reynolds, *Mat. Res. Soc. Symp. Proc.* **363** (1995) 207.

(167) T. Aaltonen, M. Ritala and M. Leskelä, *Electrochem. Solid-State Lett.* **8** (2005) C99.

(168) K. J. Park and G. N. Parsons, *Appl. Phys. Lett.* **89** (2006) 043111.

(169) D. Josell, J. E. Bonevich, T. P. Moffat, T. Aaltonen, M. Ritala and M. Leskelä, *ECS Trans.* **1** (2006) 57.

(170) D. Josell, J. E. Bonevich, T. P. Moffat, T. Aaltonen, M. Ritala and M. Leskelä, *Electrochem. Solid-State Lett.* **9** (2006) C48.

(171) D. Josell, J. E. Bonevich, T. P. Moffat, T. Aaltonen, M. Ritala and M. Leskelä, *Electrochem. Solid-State Lett.* **9** (2006) L4.

(172) J. Vila-Comamala, K. Jefimovs, T. Pilvi, M. Ritala, S. S. Sarkar, H. H. Solak, V. A. Guzenko, M. Stampanoni, F. Marone, J. Raabe, G. Tzvetkov, R. H. Fink, D. Grolimund, C. N. Borca, B. Kaulich and C. David, *J. Phys.: Conf. Ser.* **186** (2009) 012078.

(173) J. Vila-Comamala, S. Gorelick, E. Färm, C. M. Kewish, A. Diaz, R. Barrett, V. A. Guzenko, M. Ritala and C. David, *Opt. Express* **19** (2011) 175.

(174) J. Vila-Comamala, S. Gorelick, V. A. Guzenko, E. Färm, M. Ritala and C. David, *Nanotechnology* **21** (2010) 285305.

(175) C. David, S. Gorelick, S. Rutishauser, J. Krzywinski, J. Vila-Comamala, V. A. Guzenko, O. Bunk, E. Färm, M. Ritala, M. Cammarata, D. M. Fritz, R. Barrett, L. Samoylova, J. Grünert and H. Sinn, *Sci. Rep.* **1** (2011) 57.

(176) T. Weber, T. Käsebier, A. Szeghalmi, M. Knez, E.-B. Kley and A. Tünnermann, *Nanoscale Res. Lett.* **6** (2011) 558.

(177) T. Weber, T. Käsebier, A. Szeghalmi, M. Knez, E.-B. Kley and A. Tünnermann, *Microelectron. Eng.* **98** (2012) 433.

(178) K. Jefimovs, J. Laukkanen, T. Vallius, T. Pilvi, M. Ritala, T. Meilahti, M. Kaipiainen, M. Bavdaz, M. Leskelä and J. Turunen, *Microelectron. Eng.* **83** (2006) 1339.

(179) T. A. Walsh, J. A. Bur, Y.-S. Kim, T.-M. Lu and S-Y. Lin, *J. Opt. Soc. Am. B* **26** (2009) 1450.

(180) M. Kemell, V. Pore, M. Ritala and M. Leskelä, *Chem. Vap. Deposition* **12** (2006) 419.

(181) M. Kemell, M. Ritala, M. Leskelä, R. Groenen and S. Lindfors, *Chem. Vap. Deposition* **14** (2008) 347.

(182) D. J. Comstock, S. T. Christensen, J. W. Elam, M. J. Pellin and M. C. Hersam, *Electrochem. Commun.* **12** (2010) 1543.

(183) D. J. Comstock, S. T. Christensen, J. W. Elam, M. J. Pellin and M. C. Hersam, *Adv. Funct. Mater.* **20** (2010) 3099.

(184) K. Kawano, M. Takamori, K. Tada, T. Yamakawa, N. Ohshima, S. Watari, H. Fujisawa and M. Shimizu, *TOSOH Res. Technol. Rev.* **48** (2004) 3.

(185) Y. H. Lim, H. Yoo, B. H. Choi, J. H. Lee, H.-N. Lee and H. K. Lee, *Phys. Status Solidi C* **8** (2011) 891.

(186) S.-W. Kim, S.-H. Kwon, D.-K. Kwak and S.-W. Kang, *J. Appl. Phys.* **103** (2008) 023517.

(187) S.-W. Kim, S.-H. Kwon and S.-W. Kang, *ECS Trans.* **16** (2008) 309.

(188) S.-W. Kim, S-H. Kwon, S.-J. Jeong, J.-S. Park and S.-W. Kang, *Electrochem. Solid-State Lett.* **11** (2008) H303.

(189) M. J. Heikkilä, J. Hämäläinen, M. Ritala and M. Leskelä, *Z. Kristallogr. Proc.* **1** (2011) 209.

(190) S.-J. Jeong, Y.-R. Shin, W.-S. Kwack, H. W. Lee, Y.-K. Jeong, D.-I. Kim, H. C. Kim and S.-H. Kwon, *Surf. Coat. Technol.* **205** (2011) 5009.

(191) M. R. Kim, J. H. Lee and B. H. Choi, *Microelectron. Eng.* **98** (2012) 400.

(192) K. Kim and S. Lee, *J. Appl. Phys.* **100** (2006) 051604.

(193) J.-M. Koo, B.-S. Seo, S. Kim, S. Shin, J.-H. Lee, H. Baik, J.-H. Lee, J. H. Lee, B.-J. Bae, J.-E. Lim, D.-C. Yoo, S.-O. Park, H.-S. Kim, H. Han, S. Baik, J.-Y. Choi, Y. J. Park and Y. Park, in Technical Digest – International Electron Devices Meeting, IEEE, 2005, pp. 351–354.

(194) C. Dussarrat and J. Gatineau, *Proc. Electrochem. Soc.* **2005-05** (2005) 354.

(195) S. H. Kwon, S. W. Kim, S. J. Jeong, K. H. Kim and S. W. Kang, *ECS Trans.* **16** (2008) 315.

(196) S. Choi, Y.-K. Cha, B.-S. Seo, S. Park, J.-H. Park, S. Shin, K. S. Seol, J.-B. Park, Y.-S. Jung, Y. Park, Y. Park, I.-K. Yoo and S.-H. Choi, *J. Phys. D: Appl. Phys.* **40** (2007) 1426.

(197) T. Ryynänen, K. Nurminen, J. Hämäläinen, M. Leskelä and J. Lekkala, *Proc. Eng.* **5** (2010) 548.

(198) T. Ryynänen, L. Ylä-Outinen, S. Narkilahti, J. M. A. Tanskanen, J. Hyttinen, J. Hämäläinen, M. Leskelä and J. Lekkala, *J. Vac. Sci. Technol. A* **30** (2012) 041501.

(199) E. Santala, J. Hämäläinen, J. Lu, M. Leskelä and M. Ritala, *Nanosci. Nanotechnol. Lett.* **1** (2009) 218.

(200) D.-K. Joo, J.-S. Park and S.-W. Kang, *Electrochem. Solid-State Lett.* **12** (2009) H77.

(201) J. J. Senkevich, F. Tang, D. Rogers, J. T. Drotar, C. Jezewski, W. A. Lanford, G.-C. Wang and T.-M. Lu, *Chem. Vap. Deposition* **9** (2003) 258.

(202) G. A. Ten Eyck, S. Pimanpang, H. Bakhru, T.-M. Lu and G.-C. Wang, *Chem. Vap. Deposition* **12** (2006) 290.

(203) M. J. Weber, A. J. M. Mackus, M. A. Verheijen, C. van der Marel and W. M. M. Kessels, *Chem. Mater.* **24** (2012) 2973.

(204) J. W. Elam, G. Xiong, C. Y. Han, H. H. Wang, J. P. Birrell, J. N. Hryn, M. J. Pellin, J. F. Poco and J. H. Satcher Jr., *Mater. Res. Soc. Symp. Proc.* **876 E** (2005) R12.6.1.

(205) J. W. Elam, G. Xiong, C. Y. Han, H. H. Wang, J. P. Birrell, U. Welp, J. N. Hryn, M. J. Pellin, T. F. Baumann, J. F. Poco and J. H. Satcher Jr., *J. Nanomater.* **2006** (2006) 64501.

(206) G. A. Ten Eyck, J. J. Senkevich, F. Tang, D. Liu, S. Pimanpang, T. Karaback, G.-C. Wang, T.-M. Lu, C. Jezewski and W. A. Lanford, *Chem. Vap. Deposition* **11** (2005) 60.

(207) Y.-S. Kim, J. Shin, J.-H. Cho, G. A. Ten Eyck, D.-L. Liu, S. Pimanpang, T.-M. Lu, J. J. Senkevich and H.-S. Shin, *Surf. Coat. Technol.* **200** (2006) 5760.

(208) N. E. Lay and D. J. Duquette, *ECS Trans.* **3** (2007) 153.

(209) N. E. Lay, G. A. Ten Eyck, D. J. Duquette and T.-M. Lu, *Electrochem. Solid-State Lett.* **10** (2007) D13.

(210) Y.-S. Kim, G. A. Ten Eyck, D. Ye, C. Jezewski, T. Karabacak, H.-S. Shin, J. J. Senkevich and T.-M. Lu, *J. Electrochem. Soc.* **152** (2005) C376.

(211) G. A. Ten Eyck, S. Pimanpang, J. S. Juneja, H. Bakhru, T.-M. Lu and G.-C. Wang, *Chem. Vap. Deposition* **13** (2007) 307.

(212) Y.S. Kim, H.-I. Kim, J.-H. Cho, H.-K. Seo, M. A. Dar, H.-S. Shin, G. A. Ten Eyck, T.-M. Lu and J. J. Senkevich, *Electrochim. Acta* **51** (2006) 2400.

(213) T. Aaltonen, M. Ritala, T. Sajavaara, J. Keinonen and M. Leskelä, *Chem. Mater.* **15** (2003) 1924.

(214) Y. Zhou, D. M. King, X. Liang, J. Li and A. W. Weimer, *Appl. Catal. B* **101** (2010) 54.

(215) C. Henkel, S. Abermann, O. Bethge and E. Bertagnolli, *Semicond. Sci. Technol.* **24** (2009) 125013.

(216) G. Liang, H. Cheng, Z. Zhiwei, Z. Wei, W. Dongping and Z. Shili, *J. Semicond.* **33** (2012) 083003.

(217) J. R. Montague, M. Dalberth, J. M. Gray, D. Seghete, K. A. Bertness, S. M. George, V. M. Bright, C. T. Rogers and N. A. Sanford, *Sens. Actuators A* **165** (2011) 59.

(218) J. H. Shim and F. B. Prinz, *ECS Trans.* **11** (2008) 27.

(219) A. J. M. Mackus, S. A. F. Dielissen, J. J. L. Mulders and W. M. M. Kessels, *Nanoscale* **4** (2012) 4477.

(220) I. J. Hsu, D. A. Hansgen, B. E. McCandless, B. G. Willis and J. G. Chen, *J. Phys. Chem. C* **115** (2011) 3709.

(221) O. Bethge, G. Pozzovivo, C. Henkel, S. Abermann and E. Bertagnolli, *J. Micromech. Microeng.* **22** (2012) 085013.

(222) S. T. Christensen, J. W. Elam, F. A. Rabuffetti, Q. Ma, S. J. Weigand, B. Lee, S. Seifert, P. C. Stair, K. R. Poeppelmeier, M. C. Hersam and M. J. Bedzyk, *Small* **5** (2009) 750.

(223) V. A. Sivakov, K. Höflich, M. Becker, A. Berger, T. Stelzner, K.-E. Elers, V. Pore, M. Ritala and S. H. Christiansen, *Chem. Phys. Chem.* **11** (2010) 1995.

(224) J. Li, X. Liang, D. M. King, Y.-B. Jiang and A. W. Weimer, *Appl. Catal. B.* **97** (2010) 220.

(225) H. C. M. Knoops, A. J. M. Mackus, M. E. Donders, M. C. M. van de Sanden, P. H. L. Notten and W. M. M. Kessels, *ECS Trans.* **16** (2008) 209.

(226) H. C. M. Knoops, A. J. M. Mackus, M. E. Donders, M. C. M. van de Sanden, P. H. L. Notten and W. M. M. Kessels, *Electrochem. Solid-State Lett.* **12** (2009) G34.

(227) A. Niskanen, T. Hatanpää, K. Arstila, M. Leskelä and M. Ritala, *Chem. Vap. Deposition* **13** (2007) 408.

(228) M. Kariniemi, J. Niinistö, T. Hatanpää, M. Kemell, T. Sajavaara, M. Ritala and M. Leskelä, *Chem. Mater.* **23** (2011) 2901.

(229) M. Kariniemi, J. Niinistö, M. Vehkamäki, M. Kemell, M. Ritala, M. Leskelä and M. Putkonen, *J. Vac. Sci. Technol. A* **30** (2012) 01A115-1.

(230) B. S. Lim, A. Rahtu and R. G. Gordon, *Nature Mater.* **2** (2003) 749.

(231) P. R. Chalker, S. Romani, P. A. Marshall, M. J. Rosseinsky, S. Rushworth and P. A. Williams, *Nanotechnology* **21** (2010) 405602.

(232) S. T. Barry, J. P. Coyle, M. Kariniemi, J. Niinistö, M. Ritala, and M. Leskelä, ”Novel Ligand System for Group 11 Metals: Thermal and Plasma-Enhanced ALD of Copper and Gold”, poster presentation, 12th International Conference on Atomic Layer Deposition (ALD 2012), Dresden, Germany, 2012.

(233) T. J. J. Whitehorne, J. P. Coyle, A. Mahmood, W. H. Monillas, G. P. A. Yap and S. T. Barry, *Eur. J. Inorg Chem.* (2011) 3240.

(234) J. W. Klaus, S. J. Ferro and S. M. George, *Thin Solid Films* **360** (2000) 145.

(235) D. Seghete, G. B. Rayner Jr., A. S. Cavanagh, V. R. Anderson and S. M. George, *Chem. Mater.* **23** (2011) 1668.

(236) R. A. Waldo, *Microbeam. Anal.* **23** (1988) 310.

(237) M. Putkonen, T. Sajavaara, L. Niinistö and J. Keinonen, *Anal. Bioanal. Chem.* **382** (2005) 1791.

(238) I. K. Igumenov, *J. Phys. IV* **5** (1995) C5-489.

(239) A. J. Plomp, H. Vuori, A. O. I. Krause, K. P. de Jong and J. H. Bitter, *Appl. Catal. A* **351** (2008) 9.